FP 4A 2024

Collisions

Cross section and Rate coefficient

Electron collisions

Ramsauer effect

Collision cross section of IMR

Arrhenius dependence

Single collision

$$H_2^+ + Ar \Rightarrow ArH^+ + H$$

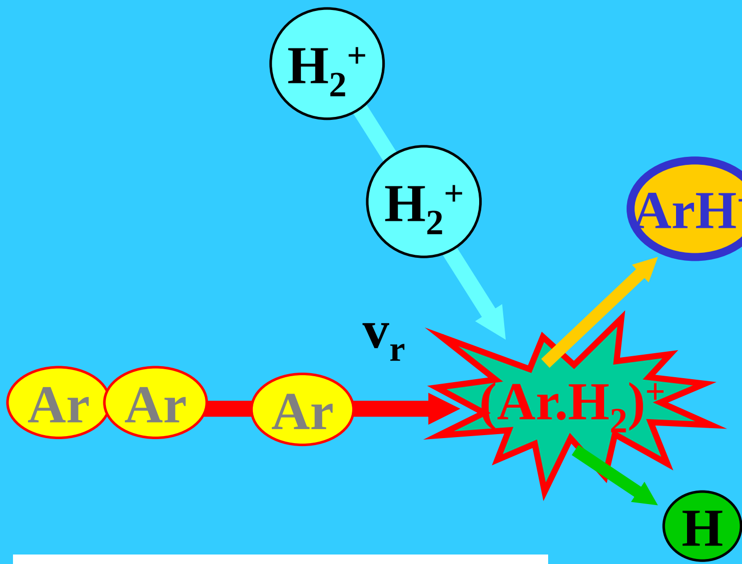

reaction cross section

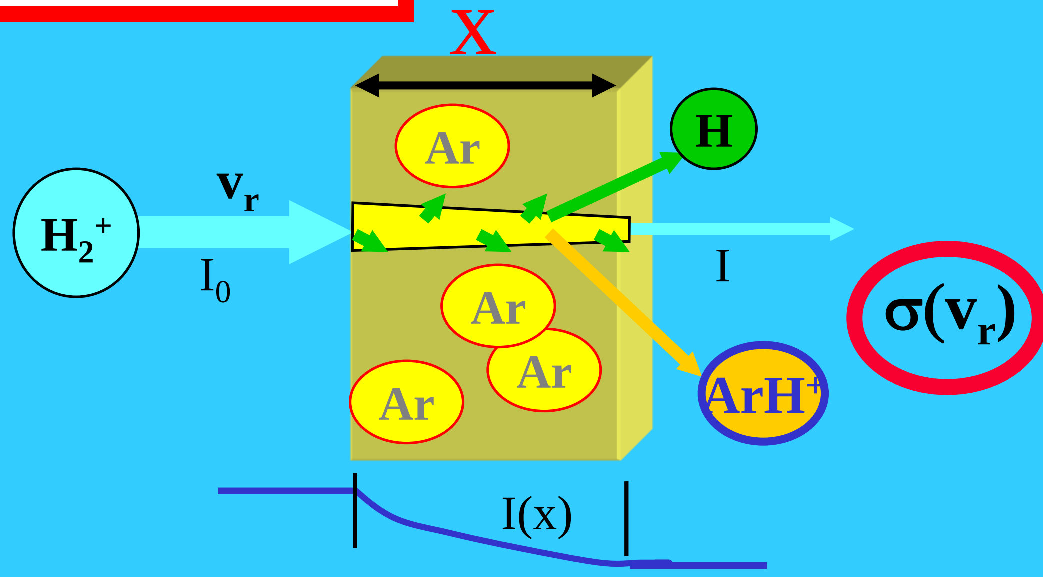

$I = I_0 \exp(-\sigma n_{Ar} x)$

$$\nu_{coll} = +nV_{rel} = +n\nu S = +n\nu\pi\delta^2 = +n\nu\sigma$$

Collisional cross section

$$\frac{dI}{dt} = -\frac{I}{\tau_{coll}} = -I\nu_{coll}$$

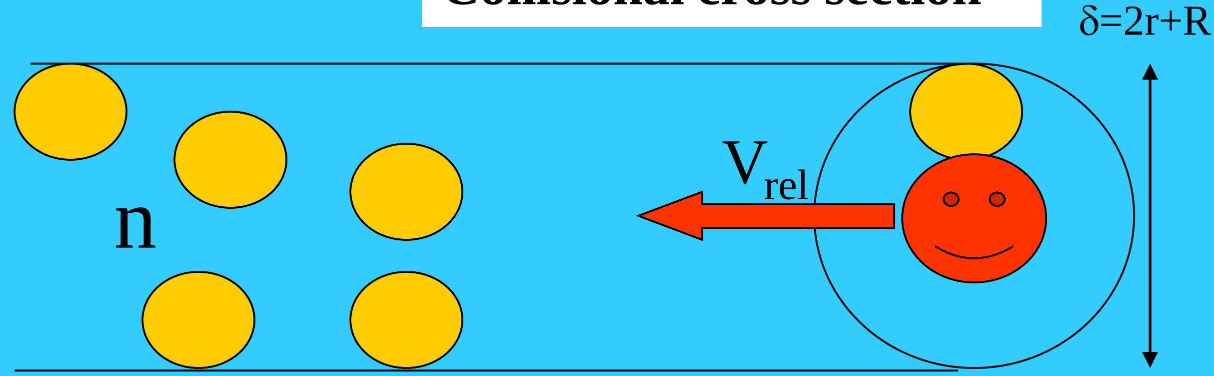

$$I(t) = I_0 \exp(-\nu_{coll} t) = I_0 \exp(-\sigma n \nu_{rel} t)$$

$I = I_0 \exp(-\sigma n_{Ar} x)$

Single collision

$$H_2^+ + Ar \Rightarrow ArH^+ + H$$

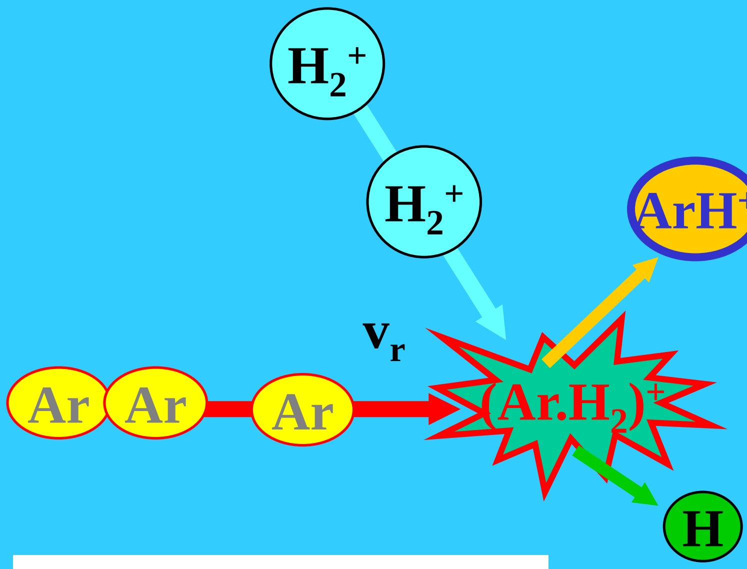

reaction cross section

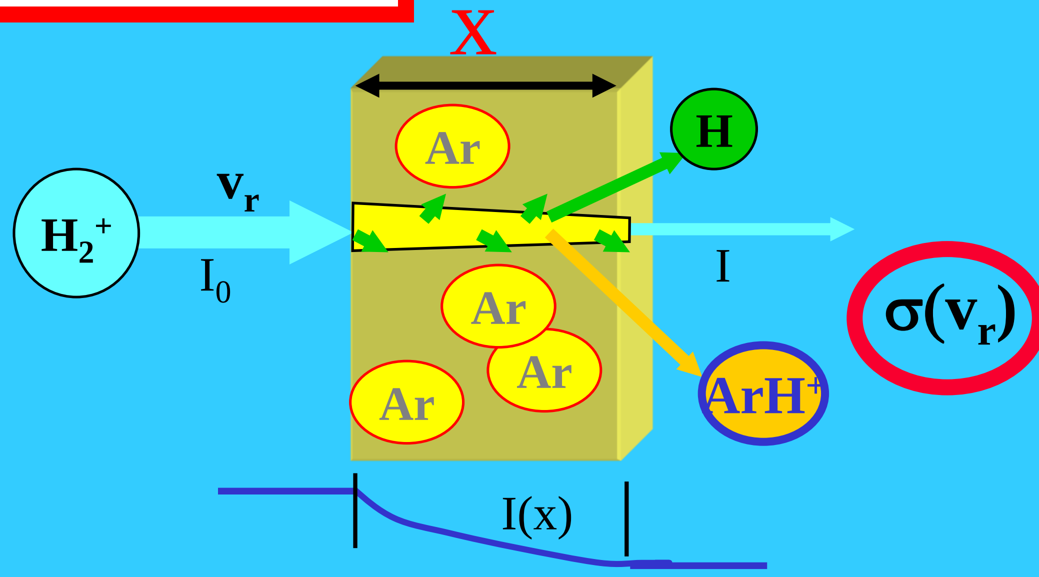

$I=I_0\exp(-\sigma n_{Ar}x)$

Proportionality factor

$$\frac{dI}{dx} \sim -INx \qquad \frac{dI}{dx} = -\sigma INx$$

$$\frac{dI}{Idx} = \frac{d\ln(I)}{dx} = -\sigma Nx$$

$$I(x) = I_0\exp(-\sigma Nx)$$

Electron impact ionization

2.3. Electron impact ionization

The electron impact ionization is the most fundamental ionization process for the operation of ion sources.

Why?

- The cross section for the impact ionization is by orders of magnitudes higher than the cross section for the photo ionization.
- The cross section depends on the mass of the colliding particle. Since the energy transfer of a heavy particle is lower, a proton needs for an identical ionization probability an ionization energy three orders of magnitudes higher than an electron

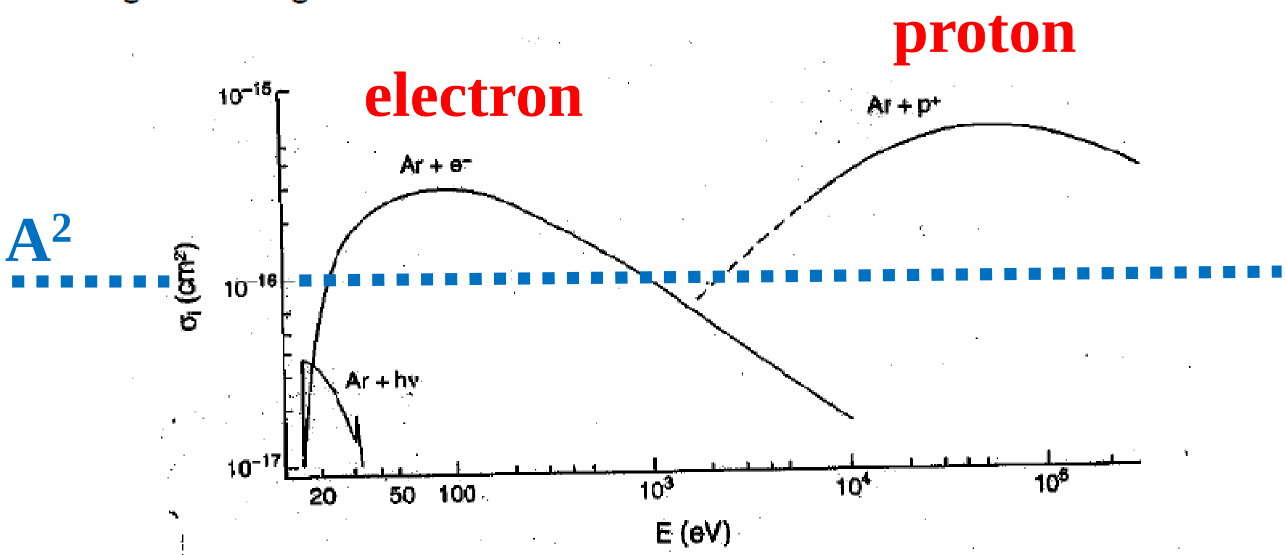

FIGURE 4
Ionization cross sections as functions of energy for ionizing collisions with fast electrons, protons, and photons. (From Winter, H., in *Experimental Methods in Heavy Ion Physics*, Springer-Verlag,

Cross sections for vibrational excitation, dissociation, ionization…H_2

$H_2 + e$	→ $H_2(v) + e$ …….	Vibrational excitation
	→ $H + H + e$…….	Dissociation
	→ $H_2^* + h\nu + e$ …	Photon excitation
	→ $H_2^+ + e + e$…..	Ionization
	→ $H^+ + H + e + e$	Dissociative Ionization

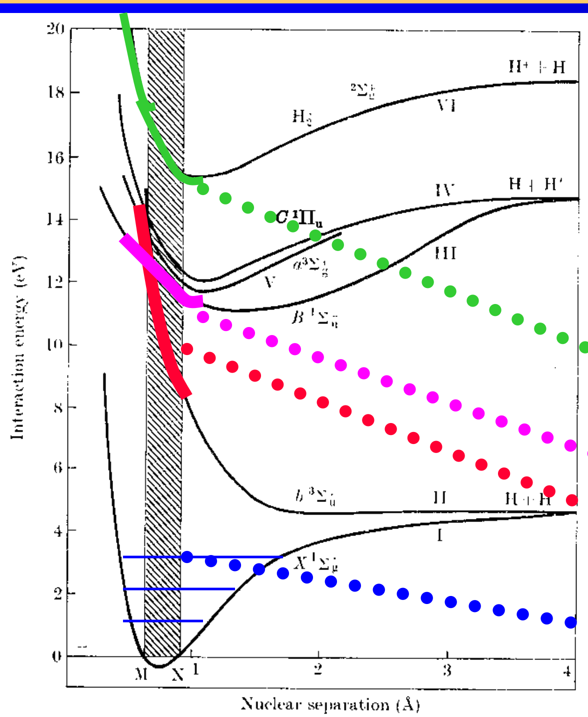

FIG. 13.1. Potential energy curves for electronic states of H_2 and H_2^+ lying within 20 eV of the ground state.

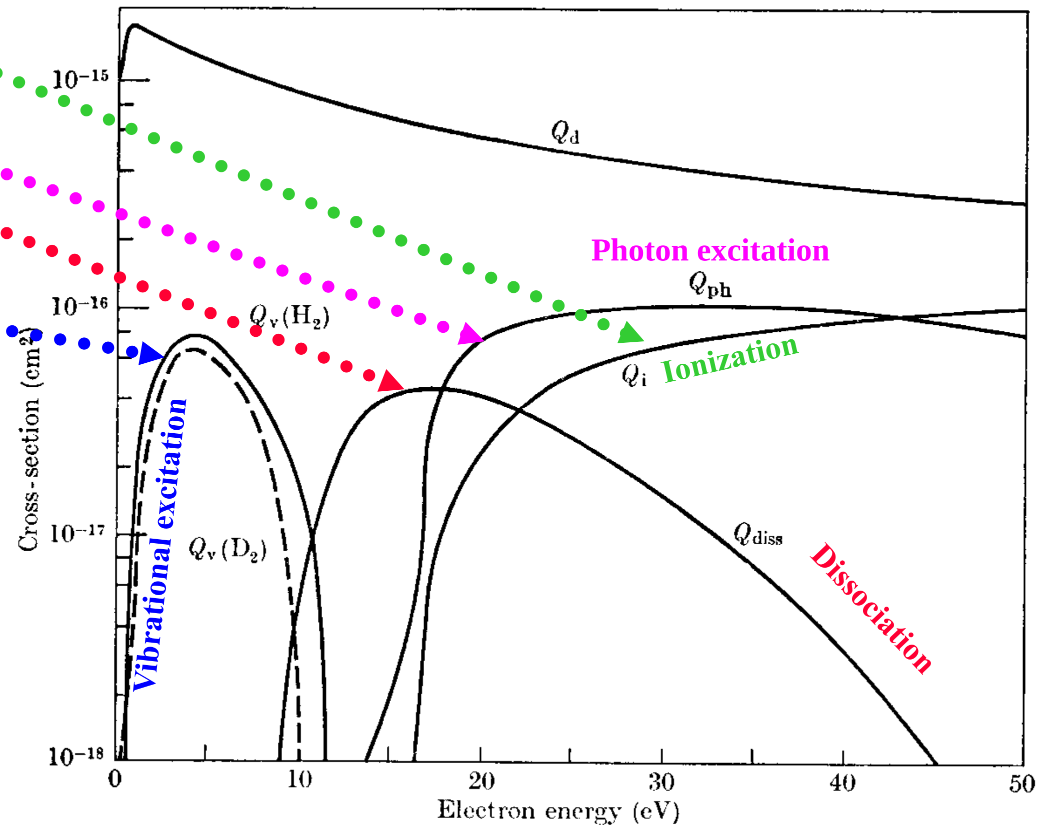

FIG. 13.37. Cross-sections assumed by Engelhardt and Phelps in their analysis of swarm data in H_2 and D_2 for electrons of characteristic energy greater than 1 eV. Q_d momentum-transfer cross-section, Q_i, ionization cross-section, Q_{diss} dissociation cross-section, Q_{ph} photon excitation cross-section, Q_v vibrational excitation cross-section (—— H_2, — — — D_2).

$$H_2^+ + Ar \Rightarrow ArH^+ + H$$

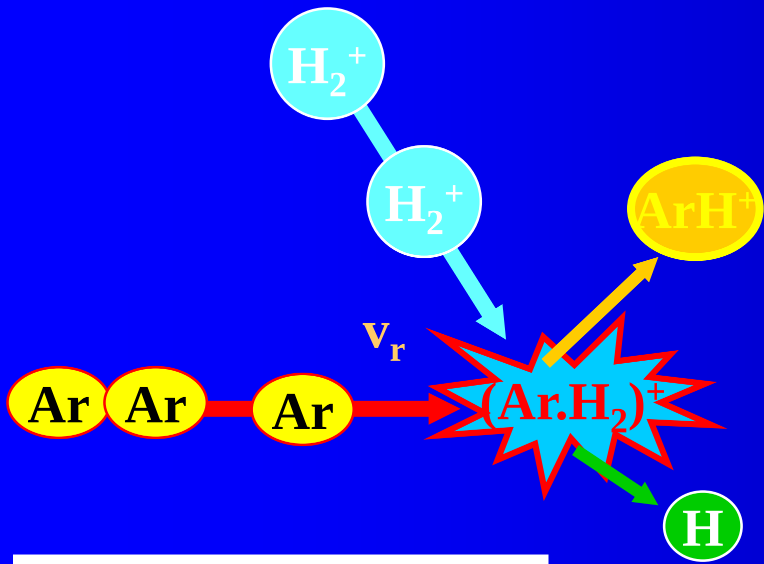

reaction cross section

$$A^+ + B \to C^+ + D$$

$$\frac{dA^+}{dt} = -k_{BIN} A^+ B$$

Identification ☺
of number densities

$$[A^+]_t = [A^+]_{t=0} \cdot e^{-k[B]t}$$

$$\nu_{coll} = -nV_{rel} = -n v S = -n v \pi \delta^2 = -n v \sigma$$

$$\frac{dI}{dt} = -\frac{I}{\tau_{coll}} = -I \nu_{coll}$$

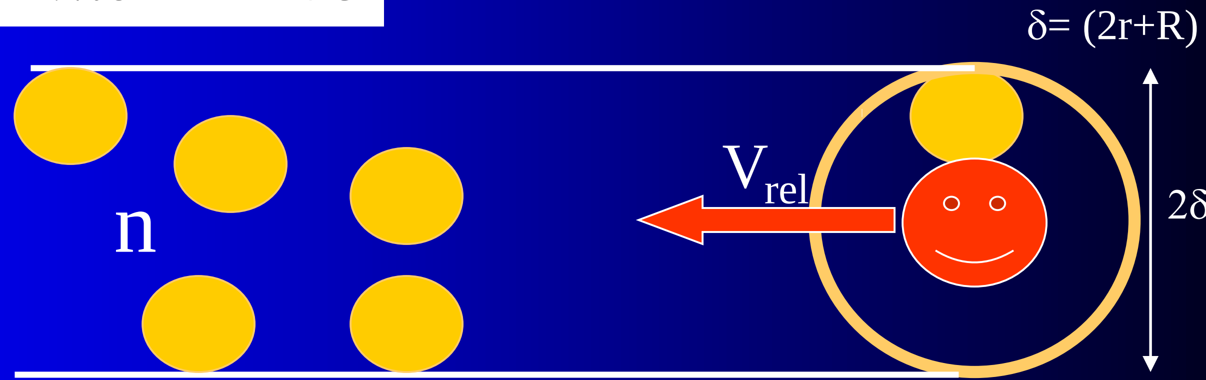

$$I(t) = I_0 \exp(-\nu_{coll} t) = I_0 \exp(-\sigma n \nu_{rel} t)$$ ↔ $$I = I_0 \exp(-\sigma n_{Ar} x)$$

Kinetics of elementary process

$$H_2^+ + Ar \Rightarrow ArH^+ + H$$

$$A^+ + B \rightarrow C^+ + D$$

$$\frac{dA^+}{dt} = -k_{BIN} A^+ B$$

$$[A^+]_t = [A^+]_{t=0} \cdot e^{-k[B]t}$$

Identification ☺
of number densities

Multiple collision

@ T

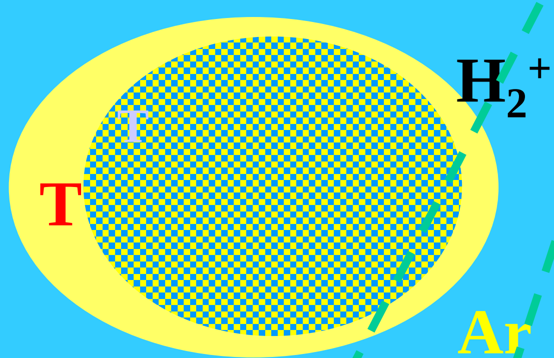

reaction rate coefficient

$d(n_{H2^+})/dt = -k\, n_{H2^+} \cdot n_{Ar}$

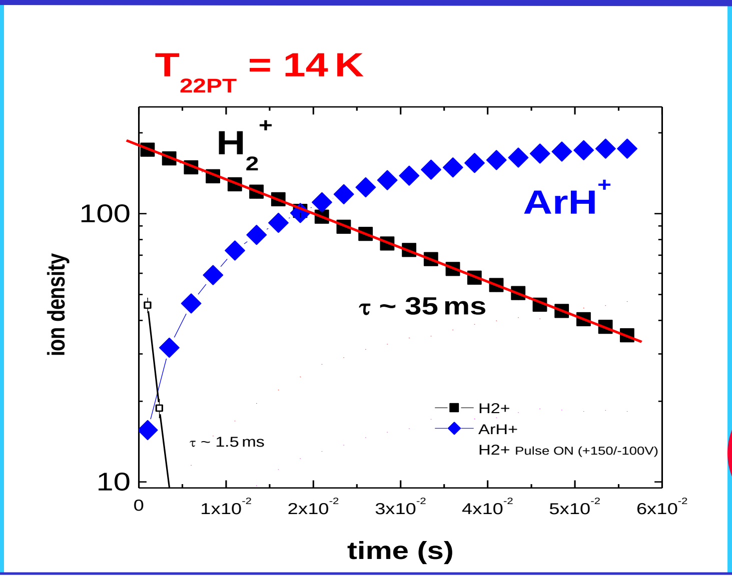

$n_{H2^+} = (n_{H2^+})_0 \exp(-k n_{Ar} t)$

k(T)

reactions

$$A^{+} \quad + \quad B \rightarrow C^{+} \quad + \quad D$$

$$\frac{dA^{+}}{dt} = -k_{BIN} A^{+} B$$

$$[k_{BIN}] = cm^{3} s^{-1}$$

$$1/\tau = k_{BIN}[B] = \ldots \; n v \rho \; \ldots = [B] v \rho \; \ldots . [B] \; \langle v \rho \rangle$$

$$k_{BIN} = \langle v \rho \rangle$$

Kinetics of elementary process

$$H_2^+ + Ar \Rightarrow ArH^+ + H$$

Single collision

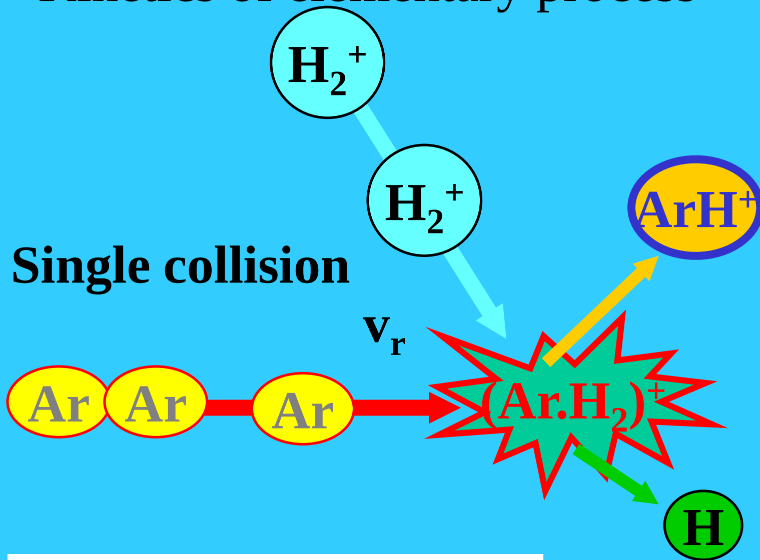

reaction cross section

$$I = I_0 \exp(-\sigma n_{Ar} x)$$

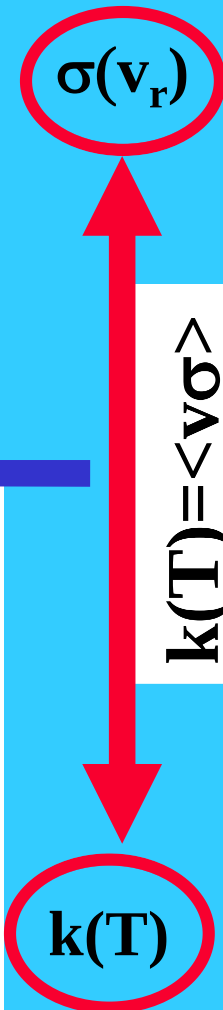

Multiple collision

@ T

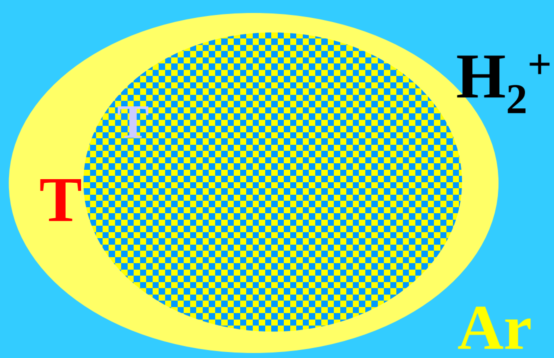

reaction rate coefficient

$$d(n_{H2^+})/dt = -k\, n_{H2^+} \cdot n_{Ar}$$

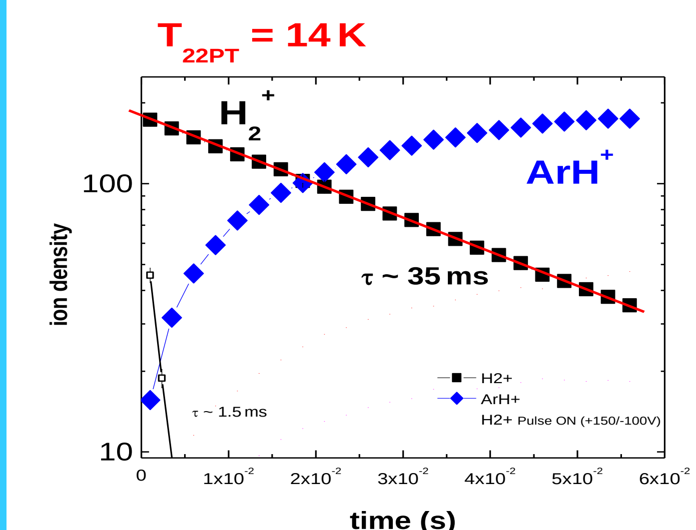

$$n_{H2^+} = (n_{H2^+})_0 \exp(-k n_{Ar} t)$$

$$A^+ \quad + \quad B \rightarrow C^+ \quad + \quad D$$

$$\sigma(v_r)$$

$$k_{BIN} = k_{BIN}(T)$$

$$k(T) = \langle v_r \sigma(v_r) \rangle$$

$$k = \int_v f_T(v).v.\sigma(v)dv = k(T)$$

Ar

Electron scattering cross-section on Ar

$$k = \int_v f_T(v).v.\sigma(v)dv = k(T)$$

Electrons – Boltzman distribution with T_e

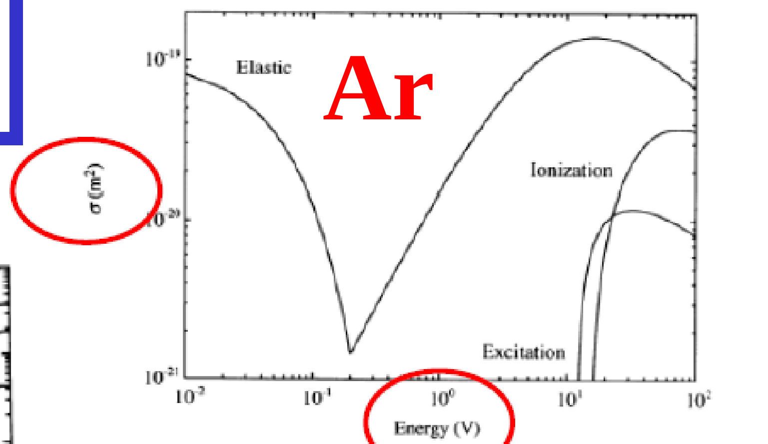

3. Ionization, excitation and elastic scattering cross sections for electrons in ...piled by Vahedi, 1993).

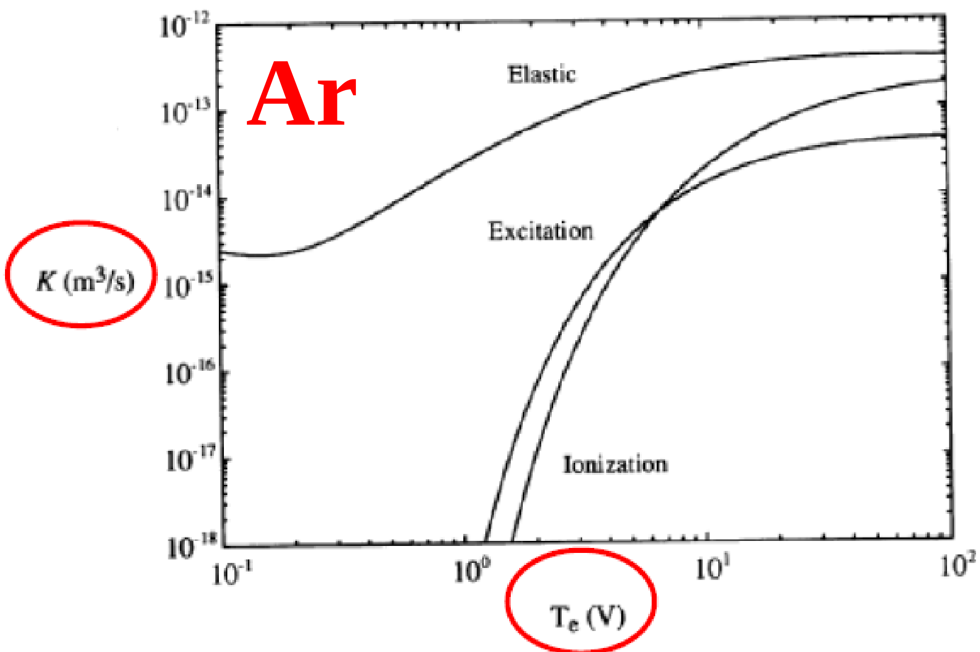

FIGURE 3.16. Electron collision rate constants K_{iz}, K_{ex} and K_m versus T_e in argon gas (compiled by Vahedi, 1993).

$$\alpha(T, T_e) \propto \int_0^\infty \sqrt{E}\,\sigma_w(E, T) f(E, T_e)\, dE$$

What if we have metastables?

Lieberman&Lichtenberg

Reaction coordinate

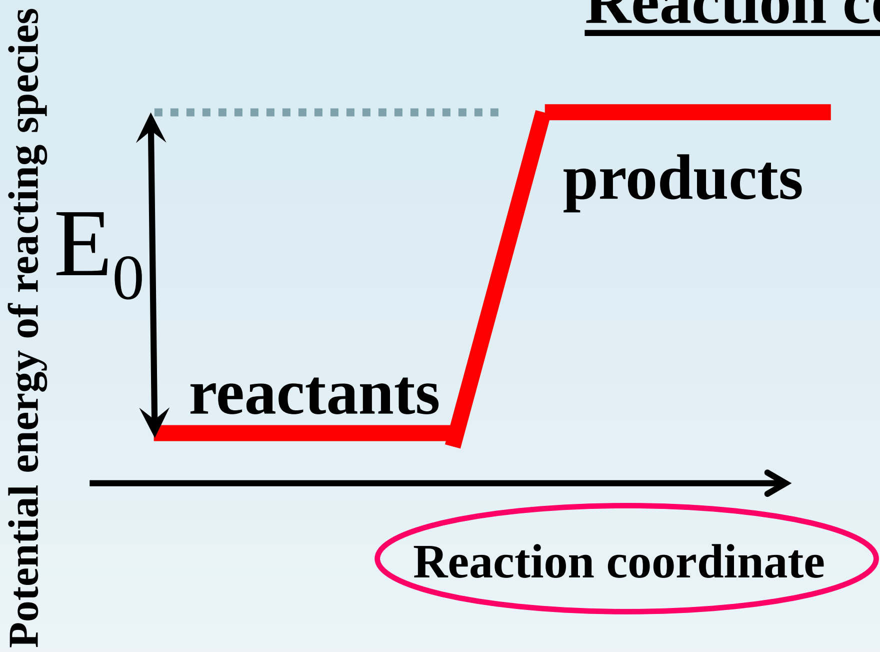

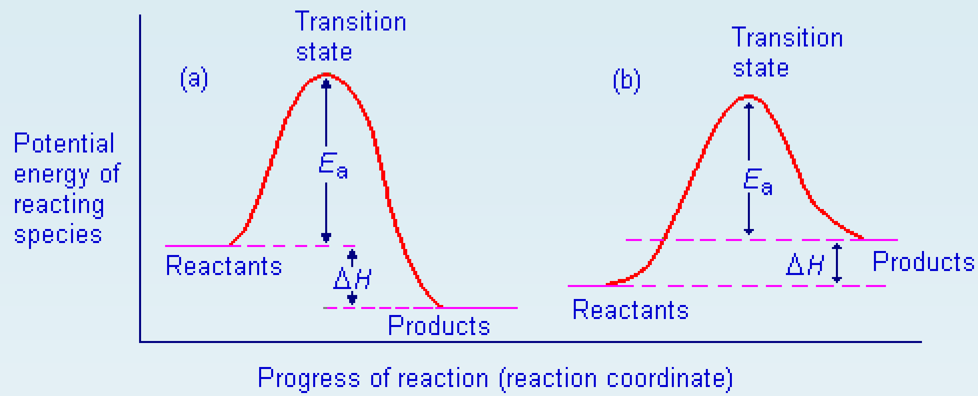

Collisional energy

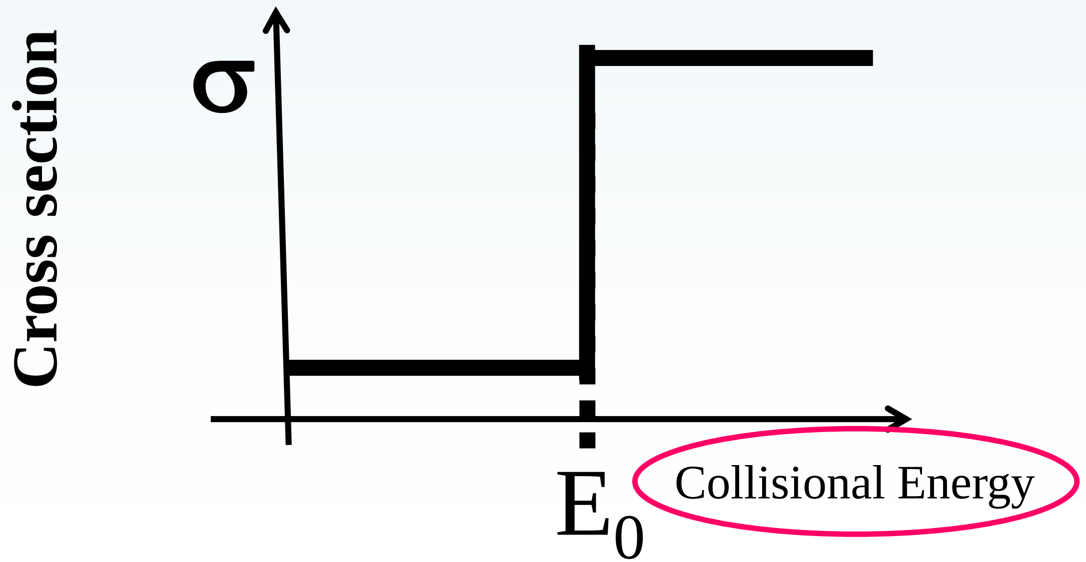

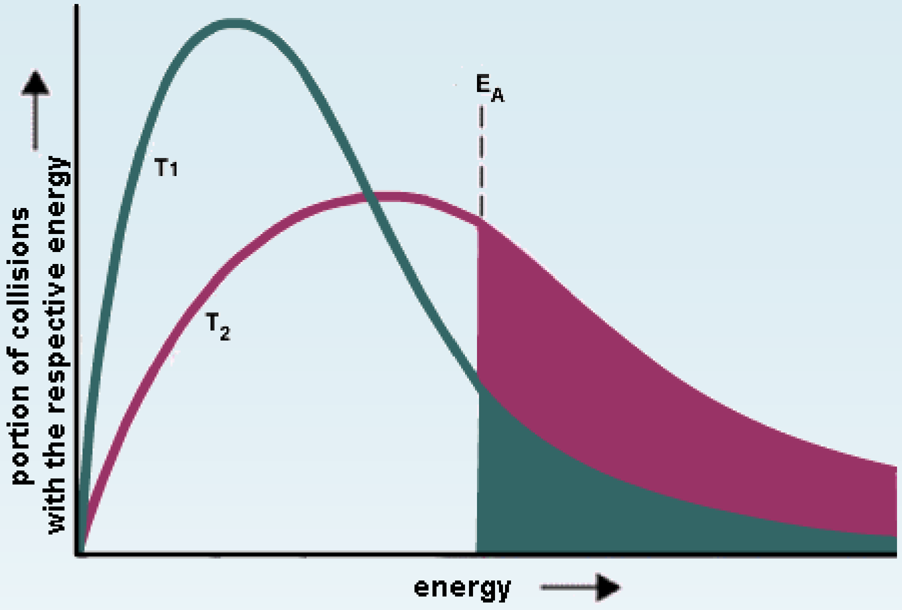
portion of collisions
with the respective energy
T1
T2
EA
energy

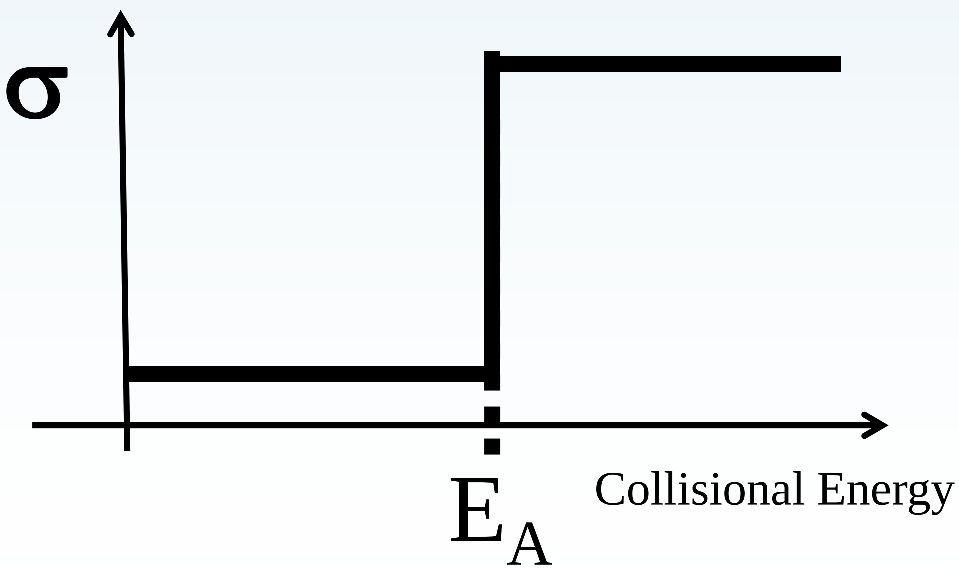
σ
EA
Collisional Energy

Higher temperatures favor products for an endothermic reaction

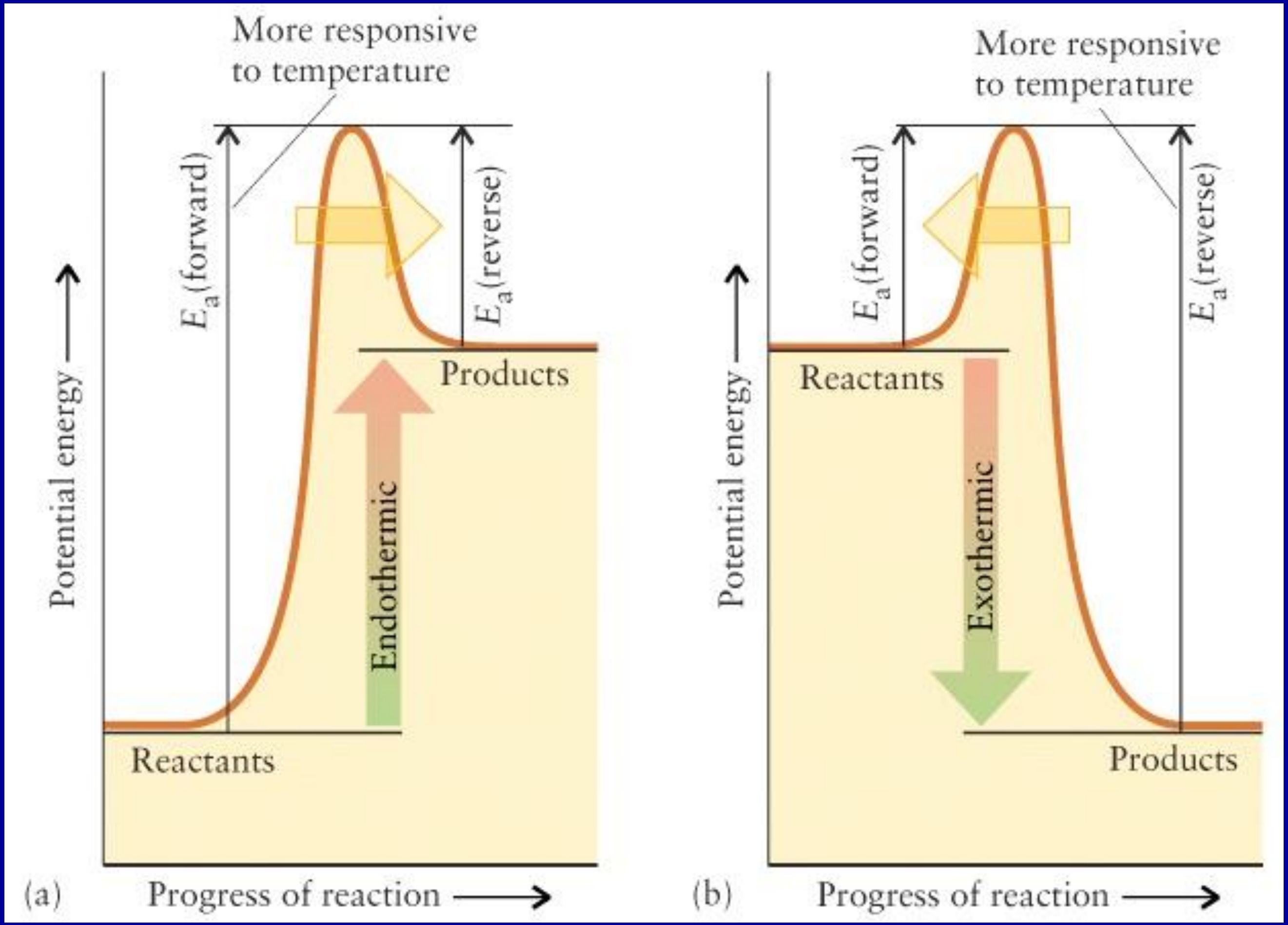

Endothermic reaction: E_a(forward) > E_a(reverse)

Exothermic reaction: E_a(forward) < E_a(reverse)

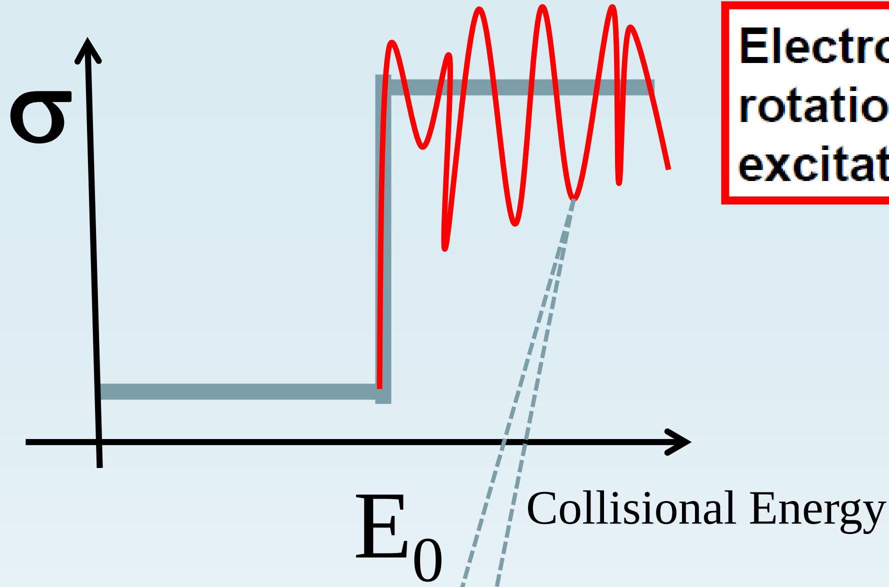

Electron impact rotational excitation of CH^+

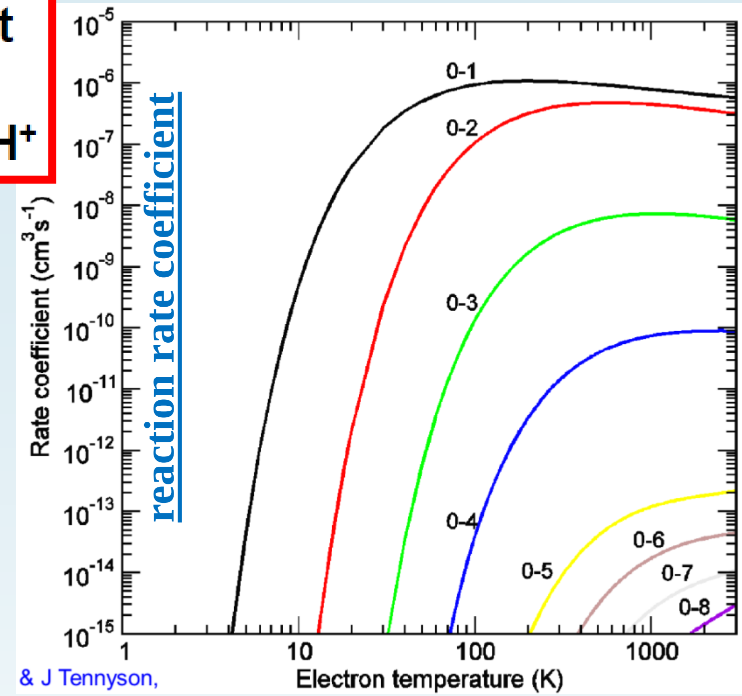

The thermally averaged rate constant $\alpha_{\mathrm{th}}(T)$ (in a.u.) is obtained from the energy-dependent cross-section $\sigma(E)$ as

$$\alpha_{\mathrm{th}}(T) = \frac{8\pi}{(2\pi kT)^{3/2}} \int_0^\infty \sigma(E_{\mathrm{el}}) e^{-\frac{E_{\mathrm{el}}}{kT}} E_{\mathrm{el}} \mathrm{d}E_{\mathrm{el}} \,, \tag{4}$$

where T is the temperature. Temperature dependencies $\alpha_{\mathrm{th}}(T)$ for different rovibrational transitions $v \rightarrow v'$ obtained using equation (4) are shown in Fig. 3 as solid lines.

For further discussion, it is convenient to represent the cross-section $\sigma(E_{\mathrm{el}})$ in the form

$$\sigma(E_{\mathrm{el}}) = \frac{\pi}{k^2} P(E_{\mathrm{el}}) \,, \tag{5}$$

where k is the wave vector of the incident electron, $P(E_{\mathrm{el}})$ is the probability for vibrational (de-)excitation at collision energy E_{el}.

Arrhenius dependence

$$k = A e^{-\frac{E_a}{RT}}$$

activation energy (E_a)

pre-exponential factor (A)

average kinetic energy (RT)

$$\ln k = \ln A - \frac{E_a}{RT}$$

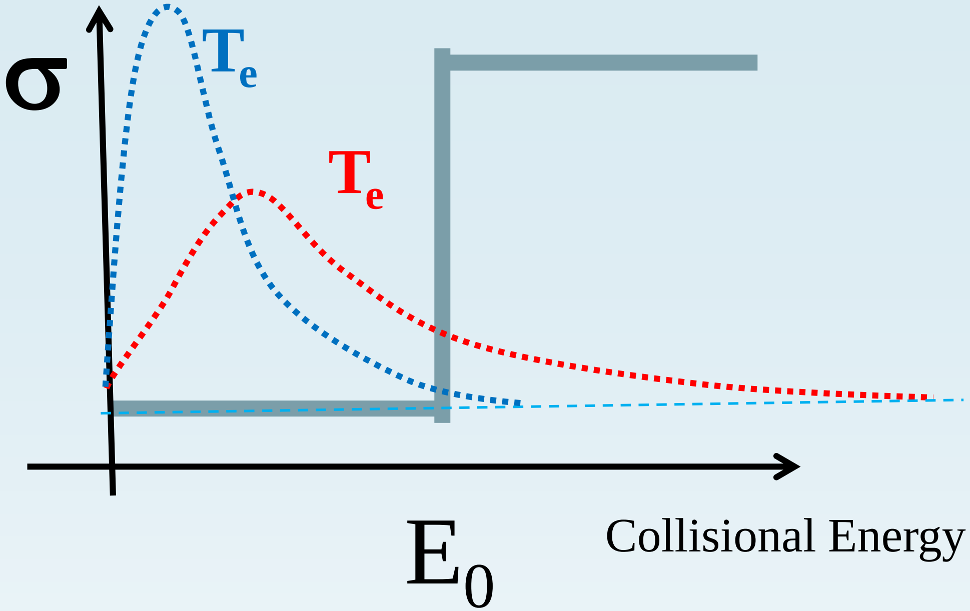

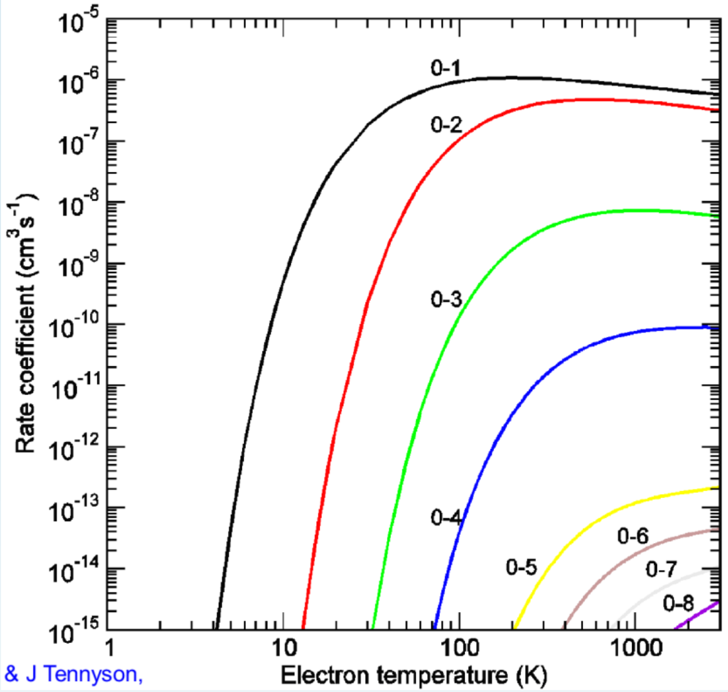

Arrhenius plot

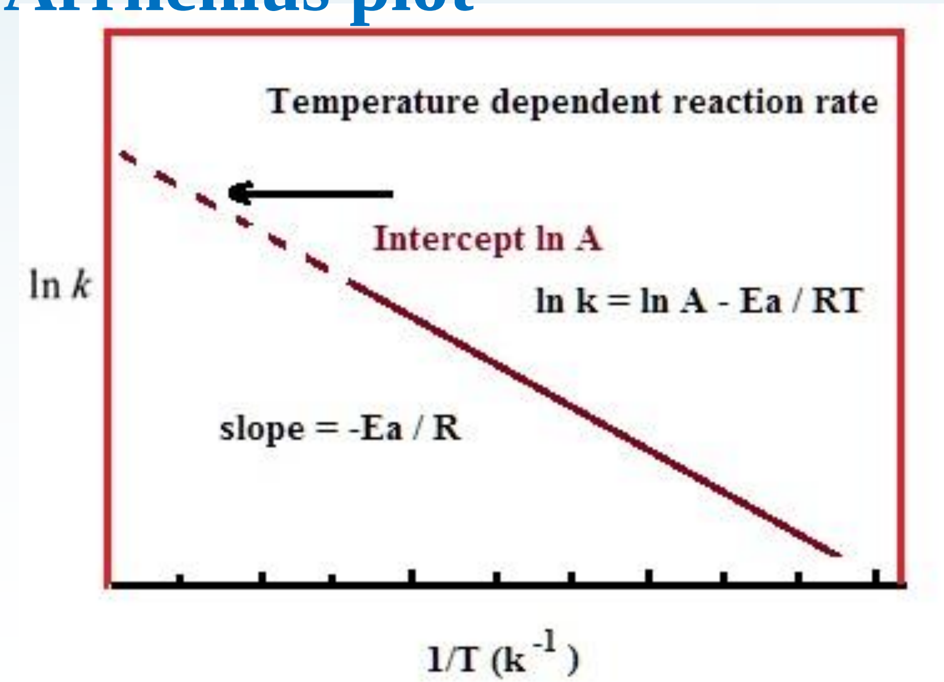

$$k = A e^{-\frac{E_a}{RT}}$$

activation energy

pre-exponential factor

average kinetic energy

$$\ln k = \ln A - \frac{E_a}{RT}$$

Older experiments and theory

Electron scattering cross-section on Ar

$$k = \int_{v} f_T(v).v.\sigma(v)dv = k(T)$$

Electrons – Boltzman distribution with T_e

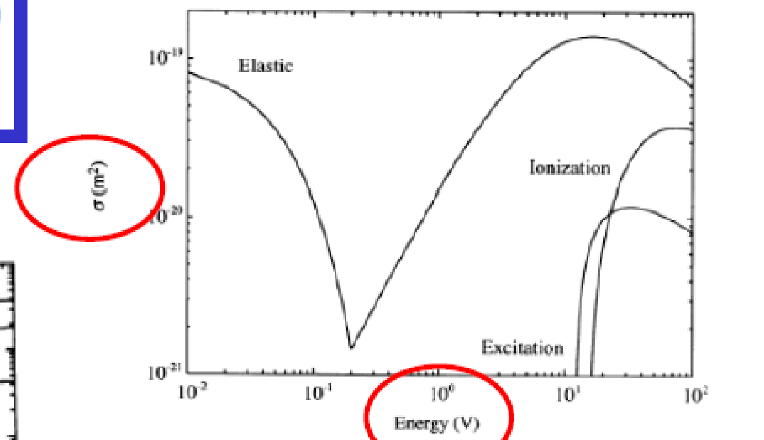

3. Ionization, excitation and elastic scattering cross sections for electrons in ...piled by Vahedi, 1993).

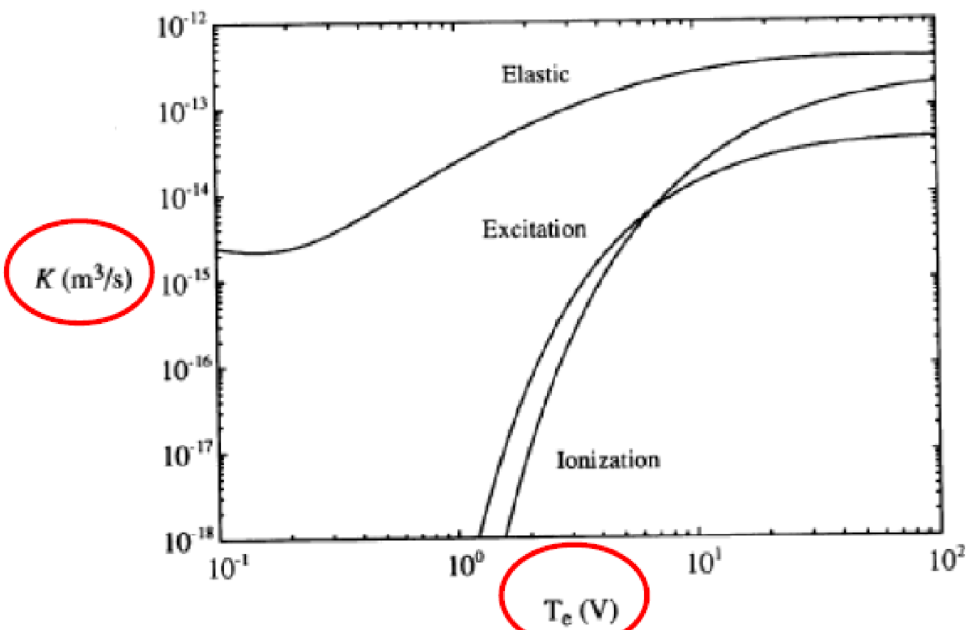

$$\alpha(T, T_e) \propto \int_0^{\infty} \sqrt{E}\,\sigma_w(E, T) f(E, T_e)\, dE$$

FIGURE 3.16. Electron collision rate constants K_{iz}, K_{ex} and K_m versus T_e in argon gas (compiled by Vahedi, 1993).

What if we have metastables?

Lieberman&Lichtenberg

Ion-Molecule reactions
Some experiments and data….

Collision cross section of IMR

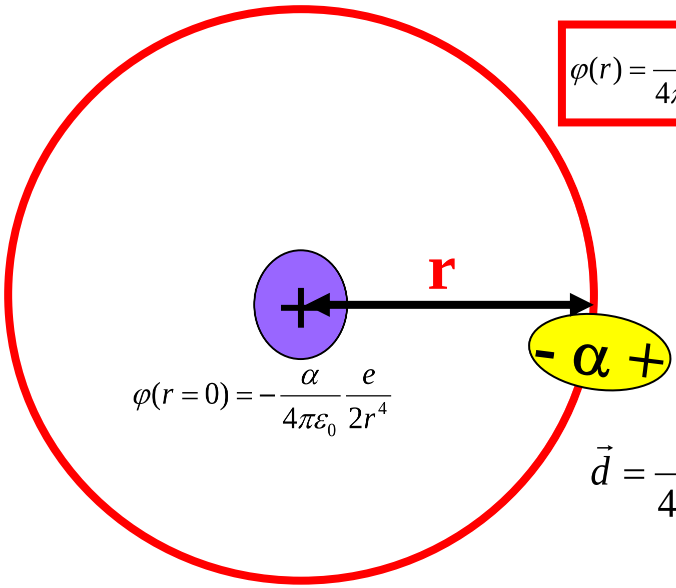

$$\varphi(r) = \frac{1}{4\pi\varepsilon_0}\frac{e}{r}$$

$$\varphi(r=0) = -\frac{\alpha}{4\pi\varepsilon_0}\frac{e}{2r^4}$$

$$\vec{d} = \frac{\alpha}{4\pi\varepsilon_0}\frac{e}{r^2}\frac{\vec{r}}{r}$$

α - polarizability

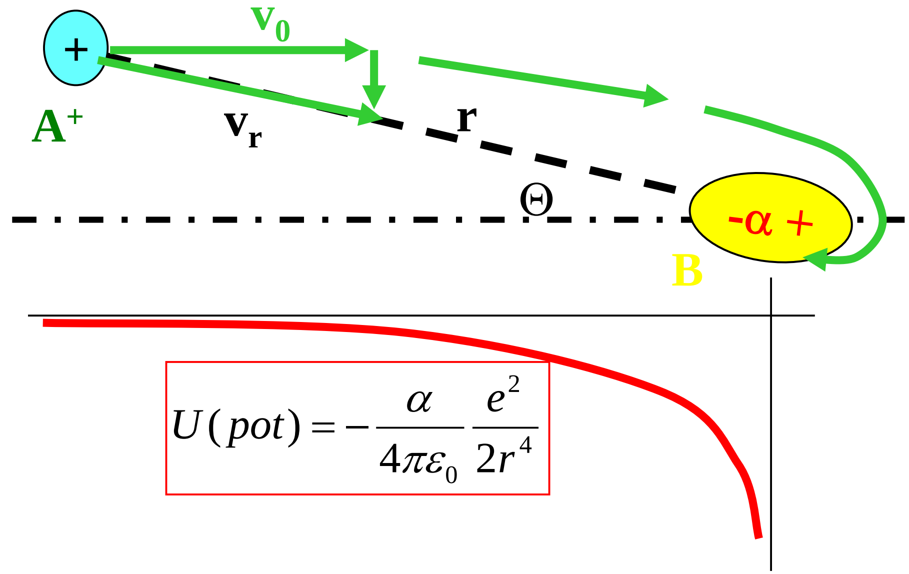

$$U(pot) = -\frac{\alpha}{4\pi\varepsilon_0}\frac{e^2}{2r^4}$$

$$\frac{\mu v_0^2}{2} = \frac{\alpha}{4\pi\varepsilon_0}\frac{e^2}{2r^4}$$

$$\sigma = \pi\rho_0^2 = \frac{2\pi e}{v_0(4\pi\varepsilon_0)}\sqrt{\frac{\alpha}{\mu}}$$

Langevin

$$\sigma = \pi\rho_0^2 \sim \frac{1}{v_0}\sqrt{\frac{\alpha}{\mu}} \sim \frac{1}{\sqrt{E}}$$

Langevin

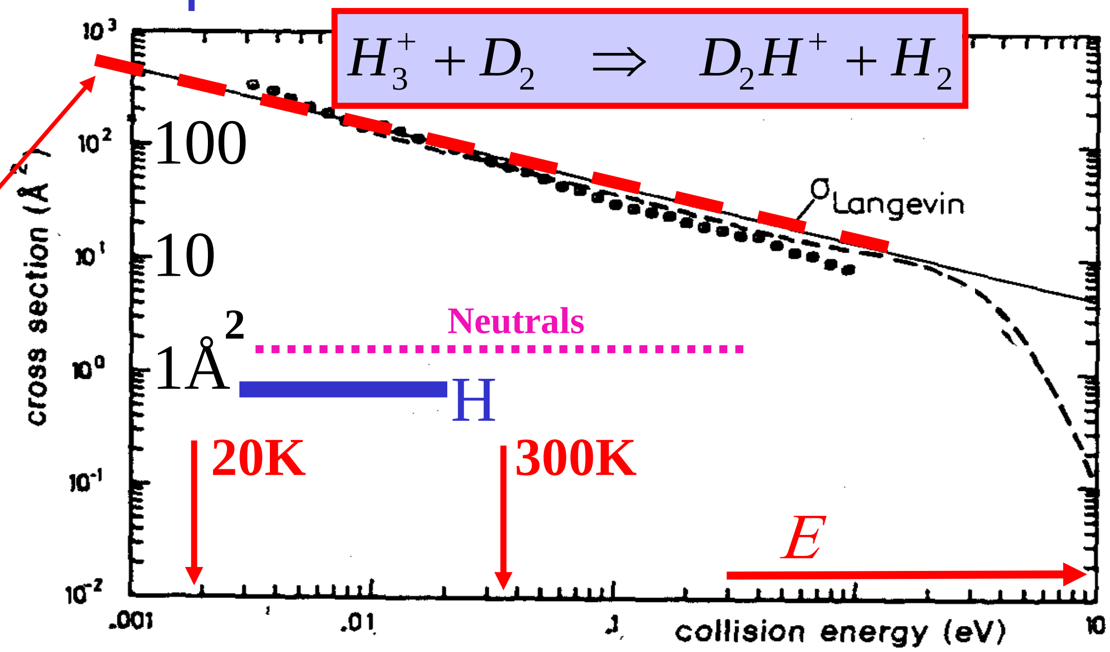

Actual experiments and theory

2020

$$H_2^+ + H_2 \rightarrow H_3^+ + H$$

ChemPhysChem

Articles
doi.org/10.1002/cphc.202000258

Very Important Paper

Formation of H_3^+ in Collisions of H_2^+ with H_2 Studied in a Guided Ion Beam Instrument

Igor Savić,*[a] Stephan Schlemmer,[b] and Dieter Gerlich[c]

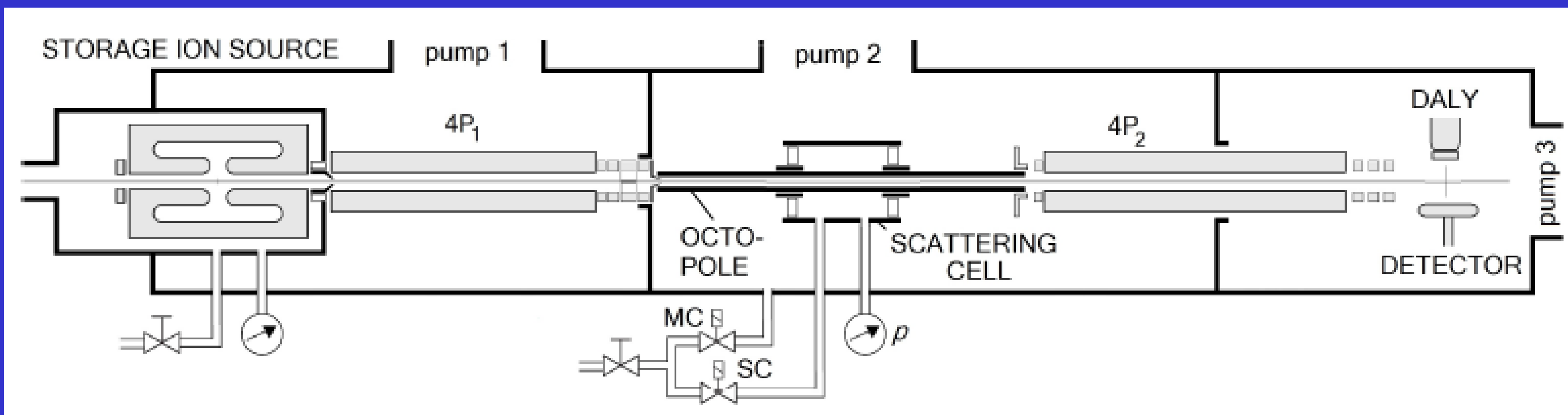

Figure 1. The Guided Ion Beam instrument *NOVion* consists of a storage ion source (SIS), a first quadrupole ($4P_1$), an octopole, guiding the ions through a scattering cell, a second quadrupole ($4P_2$), and a Daly type ion detector. Three separated vacuum chambers are pumped by turbopumps with pumping speeds of 180 l/s for hydrogen. For determining integral cross sections of ions reacting with neutrals, the target gas is leaked alternately into the scattering cell (SC) or into the main chamber (MC) containing the octopole. The net pressure p is the difference between the two values measured under these two conditions, p^{MC} and p^{SC}.

2020

$$H_2^+ + H_2 \rightarrow H_3^+ + H$$

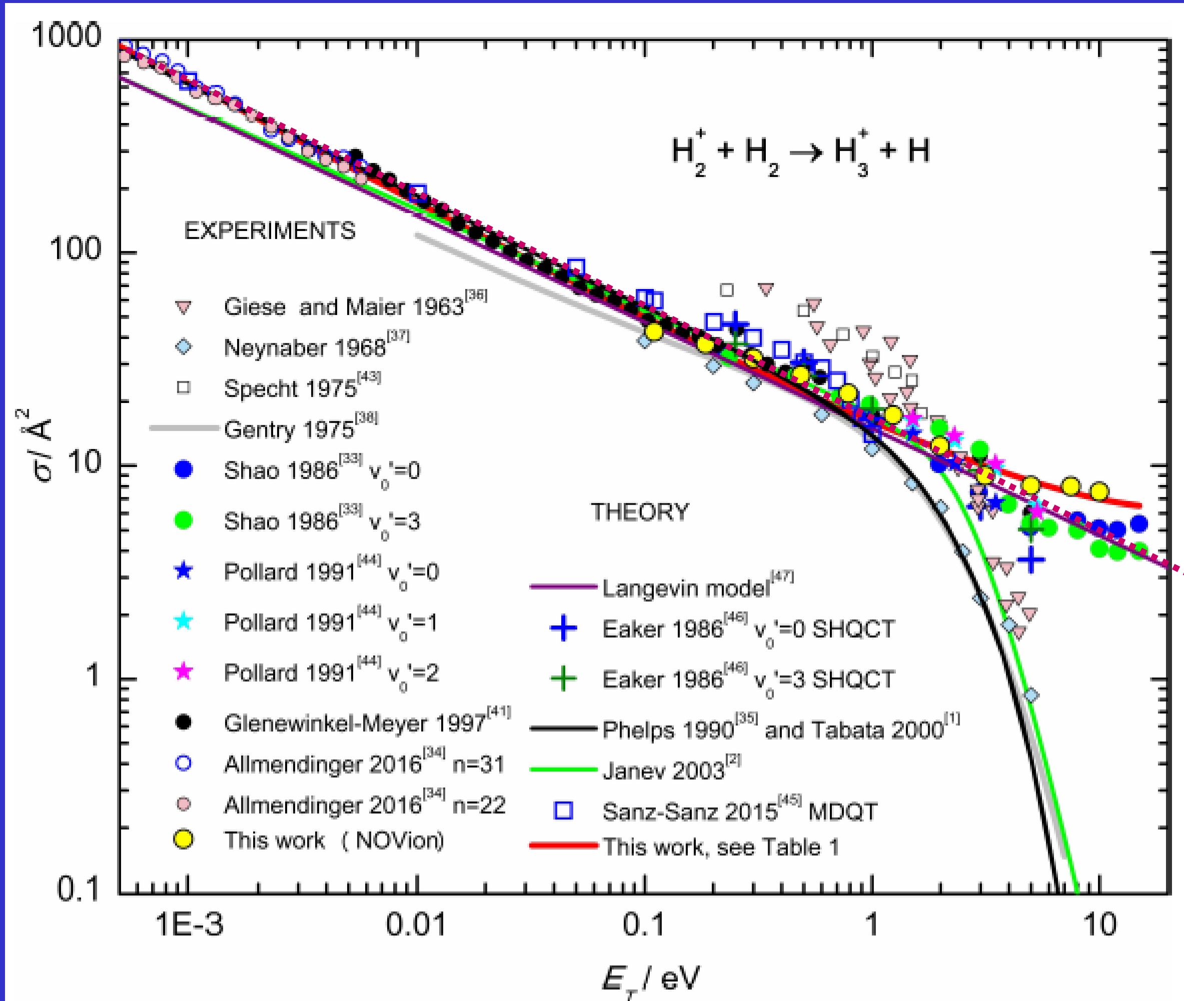

$\sigma_L(E_T)$

$$\sigma = \pi \rho_0^2 \sim \frac{1}{v_0}\sqrt{\frac{\alpha}{\mu}} \sim \frac{1}{\sqrt{E}}$$

Langevin

Figure 2. Dependence of the integral cross section for the reaction $H_2^+ + H_2 \rightarrow H_3^+ + H$ on the collision energy E_T. In the meV and sub-meV energy range, there is good agreement between two different merged beam results, Refs. [34,41]. Note that Allmendinger et al.[34] scaled their relative cross sections to the absolute ones calculated by Sanz-Sanz et al.[45] as described in the caption of figure 10 of Ref. [34]. Between thermal energies and 1 eV, most of the published and tabulated values agree more or less with the function proposed in the compilations by Tabata[1] (black line) and Janev et al.[2] (green line). However, based on results from the sixties and seventies, a steep decline has been predicted above 2 eV. In contrary, our results (yellow filled circles) do not show this trend, in accordance with the guided ion beam results from Shao et al.[33] The data presented in Ref. [35] as tabulated values and in Ref. [1] as an analytical function are nearly identical and are represented here simply by the one black line.

IMR thermal

$$\sigma = \pi\rho_0^2 = \frac{2\pi e}{v_0(4\pi\varepsilon_0)}\sqrt{\frac{\alpha}{\mu}}$$

$$k = \int_v f_T(v).v.\sigma(v)dv = k(T)$$

$$k_{col} = <v\rho> \sim <v 1/v> = \text{const.}$$

$k_{coll} \sim 10^{-9} cm^3 s^{-1}$

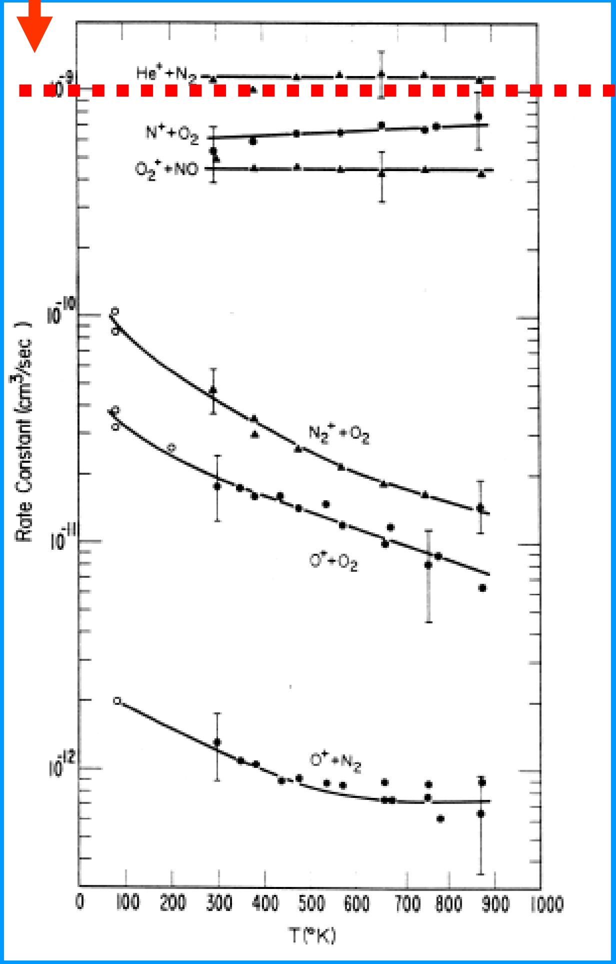

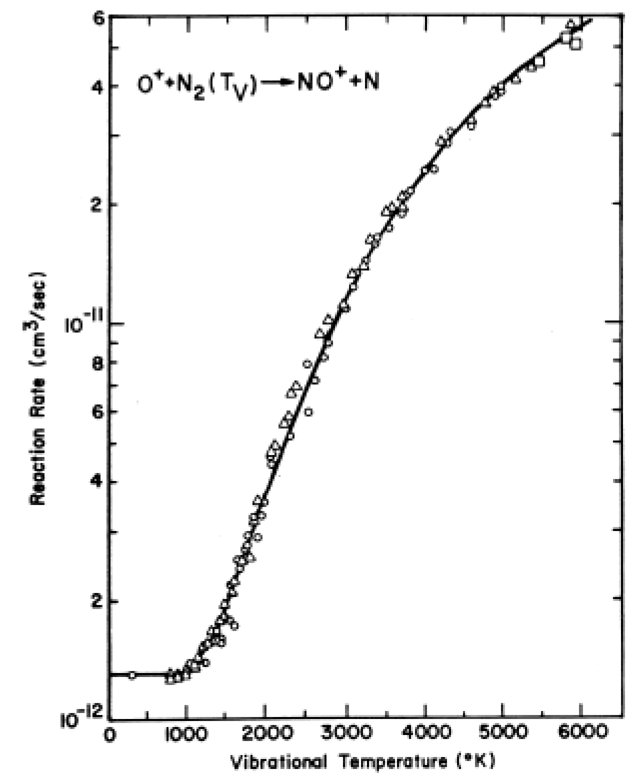

Fig. 12. Measurements of the variation of the rate coefficient for the reaction of $O^+ + N_2 \rightarrow NO^+ + N$ with the vibrational temperature of N_2 [16].

Ionic composition of the atmosphere

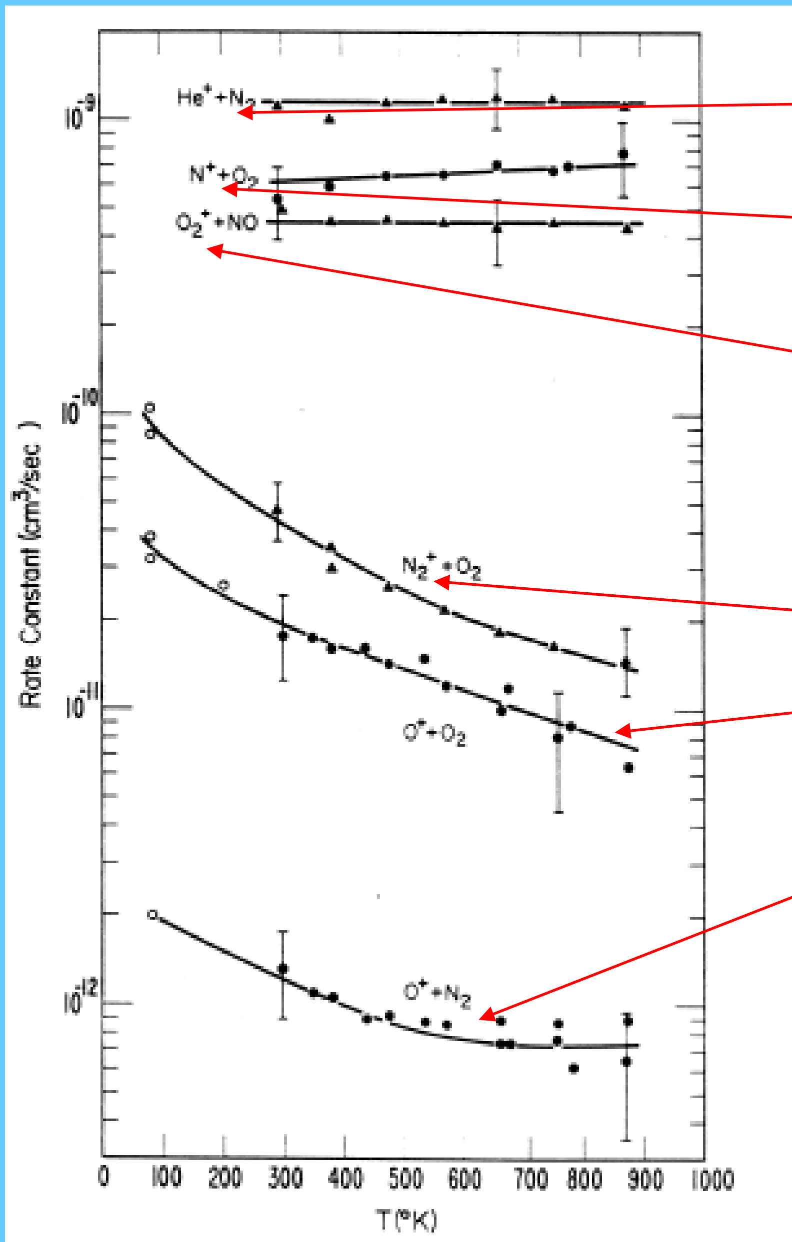

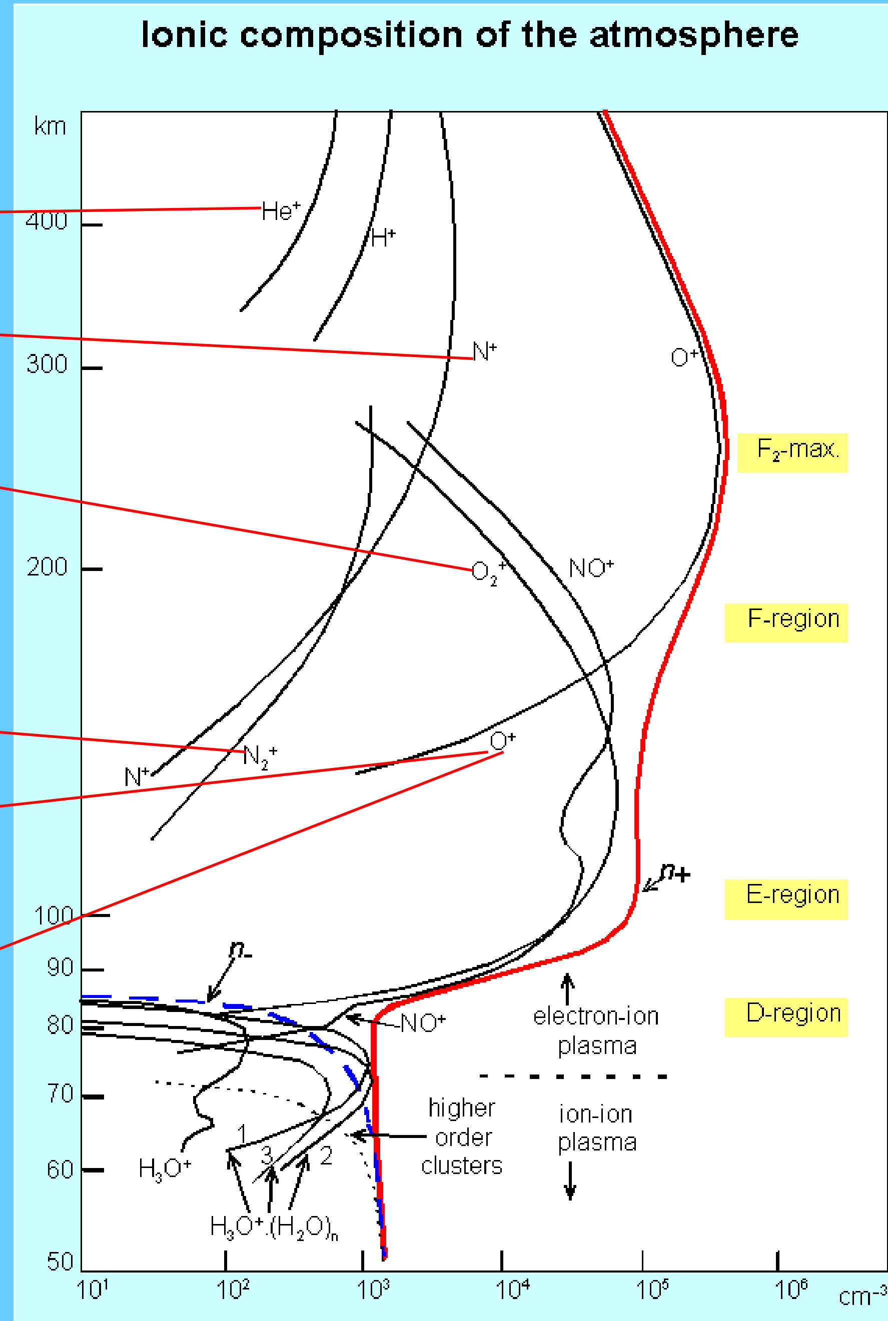

Reaction Rate of IMR relevant for ionosphere

k_{IMR}

$k_{coll} \sim 10^{-9} cm^3 s^{-1}$

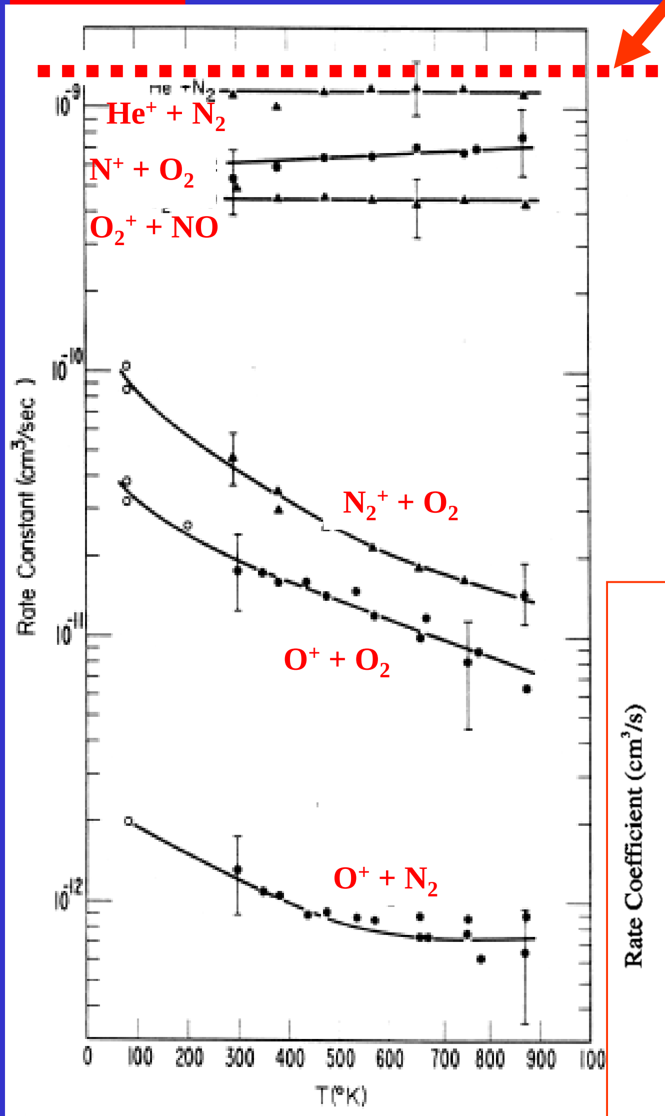

1975-90

1990-00

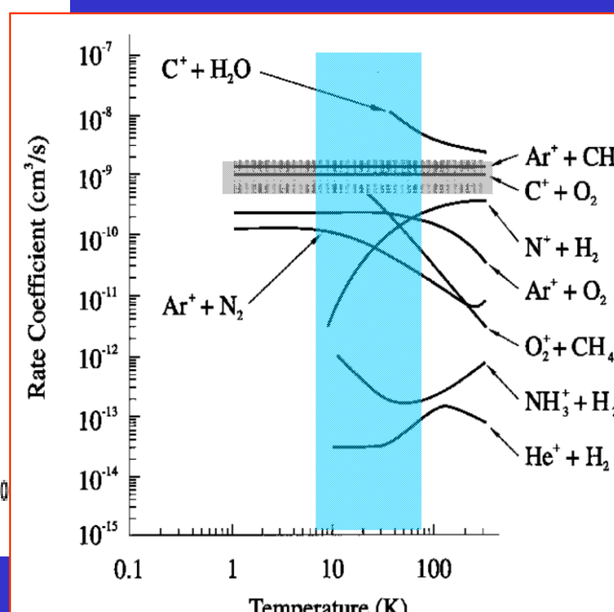

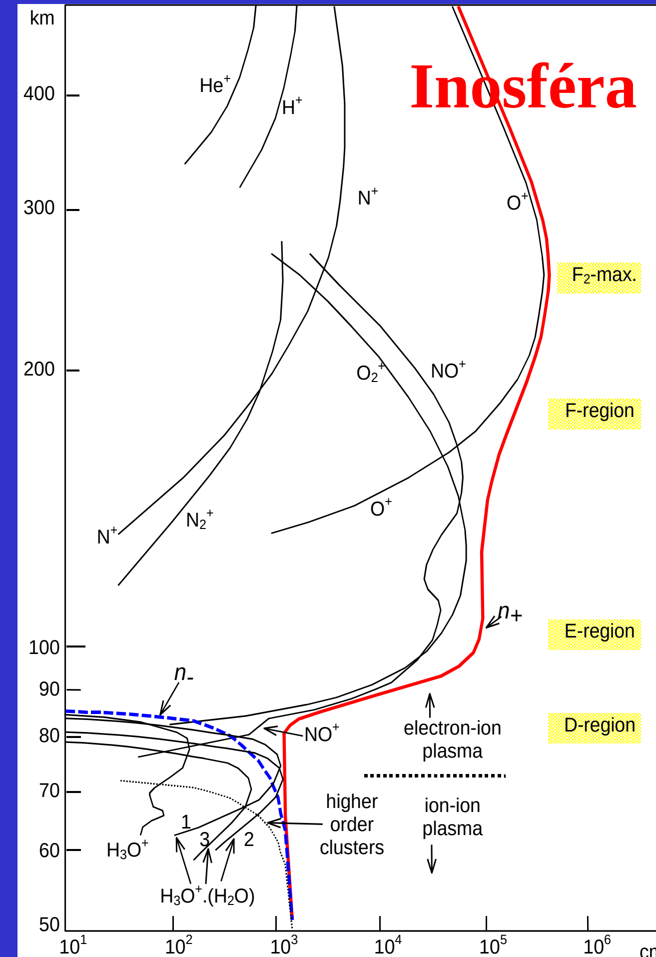

Low energy collisions with molecules

De Broglie wave length

$$\lambda = \frac{h}{p} = \frac{h}{mv}\sqrt{1 - \frac{v^2}{c^2}}$$

$$\lambda_e(4K) \sim 540\,A \sim 54x10^{-9}\,m$$

$$\lambda_e(1eV) \sim 11.6\,A \sim 1.16x10^{-9}\,m$$

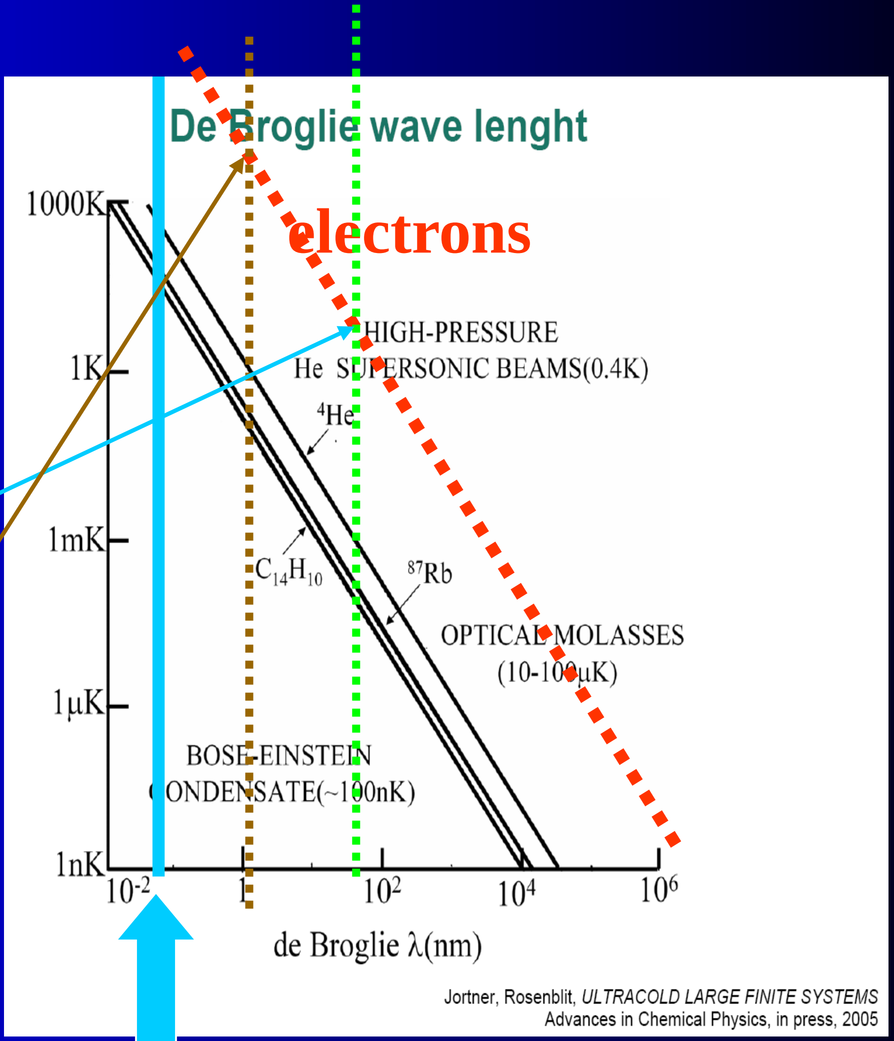

a_0

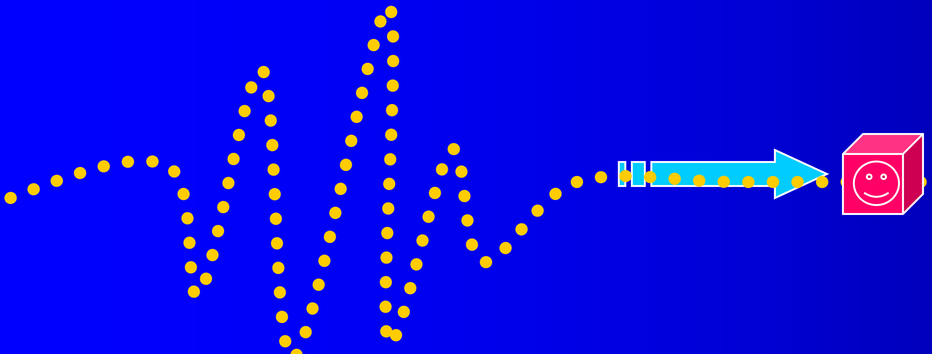

Collisions of electrons with atoms

Classical or quantum approach?

Electron:

1eV → $v = 5.9 \times 10^{7}$ cm s^{-1}

$\tau \sim a_0/v \sim 10^{-8}/\ 5.9 \times 10^{7} = 2 \times 10^{-16}$ s

$\lambda \sim 2A = 2 \times 10^{-8}$ cm de Broglie

Ar+:

1eV → $v = 2 \times 10^{5}$ cm s^{-1}

$\tau \sim a_0/v \sim 10^{-8}/\ 2 \times 10^{5} \sim 6 \times 10^{-14}$ s

$\lambda \sim 9 \times 10^{-11}$ cm de Broglie

$H_3^* + e$ at 10 K ????

$$\lambda_e(4K) \sim 540\,A \sim 54x10^{-9}\,m$$

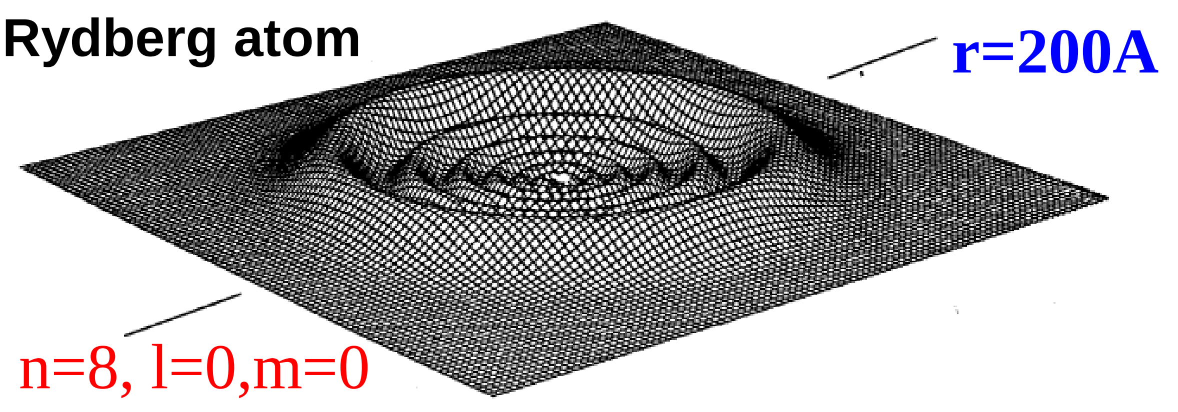

Collisions of electrons with atoms (atomic beams)

Collisions with e

CROASED BEAM METHOD

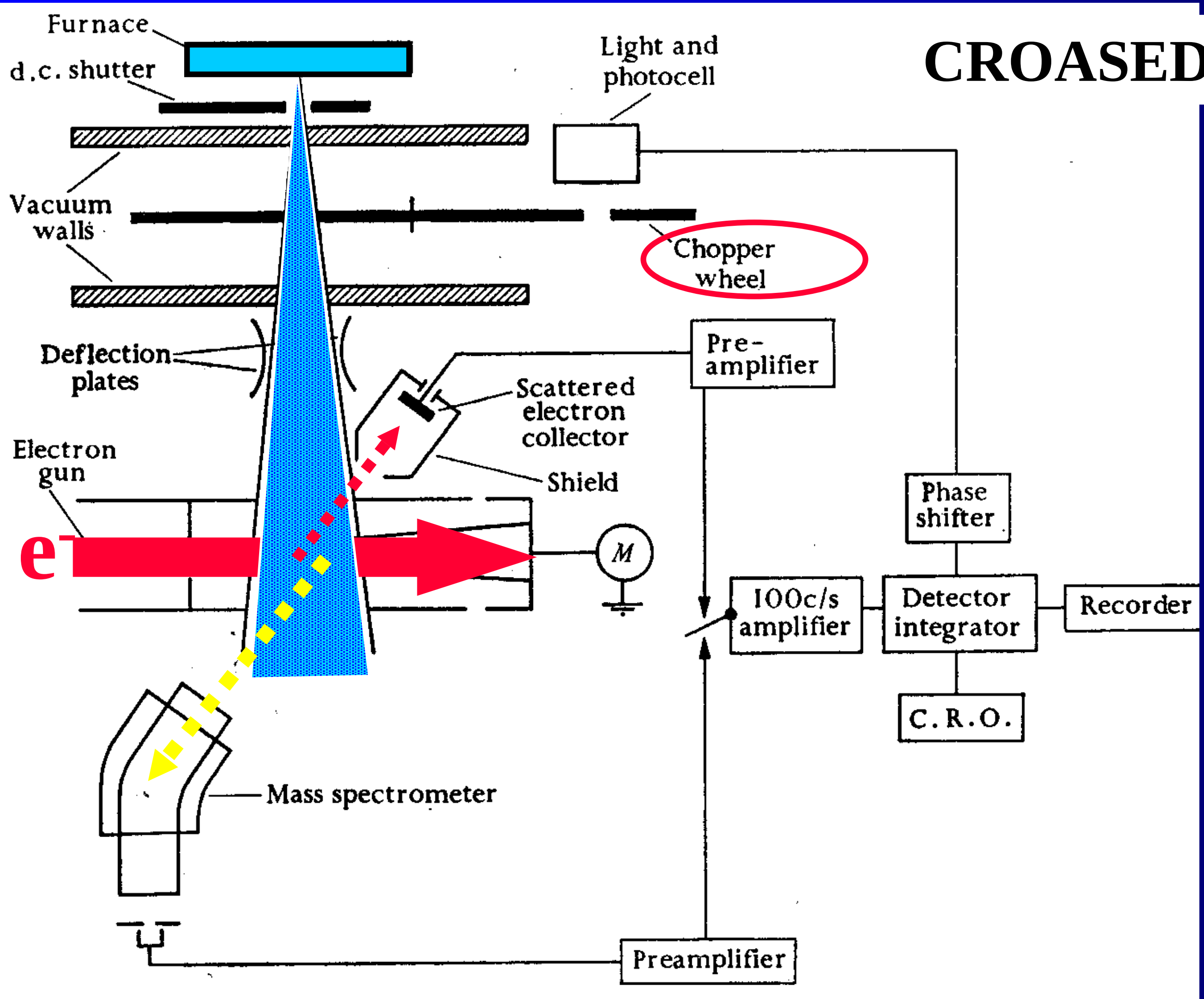

Fig. 1.2. Schematic diagram of the arrangement of apparatus used by Fite, Brackmann, and Neynaber for observation of elastic scattering of electrons by atomic hydrogen.

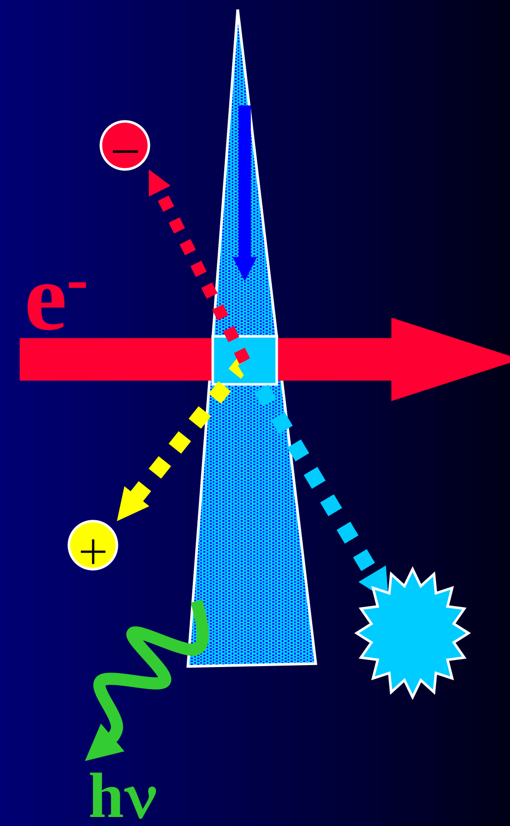

Position (angle), mass and energy sensitive detectors

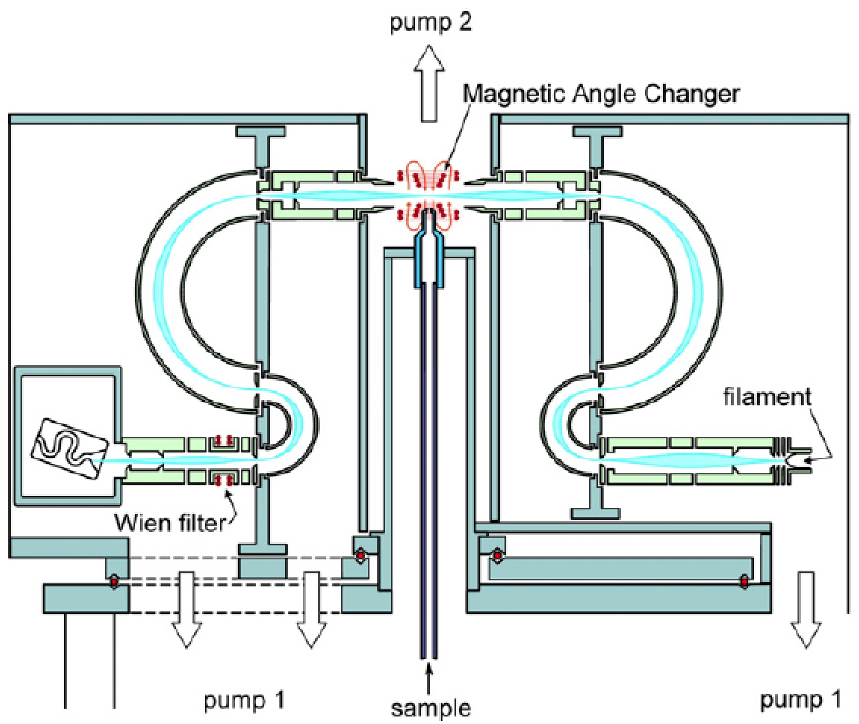

Fig. 3. The electron spectrometer of Allan (6).

Two Experimental Advances. The basic workhorse used in a large number of electron-scattering studies is the electron spectrometer. Free electrons are formed into a beam and energy selected by various combinations of electrostatic and magnetic fields. The use of electrostatic fields is most common, because they are more easily controlled and shielded than their magnetic counterparts. This is particularly important when it is essential to preserve the direction of low-energy electrons following the collision process.

Fig. 3 exhibits an example of such a spectrometer (6), which combines the characteristics of a conventional electrostatic device with an important innovation. It can be used for elastic scattering and electron impact excitation studies. The electron gun consists of a source of electrons produced by thermionic emission from a heated filament. The electrons are collimated and focused by an electrostatic lens system onto the input aperture of a double hemispherical energy selector. Those electrons within a narrow band of energies satisfying the criteria for transmission through the selector are then focused on the gas beam produced by a nozzle arrangement. Scattered electrons from the interaction region traveling in the direction of the scattered electron analyzer are similarly focused onto the input aperture of its double hemispherical analyzer, and the transmitted electrons are finally being focused into a single-channel electron multiplier detector.

One drawback of conventional electron spectrometers is that the angular range of the electron analyzer is limited by the physical presence of other components of the spectrometer. This limitation was overcome by Read and Channing (4) who applied a localized static magnetic field to the interaction region of a conventional spectrometer. The incident electron beam and the scattered electrons are, respectively, steered to and from the interaction region through angles set by the field (hence, the common name "magnetic angle changer" or "MAC"). This steering means that electrons normally scattered into inaccessible scattering angles are rotated into the accessible angular range of the electron analyzer while the magnetic field design is such that it leaves the angular distribution of the electrons undistorted. The spectrometer shown in Fig. 3 has a MAC fitted, thereby enabling the full angular range 0–180° to be accessed.

Partial cross section for excitation

Collisions with e

NO + e

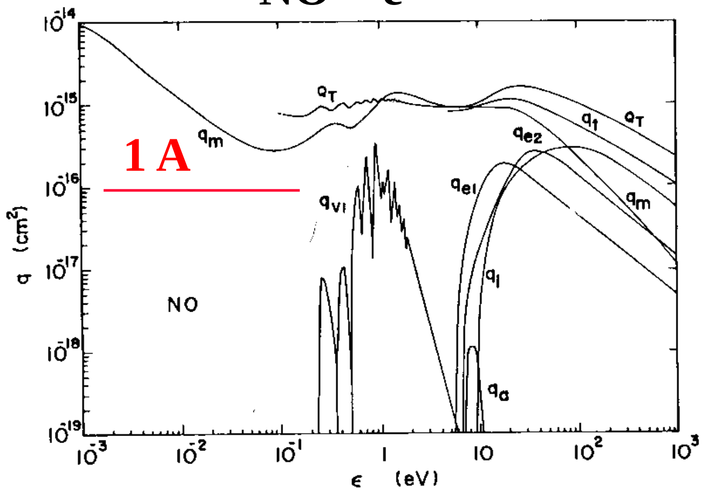

Fig. 4. Cross-section set for NO (1986).

NH_3 + e

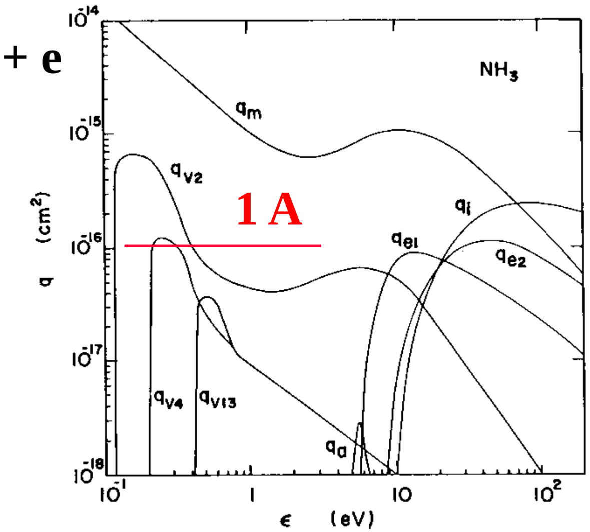

Fig. 6. Electron collision cross-section set for NH_3 (1986).

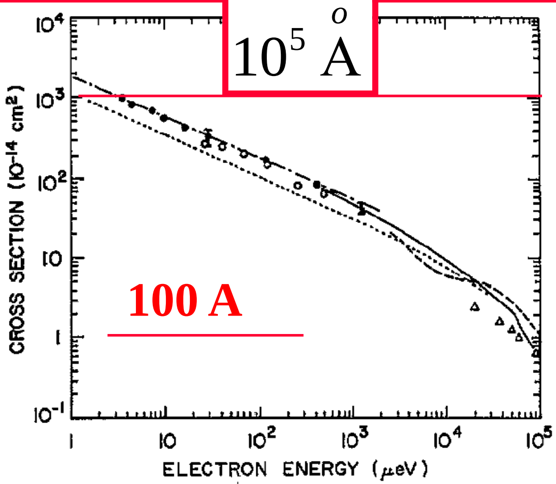

Figure 3. Cross sections for electron attachment to CCl_4. ●, $\bar{\sigma}_e$-K(np); — · —, $\sigma_e(v)$-K(np) (Frey *et al* 1994b); ○, $\bar{\sigma}_e$-K(np) (Ling *et al* 1992); ——, free electrons (Hotop 1994); - - -, free electrons (Orient *et al* 1989); △, free electrons (Christodoulides and Christophorou (1971); -----, theory (Klots 1976).

$$e^- + SF_6 \rightarrow SF_6^{-*}$$

$$e^- + CCl_4 \rightarrow CCl_4^{-*} \rightarrow CCl_3 + Cl^-$$

Total collision cross sections Na, K, Cs…

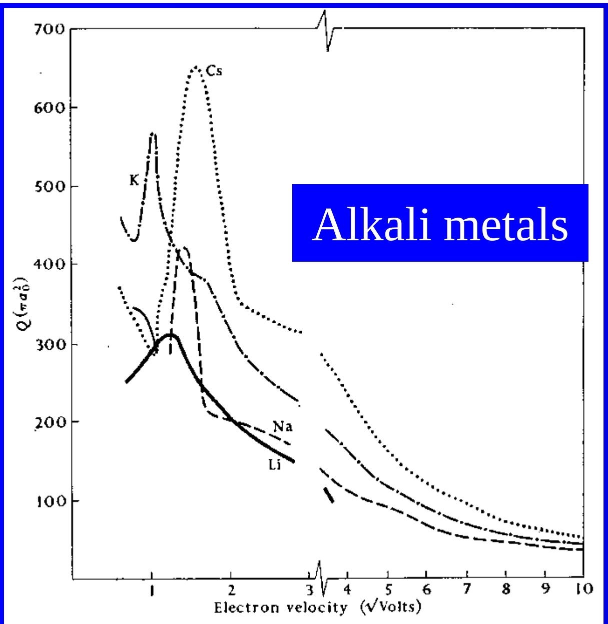

FIG. 1.16. Observed total collision cross-sections of Li, Na, K, and Cs.

Collisions with e

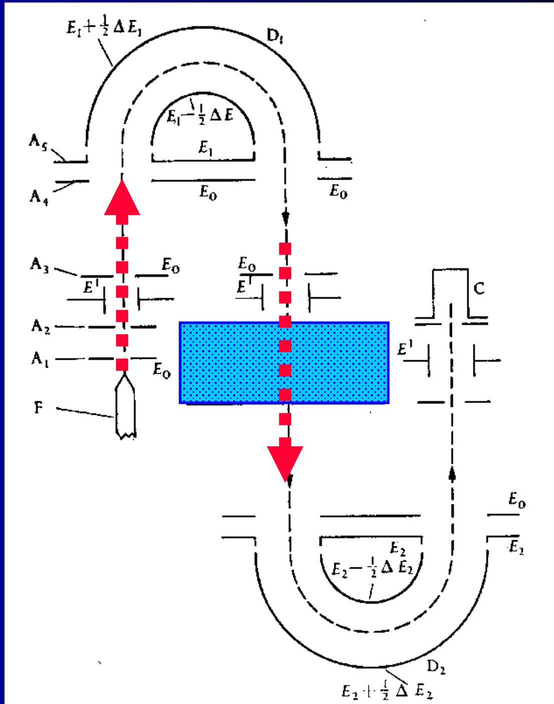

FIG. 1.6. Schematic diagram of the arrangement of apparatus developed by Simpson for observing fine structure in the variation with energy of the transmission of electrons through gases.

Cs

e^- (v)

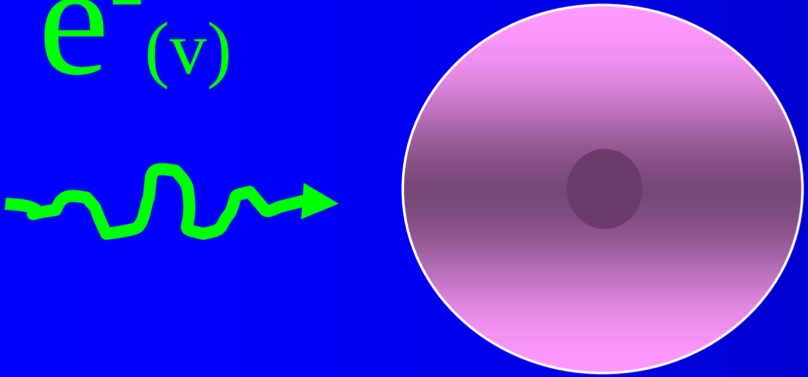

Total collision and reactive cross sections comparison

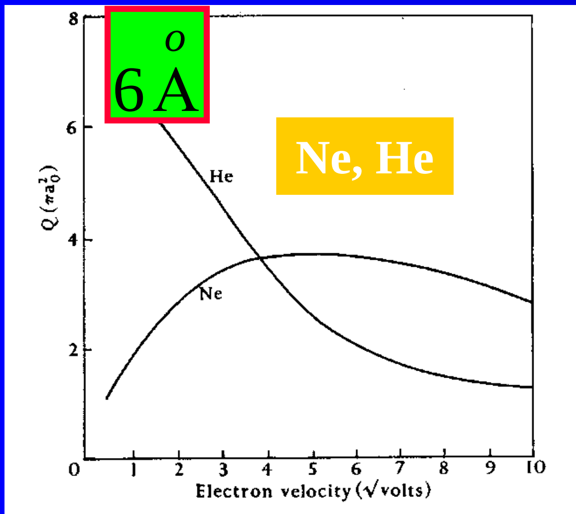

FIG. 1.10. Observed total collision cross-sections of He and Ne.

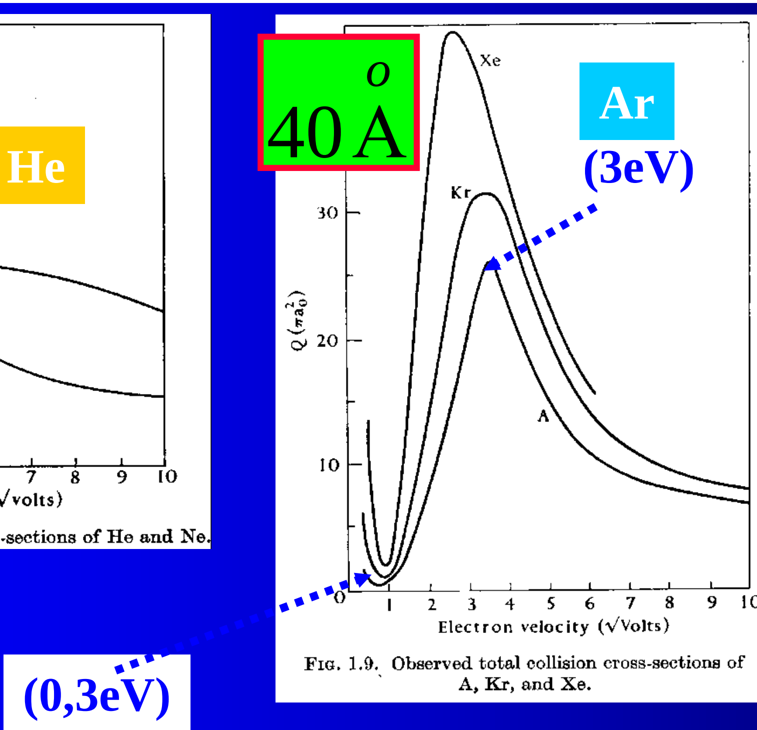

FIG. 1.9. Observed total collision cross-sections of A, Kr, and Xe.

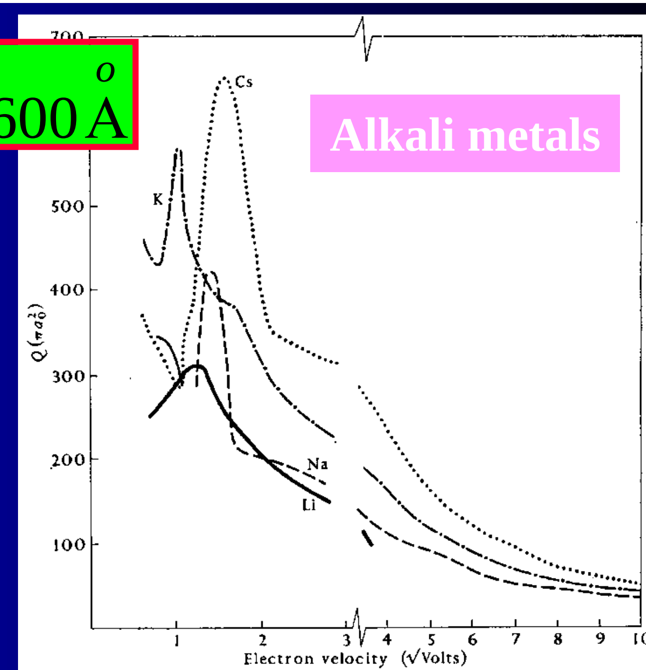

FIG. 1.16. Observed total collision cross-sections of Li, Na, K, and Cs.

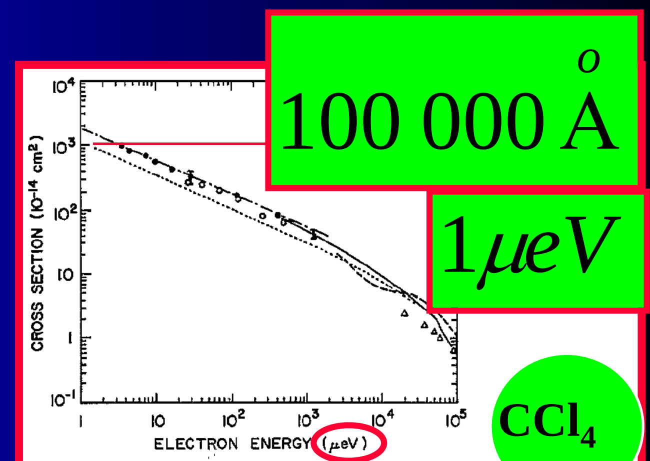

Figure 3. Cross sections for electron attachment to CCl_4. ●, $\bar{\sigma}_e$-K(np) (Frey et al 1994b); ○, $\bar{\sigma}_e$-K(np) (Ling et al 1992); ——, free electrons (Hotop 1994); – – –, free electrons (Orient et al 1989); △, free electrons (Christodoulides and Christophorou (1971); -----, theory (Klots 1976).

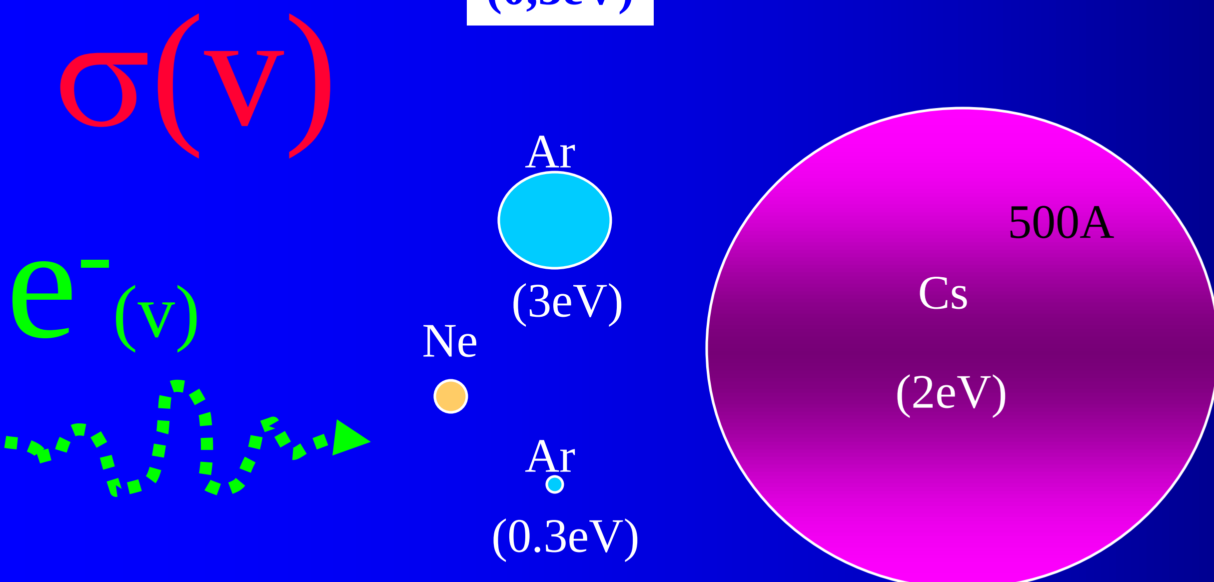

Collisions of electrons with atoms – Ramsauer's method

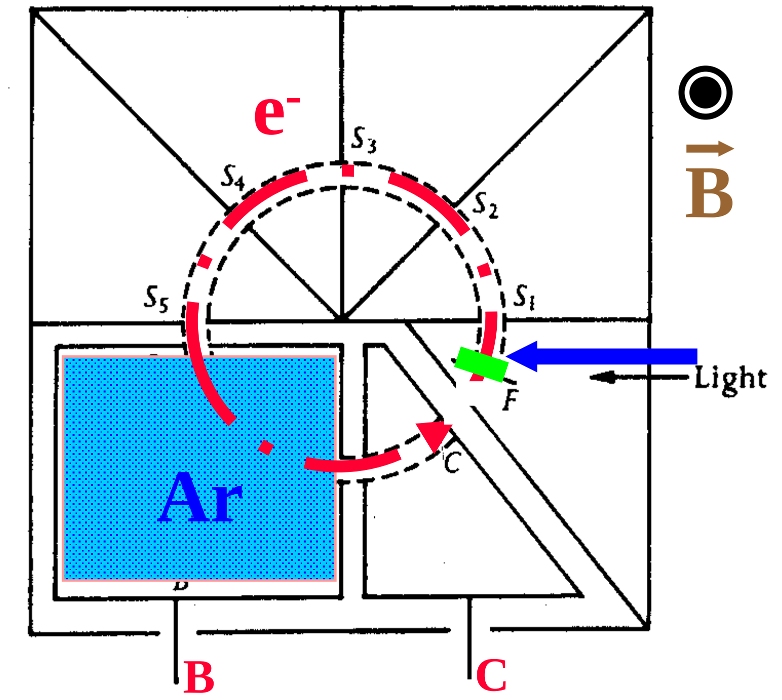

Fig. 1.1. Ramsauer's apparatus for measurement of collision cross-sections.

Lenard 1903
Akesson 1916
Ramsauer 1921

ATENUATION METHOD

$$\delta I = -N\sigma I_p\, \delta x$$

$$I_P = I_0 \exp(-\sigma N x)$$

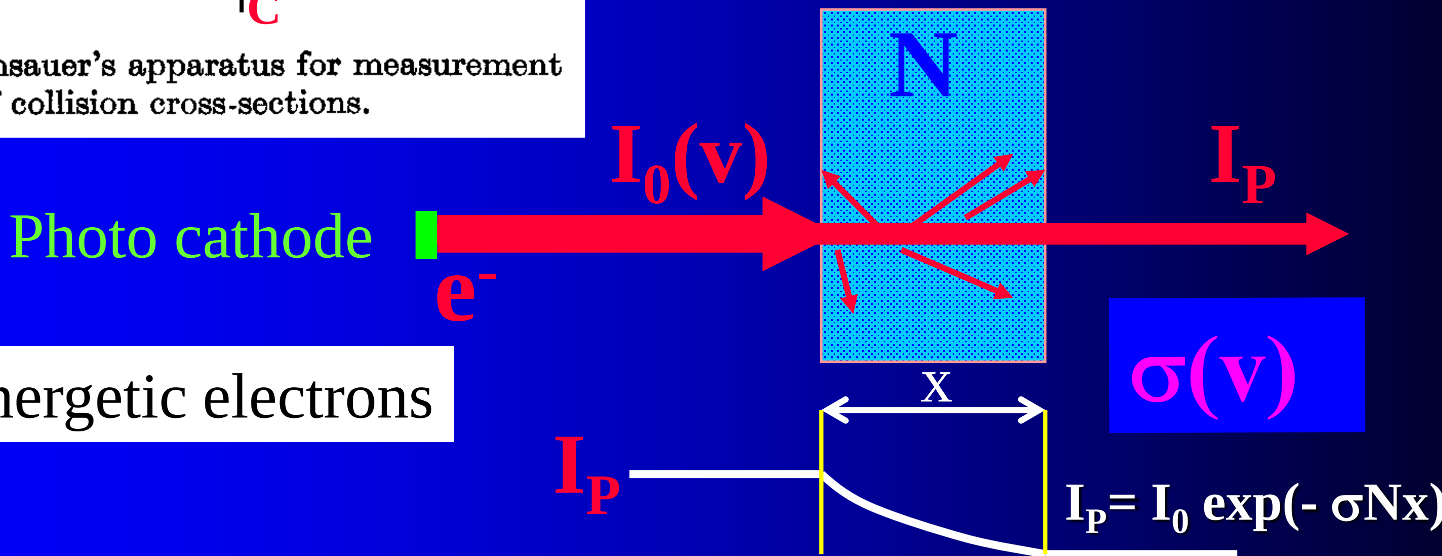

Mono energetic electrons

Collisions of electrons with atoms – Ramsauer's method

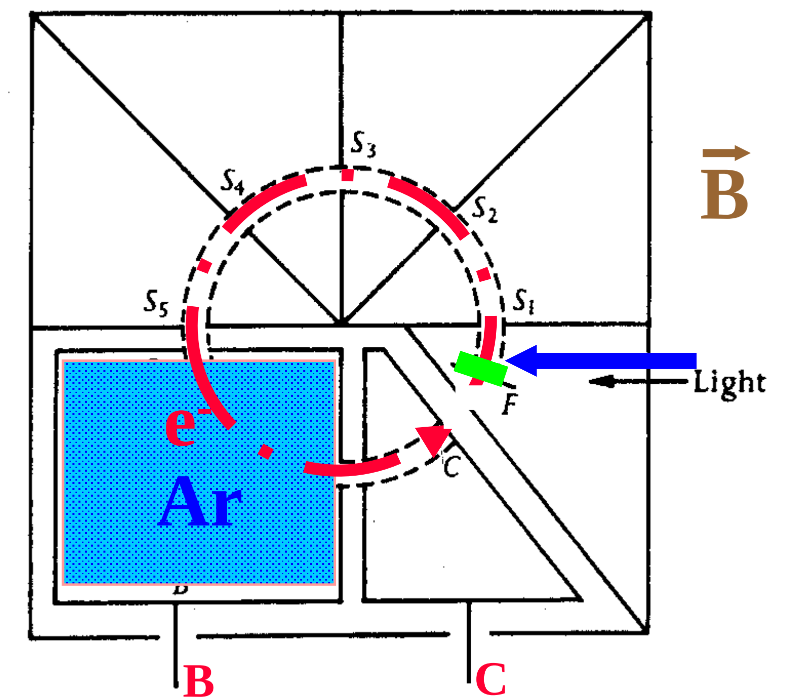

FIG. 1.1. Ramsauer's apparatus for measurement of collision cross-sections.

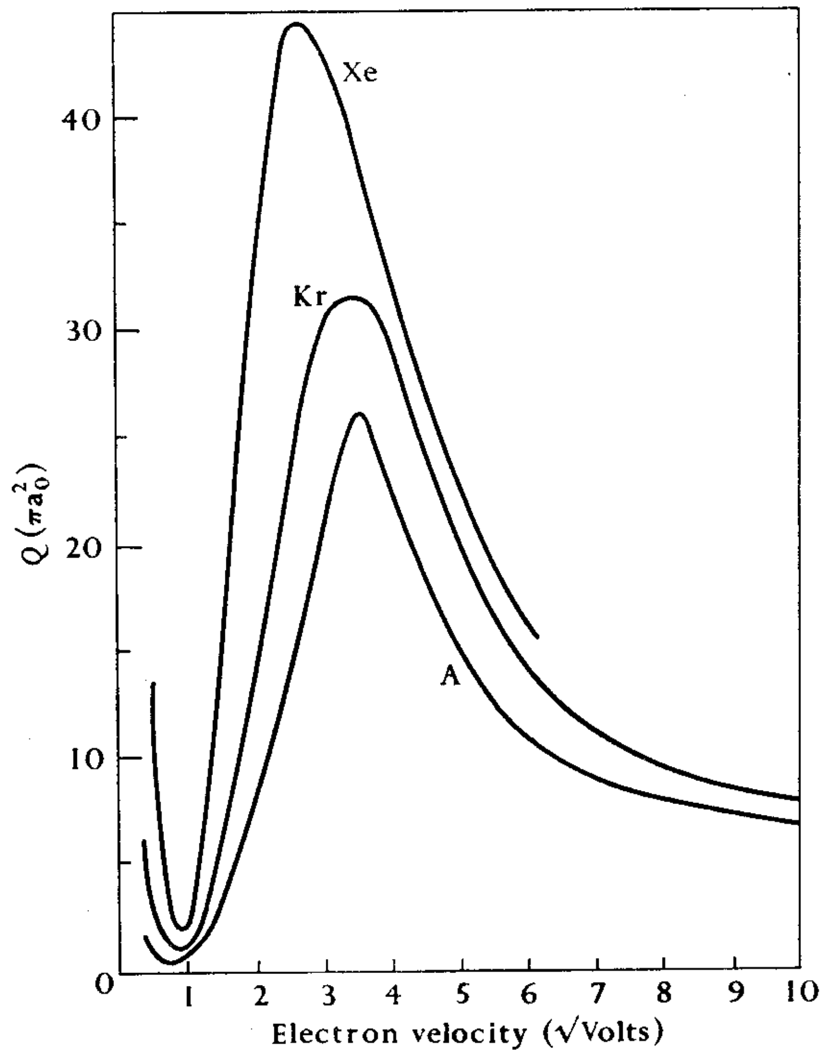

FIG. 1.9. Observed total collision cross-sections of A, Kr, and Xe.

Lenard 1903
Akesson 1916
Ramsauer 1921

Total collision cross section – e/atoms

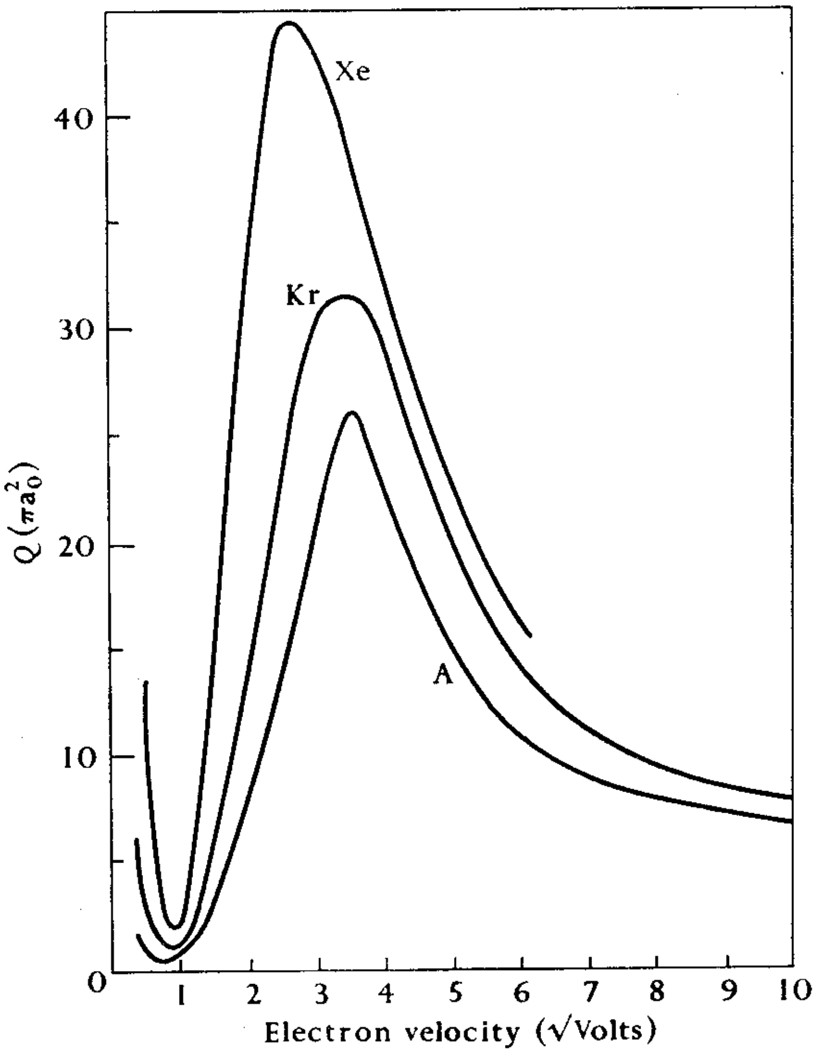

FIG. 1.9. Observed total collision cross-sections of A, Kr, and Xe.

a_0=0.53x10^{-8}cm~0.5A
Radius of the first Bohr orbit of H atom

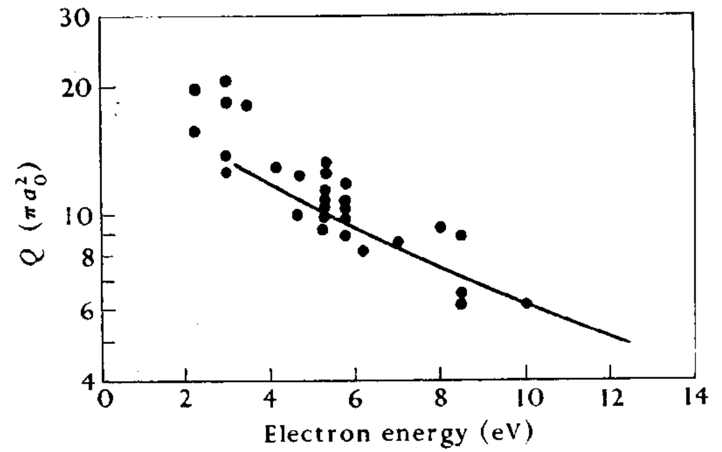

FIG. 1.11. Total collision cross-sections of atomic hydrogen. ● observed by Brackmann, Fite, and Neynaber; —— observed by Neynaber, Marino, Rothe, and Trujillo.

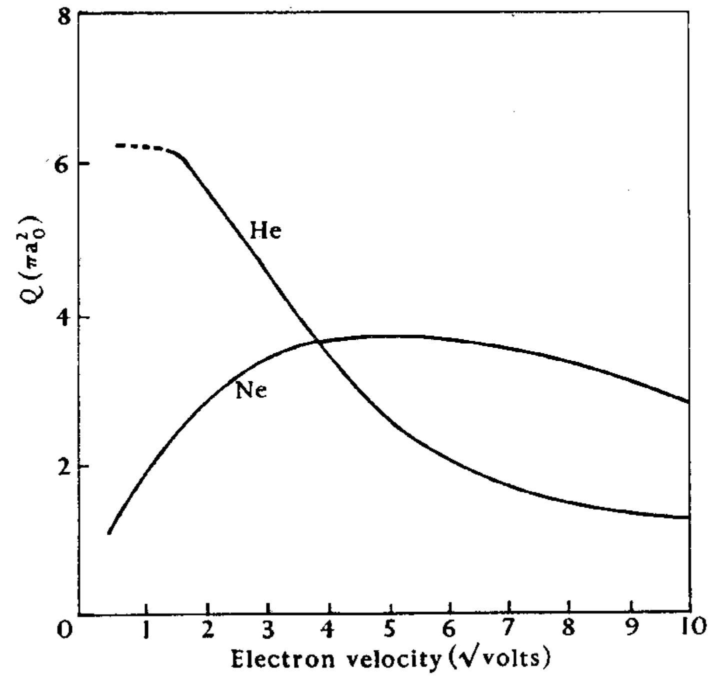

FIG. 1.10. Observed total collision cross-sections of He and Ne.

Details of Ramsauer effect

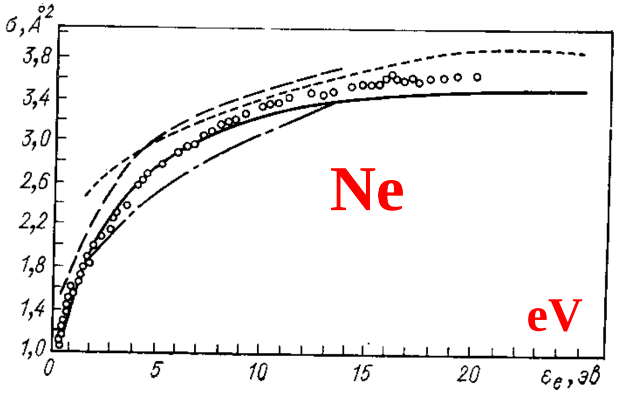

Рис. 5.8. Полное сечение рассеяния электрона на атоме неона.

Эксперимент (метод Рамзауэра): ○ — [101]; ——— — [29]; ·········· — [92]; — · — — [95]. Теория: — — — [109].

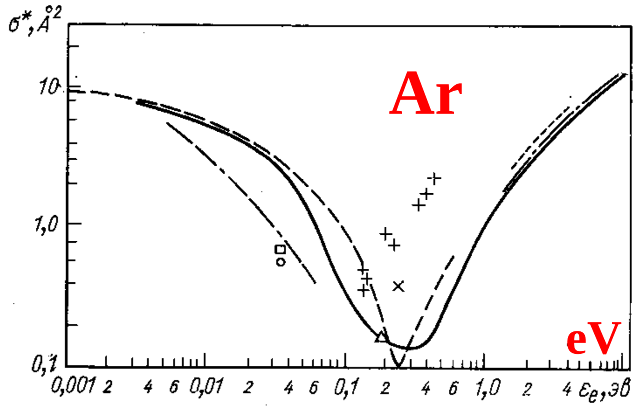

Рис. 5.9. Диффузионное сечение столкновения электрона с атомом аргона.

Эксперимент (подвижность электронов при малых полях и температурах): ·········· — [21]; ——— — [47]; × — [60]; ○ — [91]; □ — [112]; △ — [44]; — · — — [16]; — — · — — [108]; + — [43]. Теория: — — — [87].

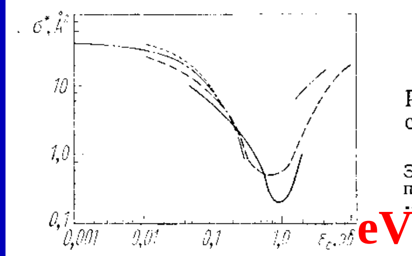

Рис. 5.12. Диффузионное сечение столкновения электрона с атомом криптона.

Эксперимент (подвижность электронов при малых полях и температурах): ·········· — [34]; — · · — — [21]; — — — [47]; ——— — [63]. Теория: — · — — [87].

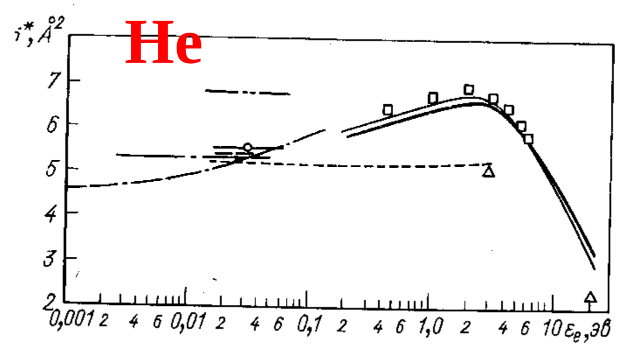

eV

Рис. 5.3. Диффузионное сечение столкновения электрона с атомом гелия.

Эксперимент (подвижность электронов при малых полях и температурах): □ — [39]; △ — [73]; — · — — [88]; — — — — [91]; ·········· — [58]; — ····· — — [13]; —○— — [62]. Теория: ——— — [75]; ——— — [32]; — — · — — — расчет по формуле (5.37).

Frequencies of elastic collisions

$$\delta I = -NQI_p\,\delta x$$
$$I_P = I_0 \exp(-QNx)$$

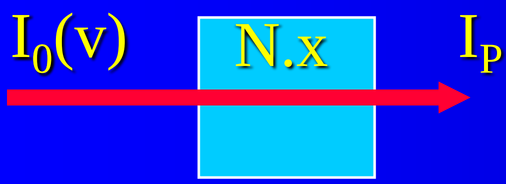

Q(v)

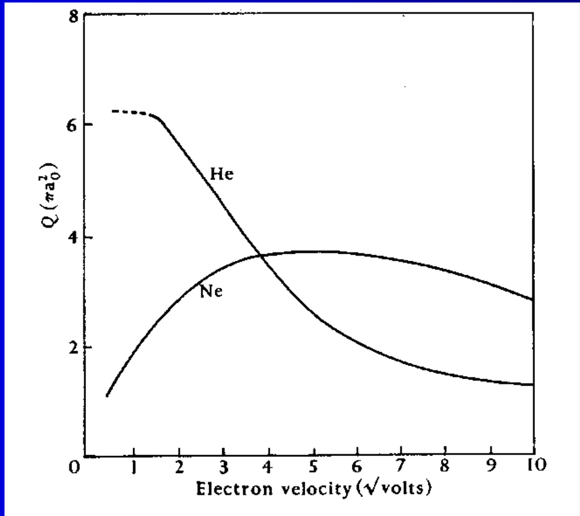

Fig. 1.10. Observed total collision cross-sections of He and Ne.

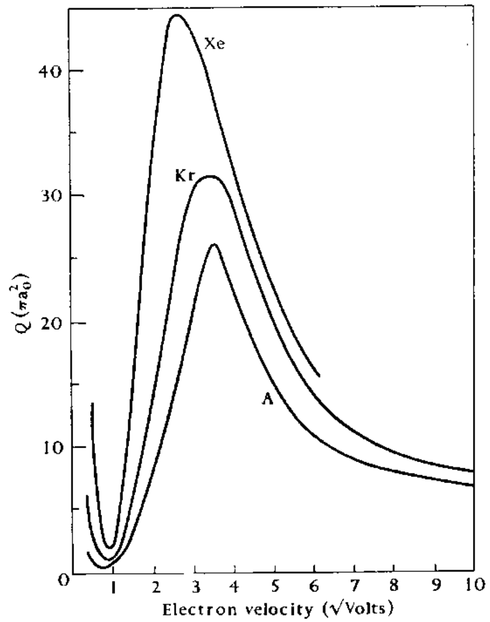

Fig. 1.9. Observed total collision cross-sections of A, Kr, and Xe.

$a_0 = 0.53 \times 10^{-8}$cm~0.5A
Radius of the first Bohr orbit of H atom

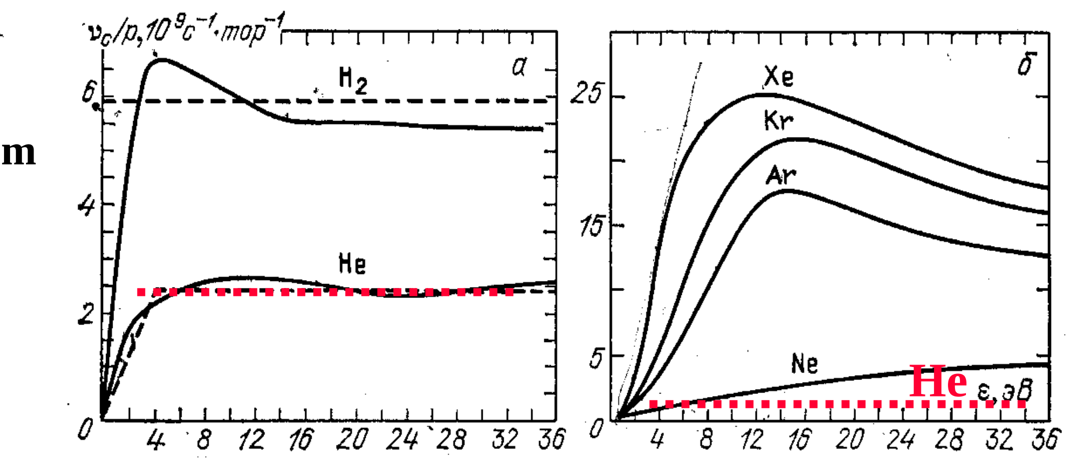

Р и с. 2.5. Частоты упругих столкновений электронов, $p=1$ тор: *а* — в H_2 и He; *б* — в инертных газах; штриховые линии — удобная аппроксимация при расчетах [24]

$$\nu \sim n v \sigma$$

Collision Frequencies

Total collision and reactive cross sections comparison

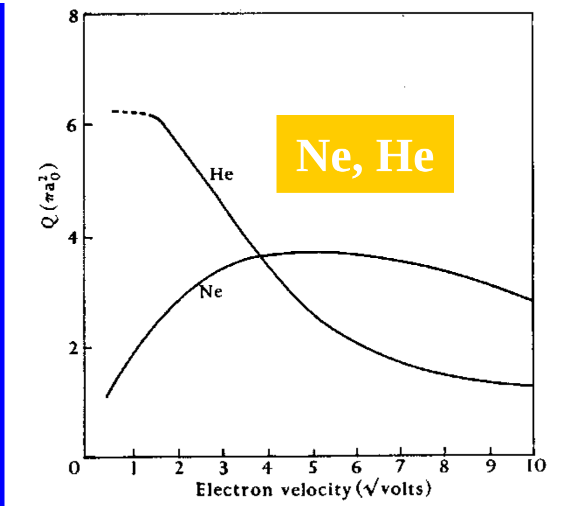

FIG. 1.10. Observed total collision cross-sections of He and Ne.

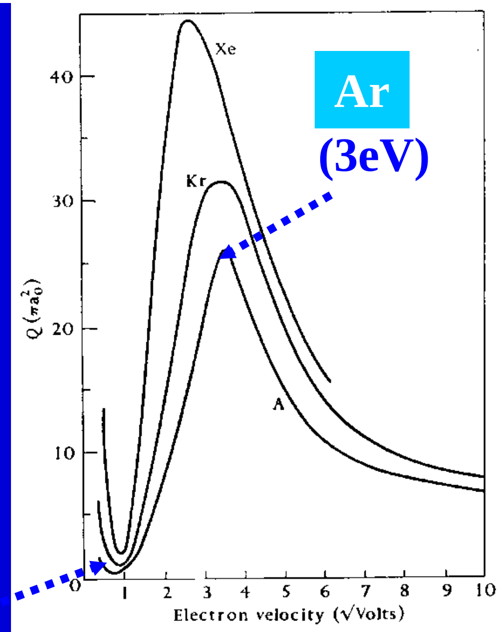

FIG. 1.9. Observed total collision cross-sections of A, Kr, and Xe.

(0,3eV)

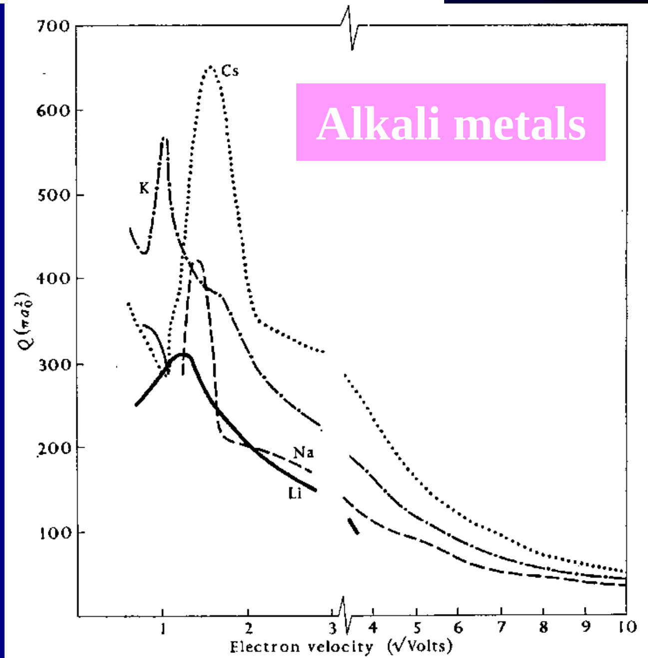

FIG. 1.16. Observed total collision cross-sections of Li, Na, K, and Cs.

$\sigma(v)$

$e^{-}(v)$

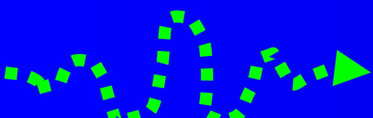

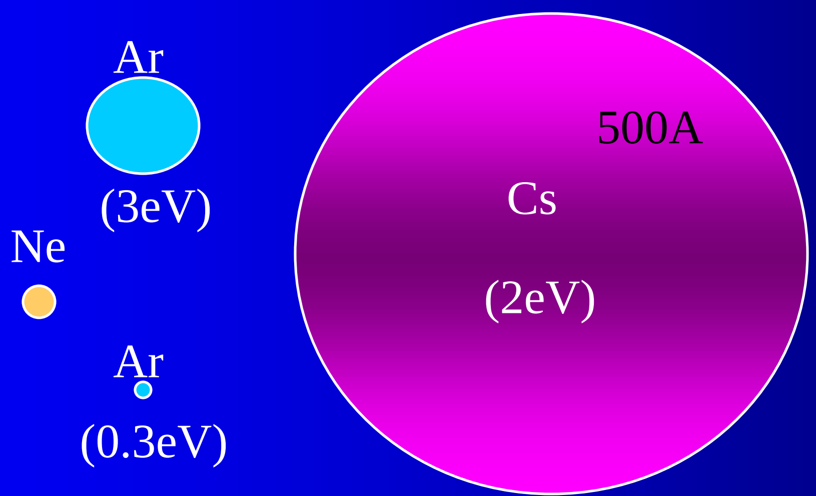

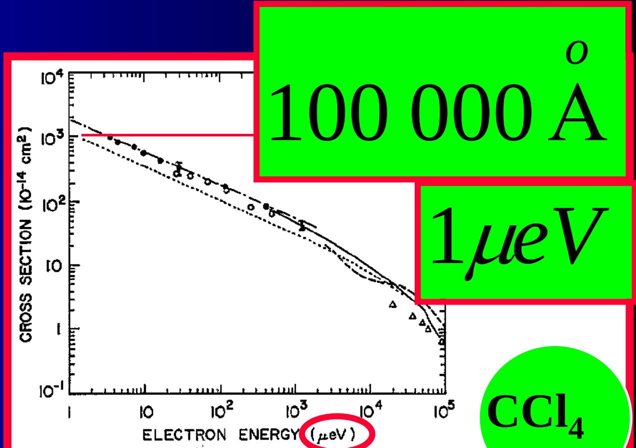

Figure 3. Cross sections for electron attachment to CCl_4. ●, $\bar{\sigma}_e$-K(np), ... K(np) (Frey et al 1994b); ○, $\bar{\sigma}_e$-K(np) (Ling et al 1992); ——, free electrons (Hotop 1994); - - -, free electrons (Orient et al 1989); △, free electrons (Christodoulides and Christophorou (1971); -----, theory (Klots 1976).

Kvantová mechanika
Jednorozměrný rozptyl

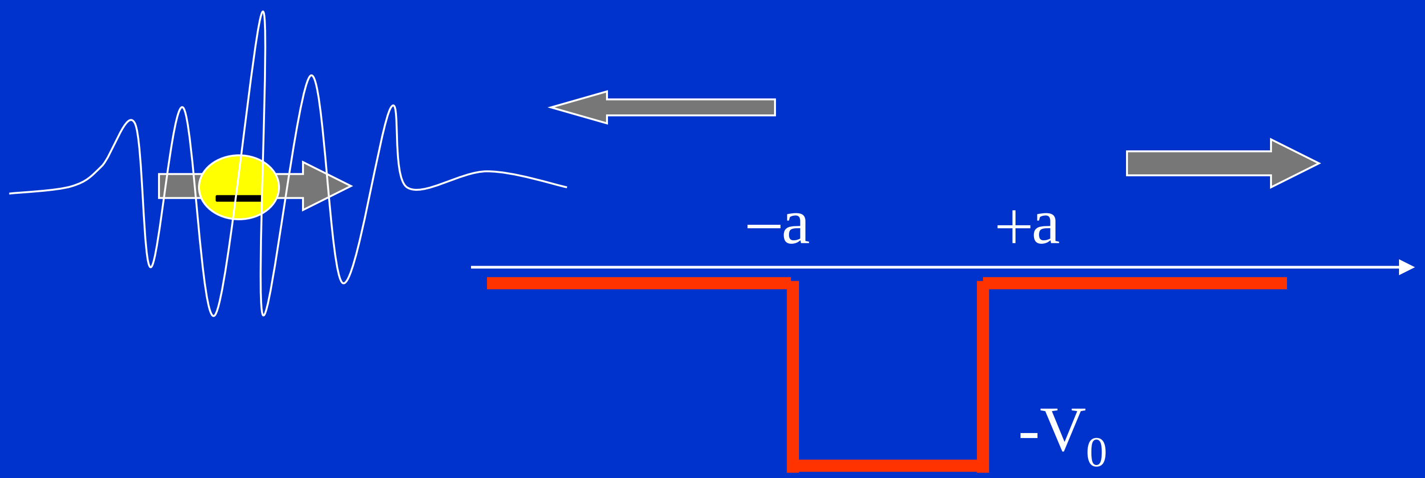

Kvantová mechanika I

J. Klíma B. Velický

MFF 1992

Jednorozměrný rozptyl

Vlnová funkce má tvar superposice Brogoliových vln

$k = \sqrt{2mE / h^2}$

$\psi_k(x,t) = (Ae^{ikx} + Be^{-ikx})e^{iE_k t/h} \qquad x \le -a$

$k = \sqrt{2mE / h^2}$

$\psi_k(x,t) = (Fe^{ikx} + \cancel{G}e^{-ikx})e^{iE_k t/h} \qquad x > a$

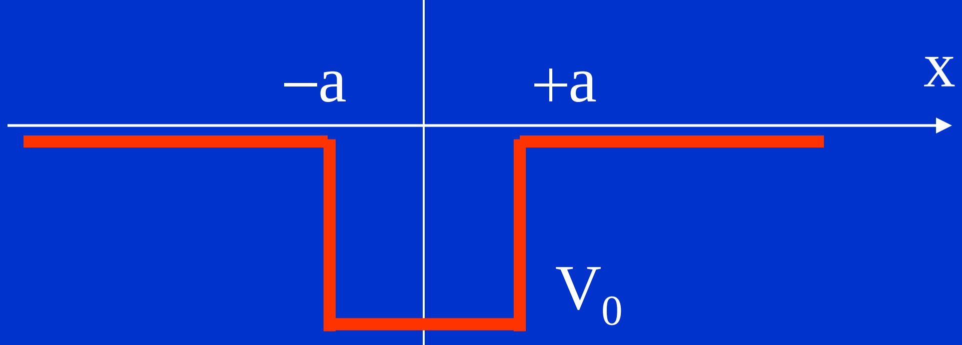

$\psi_k(x,t) = (Ce^{ik'x} + De^{-ik'x})e^{iE_k t/h} \qquad |x| \le a$

$k' = \sqrt{2m(E + V_0) / h^2}$

a) dopadající částice ➔A

b) odražená částice ➔B

c) procházející částice ➔F≠0, G=0

Jednorozměrný rozptyl

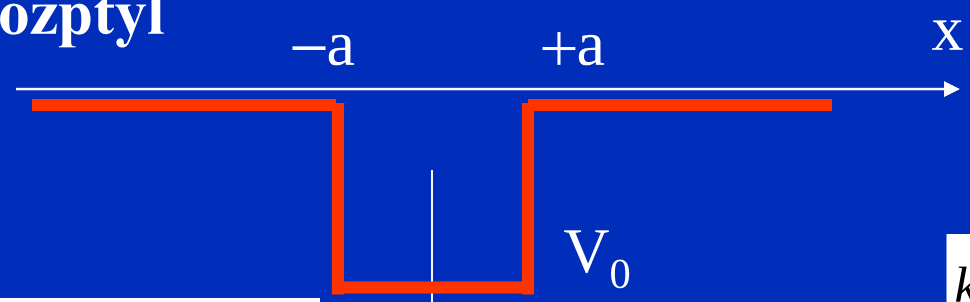

$$k = \sqrt{2mE/h^2}$$

$$k' = \sqrt{2m(E+V_0)/h^2}$$

$$\psi_k(x,t) = (Ae^{ikx} + Be^{-ikx})e^{iE_k t/h} \qquad x \le -a$$

$$\psi_k(x,t) = (Ce^{ik'x} + De^{-ik'x})e^{iE_k t/h} \qquad |x| \le a$$

$$\psi_k(x,t) = (Fe^{ikx})e^{iE_k t/h} \qquad x > a$$

Parametry jsou E, V_0, a

Hladkost řešení v bodech ±a
Určí konstanty B, C, D, G,
Hodnota A je vstupní parametr

Tok dopadajících částic $$j_{in} = \frac{hk}{m}|A|^2$$

Tok odražených částic $$j_{rf} = \frac{hk}{m}|B|^2$$

Tok prošlých částic $$j_{tr} = \frac{hk}{m}|F|^2$$

Jednorozměrný rozptyl

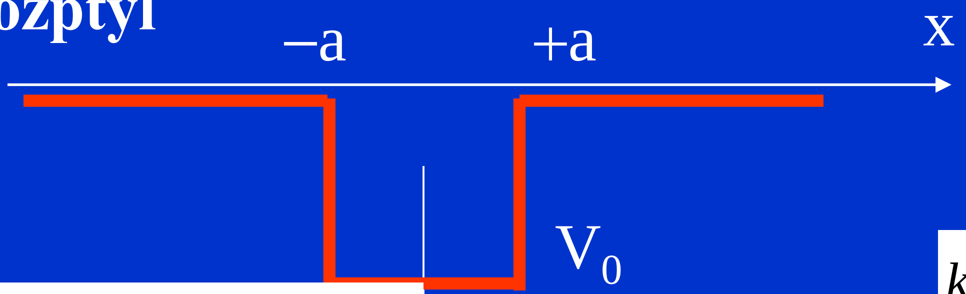

$$k = \sqrt{2mE / h^2}$$

$$k' = \sqrt{2m(E + V_0) / h^2}$$

$$\psi_k(x,t) = (Ae^{ikx} + Be^{-ikx})e^{iE_k t/h} \qquad x \le -a$$

$$\psi_k(x,t) = (Ce^{ik'x} + De^{-ik'x})e^{iE_k t/h} \qquad |x| \le a$$

$$\psi_k(x,t) = (Fe^{ikx})e^{iE_k t/h} \qquad x > a$$

Parametry jsou E, V_0, a

Hladkost řešení v bodech ±a
Urči konstanty B, C, D, G,
Hodnota A je vstupní parametr

Tok dopadajících částic $j_{in} = \frac{hk}{m}|A|^2$

$$C = \frac{F}{2}(1 + k/k')e^{i(k-k')a}$$

Tok odražených částic $j_{rf} = \frac{hk}{m}|B|^2$

$$D = \frac{F}{2}(1 - k/k')e^{i(k+k')a}$$

Tok prošlých částic $j_{tr} = \frac{hk}{m}|F|^2$

Jednorozměrný rozptyl

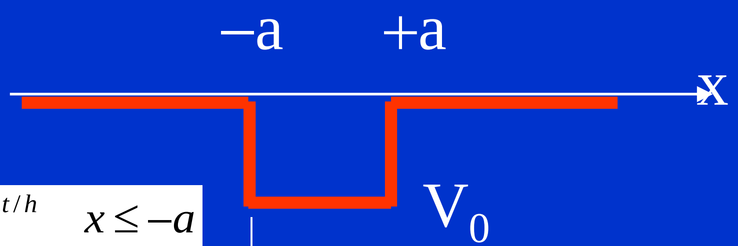

$$k = \sqrt{2mE / h^2}$$

$$k' = \sqrt{2m(E + V_0) / h^2}$$

$$\psi_k(x,t) = (Ae^{ikx} + Be^{-ikx})e^{iE_k t/h} \qquad x \le -a$$

$$\psi_k(x,t) = (Ce^{ik'x} + De^{-ik'x})e^{iE_k t/h} \qquad |x| \le a$$

$$\psi_k(x,t) = (Fe^{ikx})e^{iE_k t/h} \qquad x > a$$

Parametry jsou E, V_0, a

$$j_{in} = \frac{hk}{m}|A|^2$$

$$j_{rf} = \frac{hk}{m}|B|^2$$

$$j_{tr} = \frac{hk}{m}|F|^2$$

Hladkost řešení v bodech ±a
Urči konstanty B, C, D, F,
Hodnota A je vstupní parametr

$$\varepsilon = \frac{k'}{k} + \frac{k}{k'}$$

$$A = e^{2ika}(\cos(2k'a) - i(\varepsilon/2)\sin(2k'a))F$$

Koeficient průchodu T, koeficient odrazu R

$$\frac{1}{T} = \left|A/F\right|^2 = 1 + \frac{V_0^2}{4E(E+V)}\sin^2(2k'a)$$

Jednorozměrný rozptyl

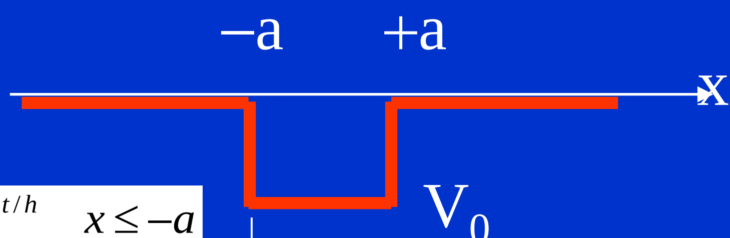

$$k = \sqrt{2mE/h^2}$$

$$k' = \sqrt{2m(E+V_0)/h^2}$$

$$\psi_k(x,t) = (Ae^{ikx} + Be^{-ikx})e^{iE_k t/h} \qquad x \le -a$$

$$\psi_k(x,t) = (Ce^{ik'x} + De^{-ik'x})e^{iE_k t/h} \qquad |x| \le a$$

$$\psi_k(x,t) = (Fe^{ikx})e^{iE_k t/h} \qquad x > a$$

Parametry jsou E, V_0 , a

$$j_{in} = \frac{hk}{m}|A|^2$$

$$j_{rf} = \frac{hk}{m}|B|^2$$

$$j_{tr} = \frac{hk}{m}|F|^2$$

Koeficient průchodu T, koeficient odrazu R

Pro velké E se T→1,

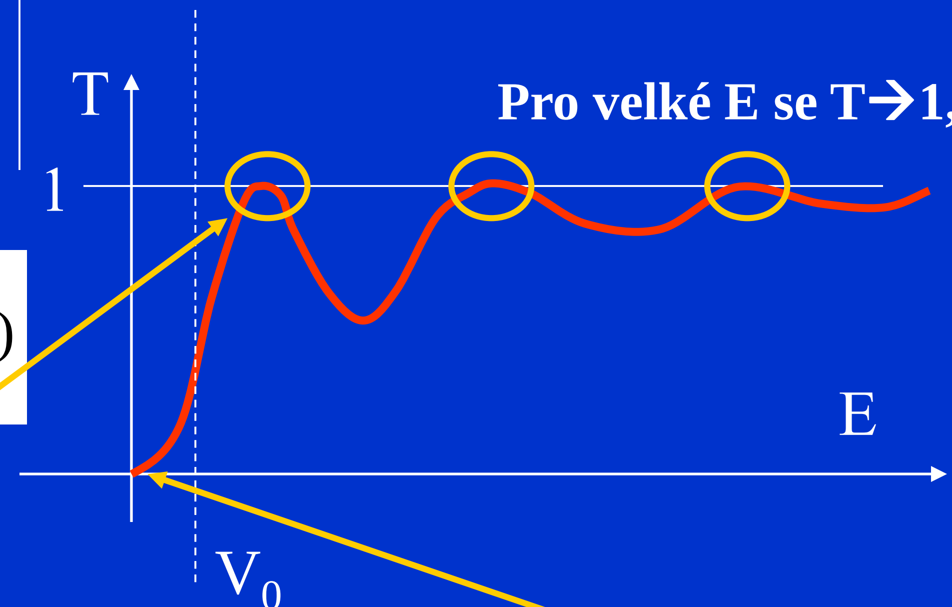

$$\frac{1}{T} = \left|A/F\right|^2 = 1 + \frac{V_0^2}{4E(E+V_0)}\sin^2(2k'a)$$

T=1 pro

$$2k_n'a = n\pi$$

$$\lim_{E\to 0}\frac{1}{T} \sim 1 + \frac{V_0^2}{4EV_0}\sin^2(2k'a) \sim 1 + \frac{V_0}{4E}\sin^2(2\sqrt{2mV_0/h^2}\,a) \sim 1 + \frac{V_0}{4E}const \sim \infty$$

$$\lim_{E\to 0} T \sim 0$$

Efekt Ramsauera - Kr

Parametry jsou E, V_0 , a

Pro velké E se T→1,

$$\frac{1}{T} = \left|\frac{A}{F}\right|^2 = 1 + \frac{V_0^2}{4E(E+V_0)}\sin^2(2k'a)$$

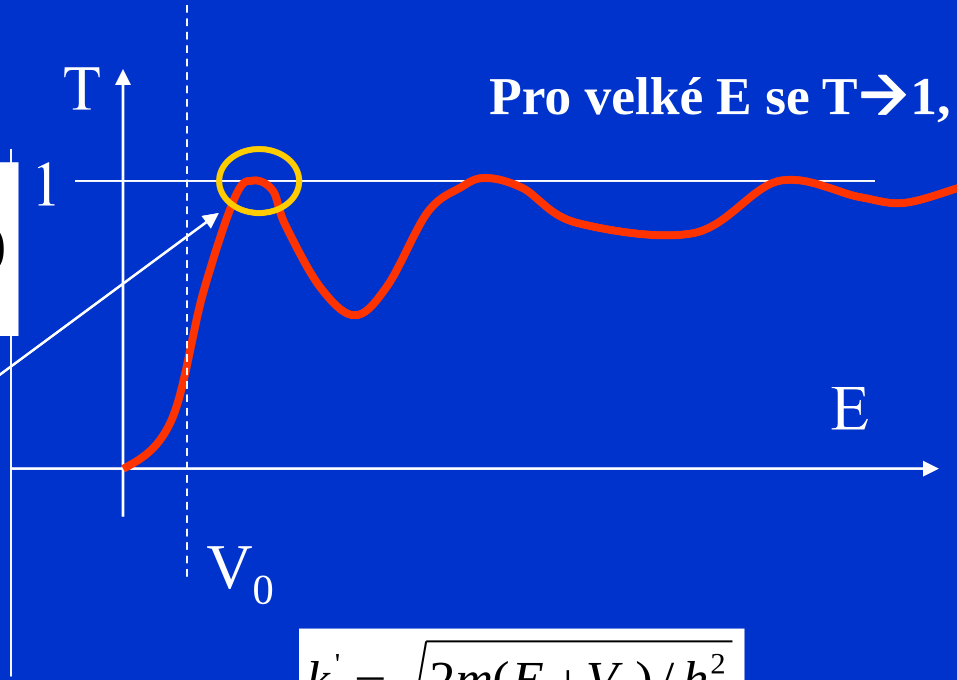

T=1 pro $2k_n'a = n\pi$

$$k' = \sqrt{2m(E+V_0)/h^2}$$

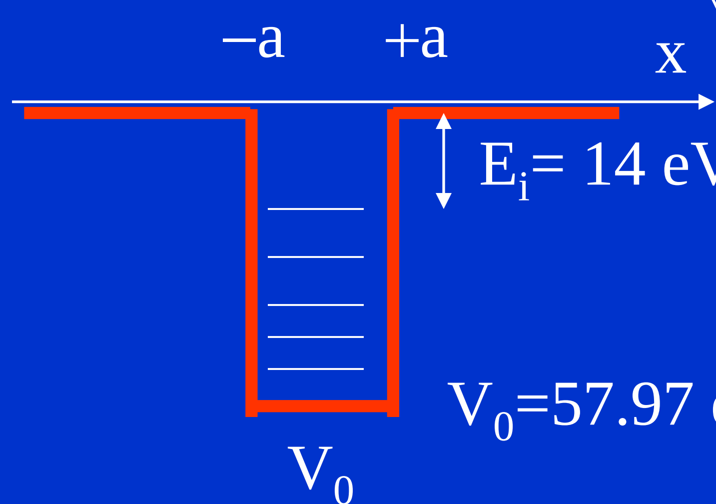

E_i= 14 eV

V_0=57.97 eV

Kr; a=2Å

E_i= 14 eV → V_0=57.97 eV

E=0.013 V_0=0.75 eV

Jednorozměrný rozptyl

Parametry jsou **E, V_0, a**

T+R=1

Pro velké E se T→1,

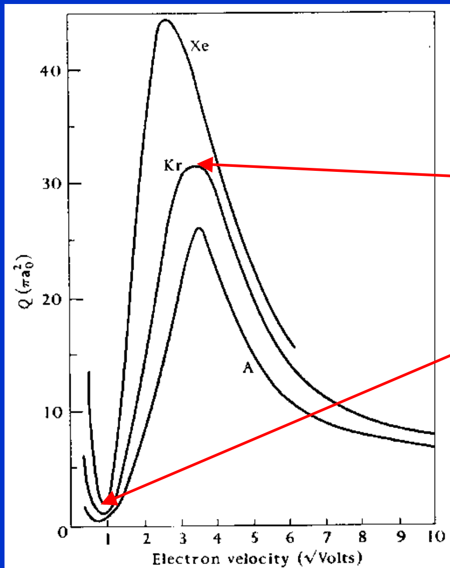

FIG. 1.9. Observed total collision cross-sections of A, Kr, and Xe.

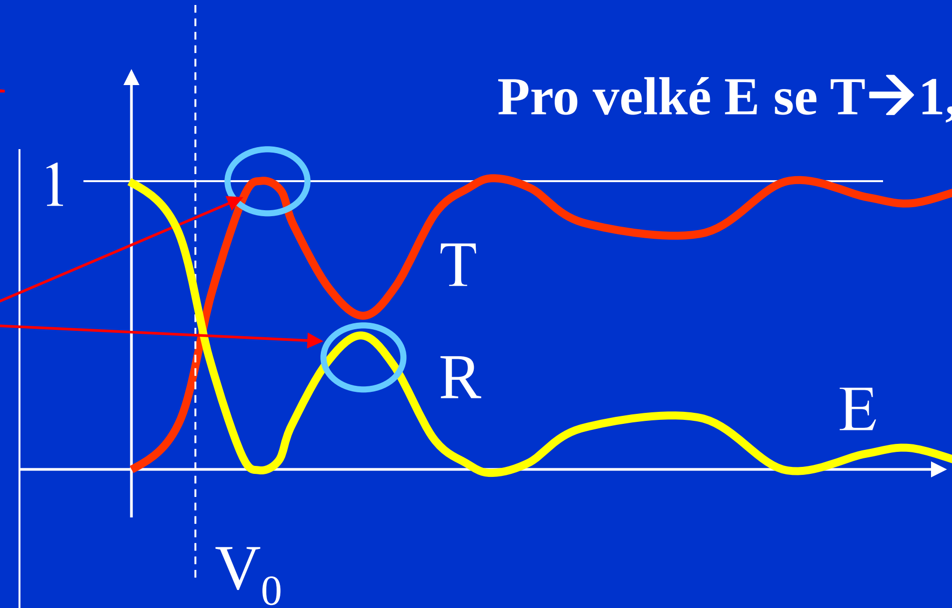

$$2k_n' a = n\pi$$

$$k' = \sqrt{2m(E+V_0)/h^2}$$

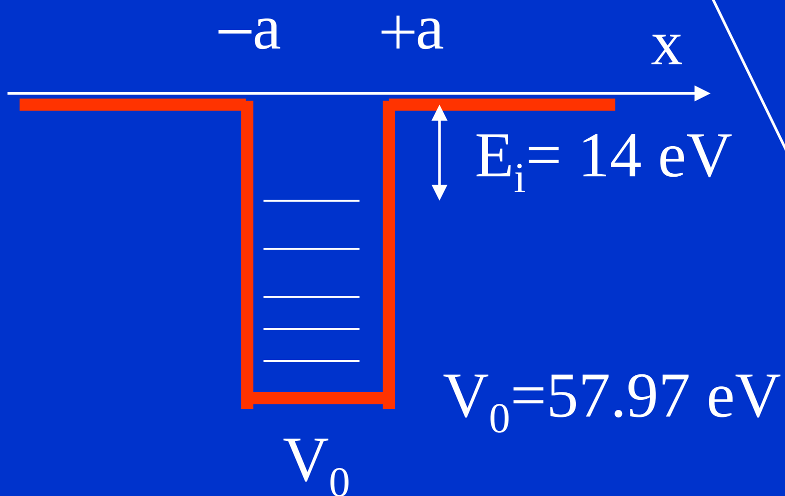

Kr; a=2Å

E_i= 14 eV → V_0=57.97 eV

E=0.013 V_0=0.75 eV

Frequencies of elastic collisions

$$\delta I = -NQI_p\,\delta x$$
$$I_P = I_0 \exp(-QNx)$$

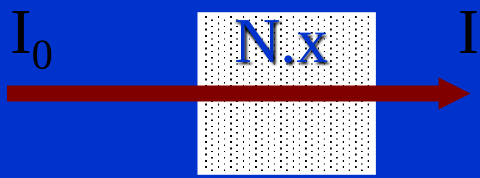

Q(v)

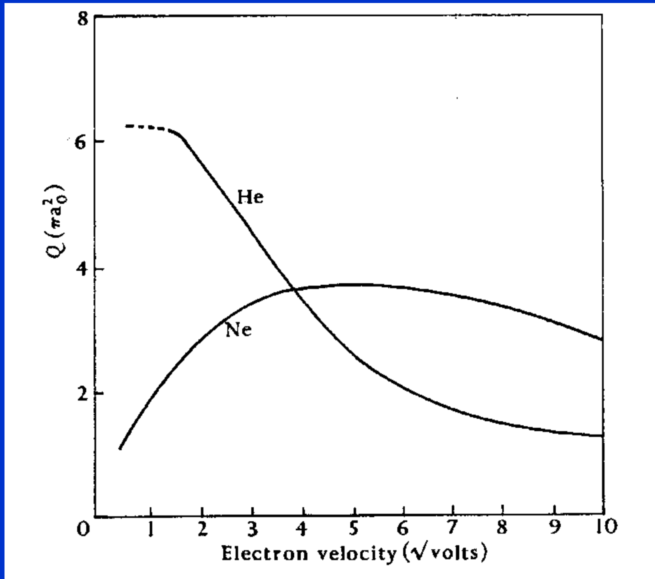

FIG. 1.10. Observed total collision cross-sections of He and Ne.

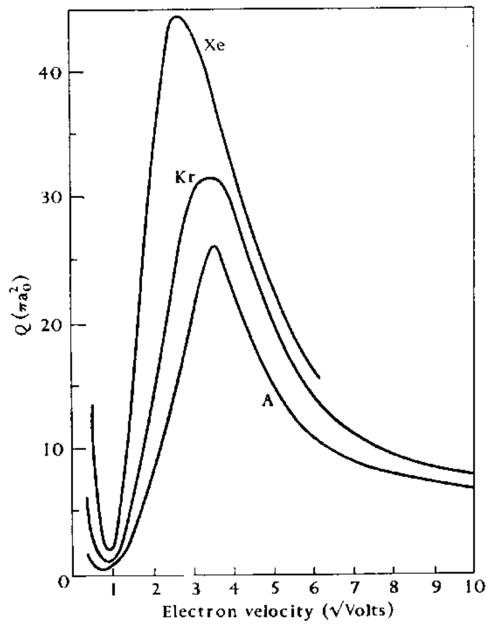

FIG. 1.9. Observed total collision cross-sections of A, Kr, and Xe.

Collision Frequencies

$$\nu \sim n v \sigma$$

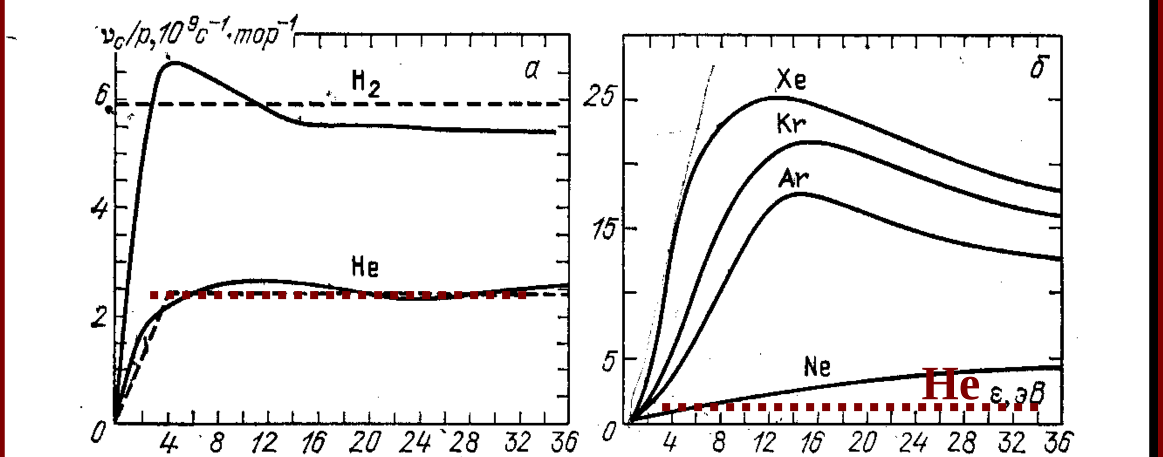

Рис. 2.5. Частоты упругих столкновений электронов, $p=1$ тор: *а* — в H_2 и He; *б* — в инертных газах; штриховые линии — удобная аппроксимация при расчетах [24]

$a_0 = 0.53\times10^{-8}$cm~0.5A
Radius of the first Bohr orbit of H atom

Very low collision energies

1995

TOPICAL REVIEW

Electron–molecule collisions at very low electron energies

F B Dunning

Department of Physics and the Rice Quantum Institute, Rice University, PO Box 1892, Houston, TX 77251, USA

J. Phys. B: At. Mol. Opt. Phys. 28 (1995) 1645–1672. Printed in the UK

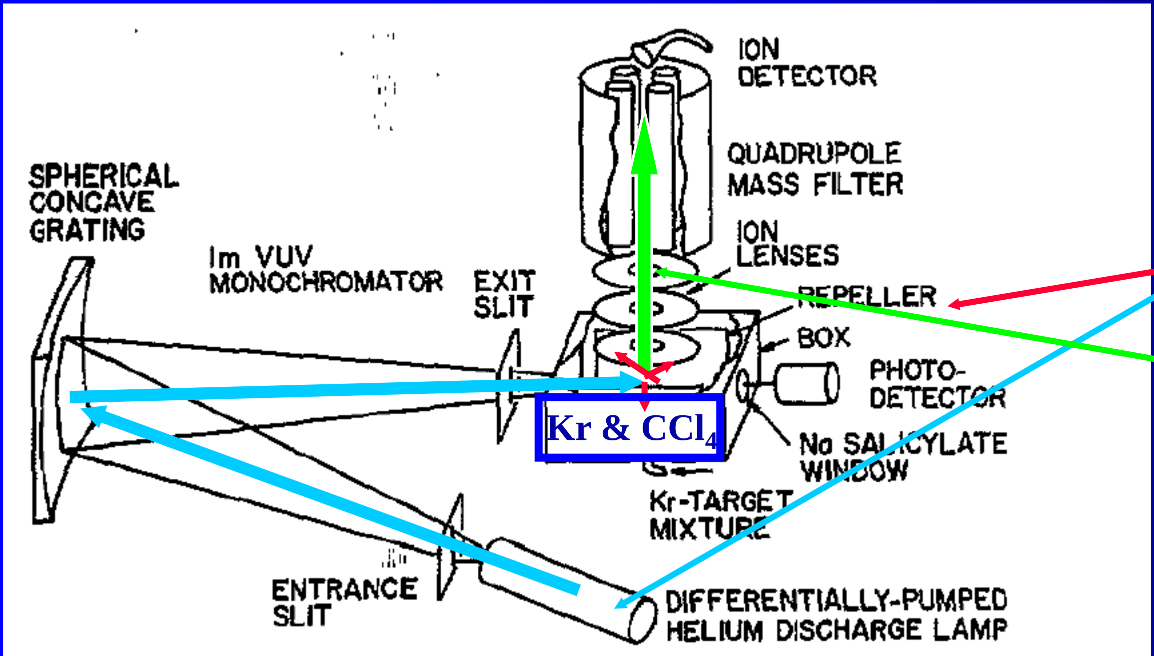

Figure 1. Schematic diagram of the vuv photoionization apparatus used for attachment studies (Chutjian and Alajajian 1985a, b).

$$Kr(^1S_0) + \hbar\omega \rightarrow Kr^+(^2P_{1/2}) + e^-(\varepsilon)$$

$$e^- + CCl_4 \rightarrow CCl_4^{-*} \rightarrow CCl_3 + Cl^-$$

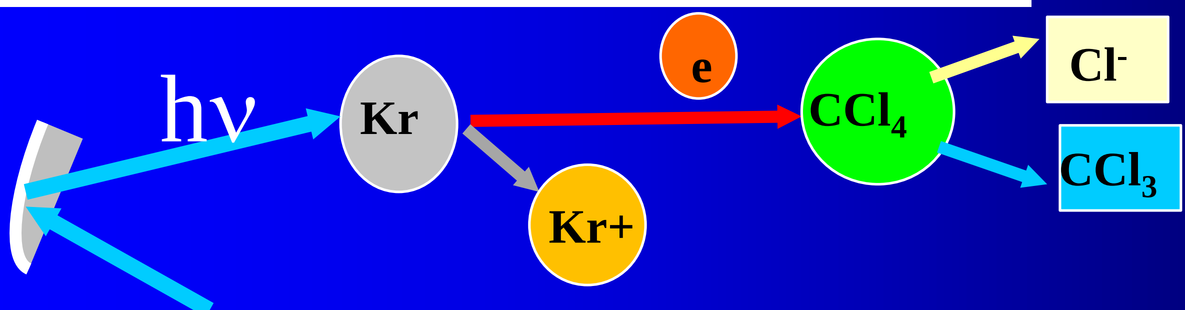

Very low collision energies

TOPICAL REVIEW

Electron–molecule collisions at very low electron energies

F B Dunning

Department of Physics and the Rice Quantum Institute, Rice University, PO Box 1892, Houston, TX 77251, USA

J. Phys. B: At. Mol. Opt. Phys. 28 (1995) 1645–1672. Printed in the UK

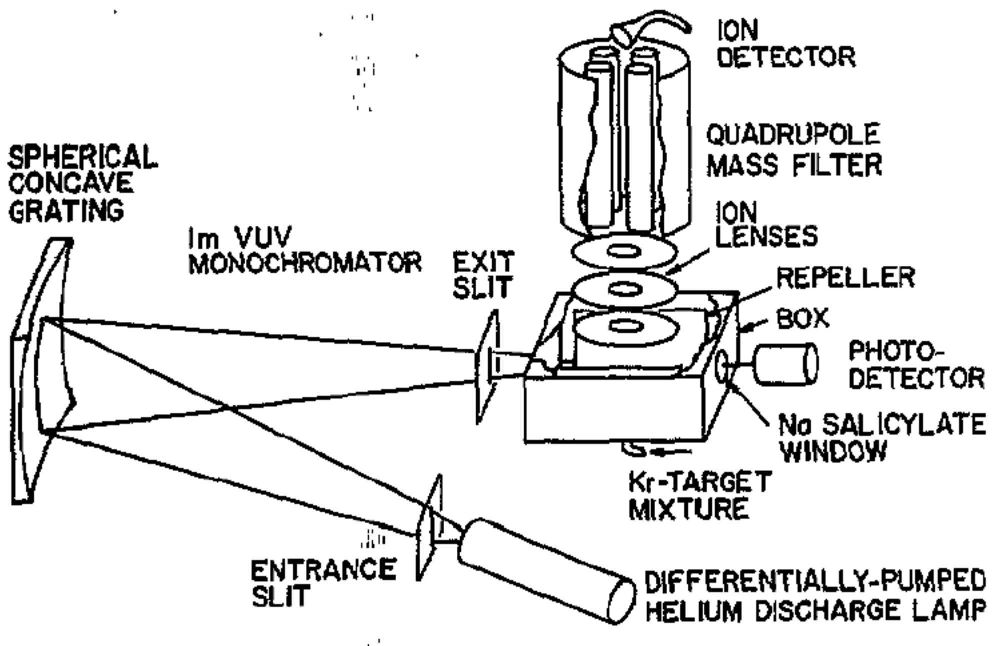

Figure 1. Schematic diagram of the vuv photoionization apparatus used for attachment studies (Chutjian and Alajajian 1985a, b).

$$Kr(^1S_0) + \hbar\omega \rightarrow Kr^+(^2P_{1/2}) + e^-(\varepsilon)$$

$$e^- + SF_6 \rightarrow SF_6^{-*}$$

$$e^- + CCl_4 \rightarrow CCl_4^{-*} \rightarrow CCl_3 + Cl^-$$

Very low collision energies

$$Kr(^1S_0) + \hbar\omega \rightarrow Kr^+(^2P_{1/2}) + e^-(\varepsilon)$$

$$e^- + SF_6 \rightarrow SF_6^{-*}$$

$$e^- + CCl_4 \rightarrow CCl_4^{-*} \rightarrow CCl_3 + Cl^-$$

TOPICAL REVIEW

J. Phys. B: At. Mol. Opt. Phys. 28 (1995) 1645–1672. Printed in the UK

Electron–molecule collisions at very low electron energies

F B Dunning

Department of Physics and the Rice Quantum Institute, Rice University, PO Box 1892, Houston, TX 77251, USA

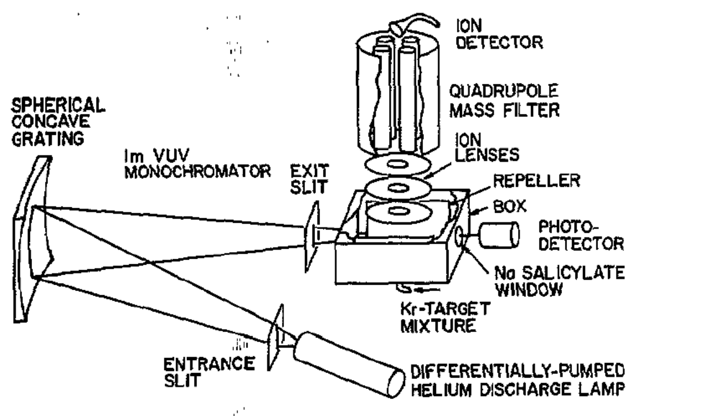

Figure 1. Schematic diagram of the vuv photoionization apparatus used for attachment studies (Chutjian and Alajajian 1985a, b).

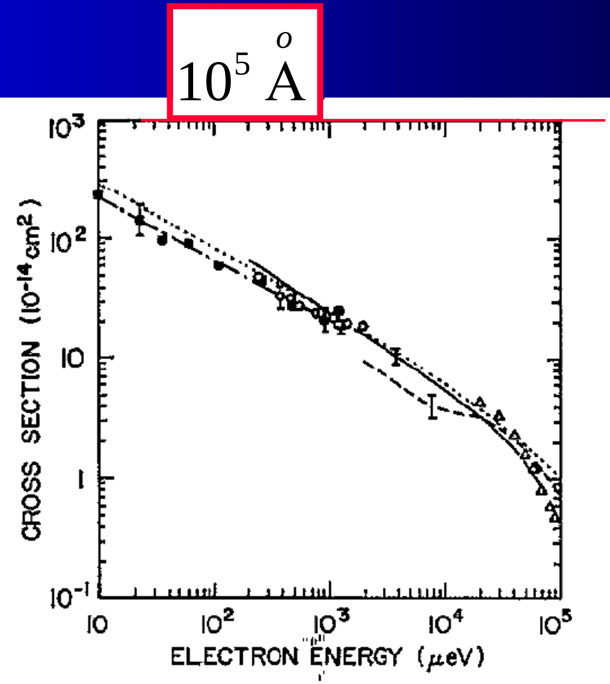

Figure 2. Cross section for electron attachment to SF_6. ■, $\bar{\sigma}_e$–K(np); — · —, $\sigma_e(v)$–K(np) (Ling *et al* 1992). ○, $\bar{\sigma}_e$–Rb(ns) (Zollars *et al* 1985); ——, free electrons (Klar *et al* 1992a, b); – – –, free electrons (Chutjian and Alajajian 1985); △, free electrons (Pai *et al* 1979, Chutjian and Alajajian 1985a); -----, theory (Klots 1976).

Electron attachment at very low electron energies

10^5 Å

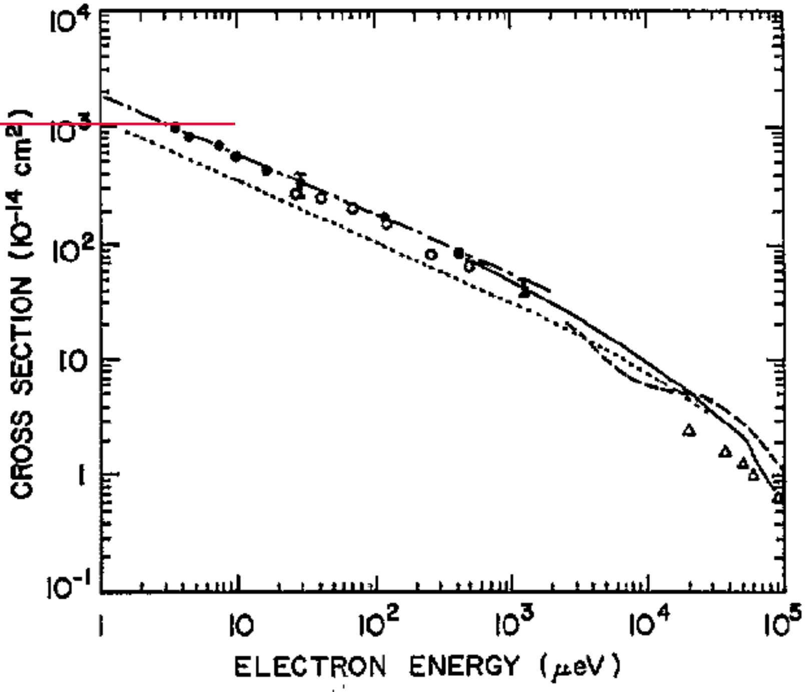

Figure 3. Cross sections for electron attachment to CCl_4. ●, $\bar{\sigma}_e$–K(np); — · —, $\sigma_e(\nu)$–K(np) (Frey *et al* 1994b); ○, $\bar{\sigma}_e$–K(np) (Ling *et al* 1992); ——, free electrons (Hotop 1994); – – –, free electrons (Orient *et al* 1989); △, free electrons (Christodoulides and Christophorou (1971); -----, theory (Klots 1976).

10^5 Å

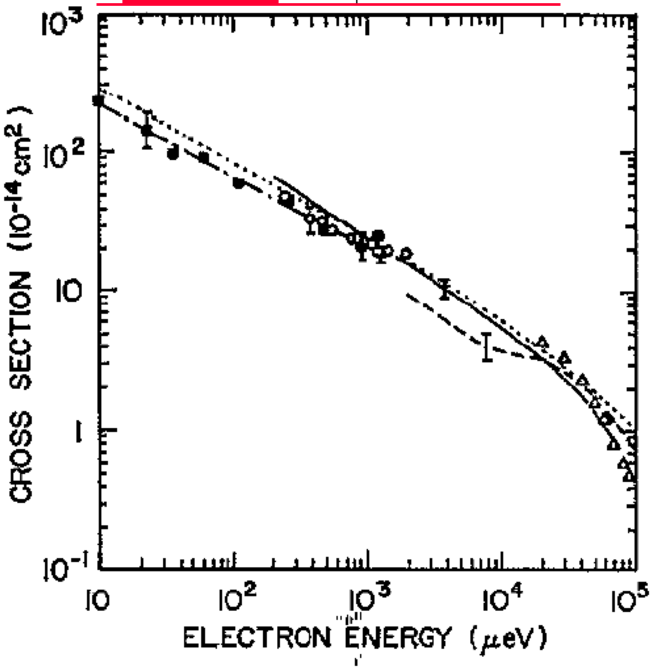

Figure 2. Cross section for electron attachment to SF_6. ■, $\bar{\sigma}_e$–K(np); — · —, $\sigma_e(\nu)$–K(np) (Ling *et al* 1992). ○, $\bar{\sigma}_e$–Rb(ns) (Zollars *et al* 1985); ——, free electrons (Klar *et al* 1992a, b); – – –, free electrons (Chutjian and Alajajian 1985); △, free electrons (Pai *et al* 1979, Chutjian and Alajajian 1985a); -----, theory (Klots 1976).

Molecules

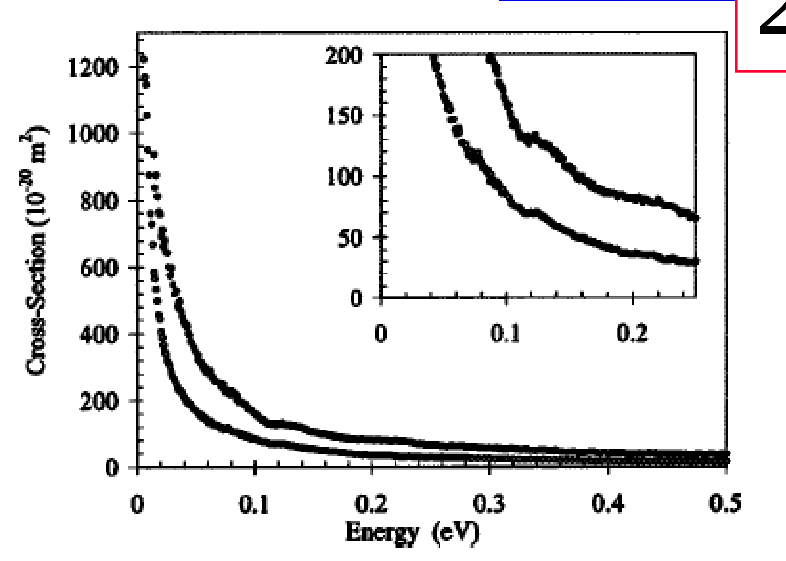

2004

PHYSICAL REVIEW A **69**, 052716 (2004)

Cold electron scattering in SF_6 and C_6F_6: Bound and virtual state channels

D. Field,[1,*] N. C. Jones,[1] and J.-P. Ziesel[2]
[1]*Department of Physics and Astronomy, University of Aarhus, DK- 8000 Aarhus C, Denmark*
[2]*Laboratoire Collisions Agrégats Réactivité (CNRS UMR5589), Université Paul Sabatier, 31062 Toulouse, France*
(Received 26 November 2003; published 20 May 2004)

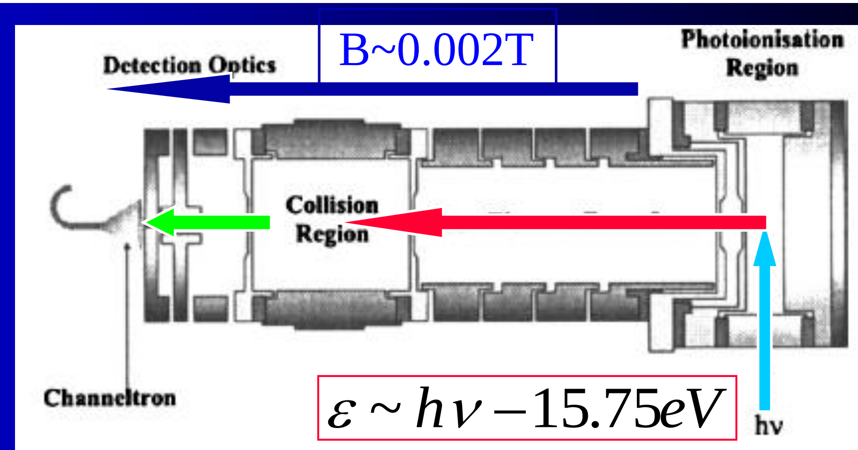

FIG. 1. A scale diagram of the apparatus. Monochromatic synchrotron radiation from ASTRID ($h\nu$) enters a photoionization region containing Ar. Photoelectrons, expelled by a weak electric field, are focused by a four-element lens [38] into a collision chamber containing the target gas. Transmitted electrons are detected at the channel electron multiplier (channeltron) situated beyond some further electron optics. The apparatus may be immersed in an axial magnetic field of 2×10^{-3} T.

The general process which we study involves electron attachment,

$$e^- + M \rightarrow M^{-*}, \quad M = SF_6, C_6F_6, \qquad (1)$$

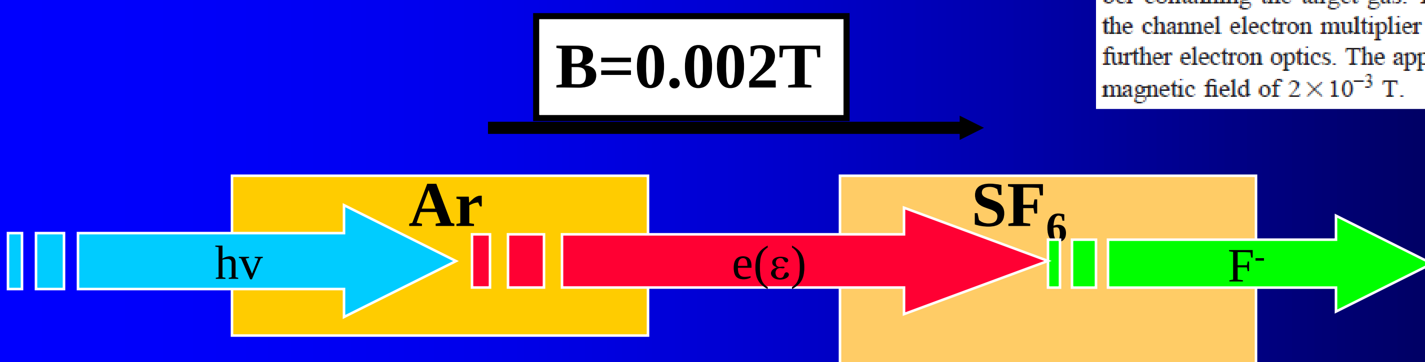

Ar +hν➔Ar⁺+e(ε)

$\varepsilon \sim h\nu - 15.75eV$

SF_6 + e(ε)➔ X^- +Y

Molecules

2008

PHYSICAL REVIEW A **78**, 042714 (2008)

Scattering of cold electrons by ammonia, hydrogen sulfide, and carbonyl sulfide

N. C. Jones,[1] D. Field,[2,*] S. L. Lunt,[3] and J.-P. Ziesel[4]
[1] *Institute for Storage Ring Facilities (ISA), University of Aarhus, DK-8000 Aarhus C, Denmark*
[2] *Department of Physics and Astronomy, University of Aarhus, DK-8000 Aarhus C, Denmark*
[3] *Kittiwake Developments Ltd, Littlehampton, West Sussex BN17 7LU, United Kingdom*
[4] *Laboratoire Collisions Agrégats Réactivité (CNRS-UPS UMR5589), Université Paul Sabatier, 31062 Toulouse, France*
(Received 2 July 2008; published 29 October 2008)

Experimental data obtained with a high-resolution transmission experiment are presented for the scattering of electrons in the energy range 20 meV–10 eV for NH_3, 25 meV–10 eV for H_2S, and 15 meV–2.5 eV for OCS. Data include cross sections for both integral scattering and scattering into the backward hemisphere, the latter up to 650 meV impact energy, with an electron energy resolution of between 1.6 and 3.5 meV. The new data allow the first detailed comparison with theory for the energy regime dominated by rotationally inelastic and elastic scattering for these species. It is evident that theory still lacks quantitative predictive power at low energy, although qualitative agreement is consistently good for all three species. A discussion is given of the possible presence of a virtual state in OCS scattering as recently proposed on theoretical grounds.

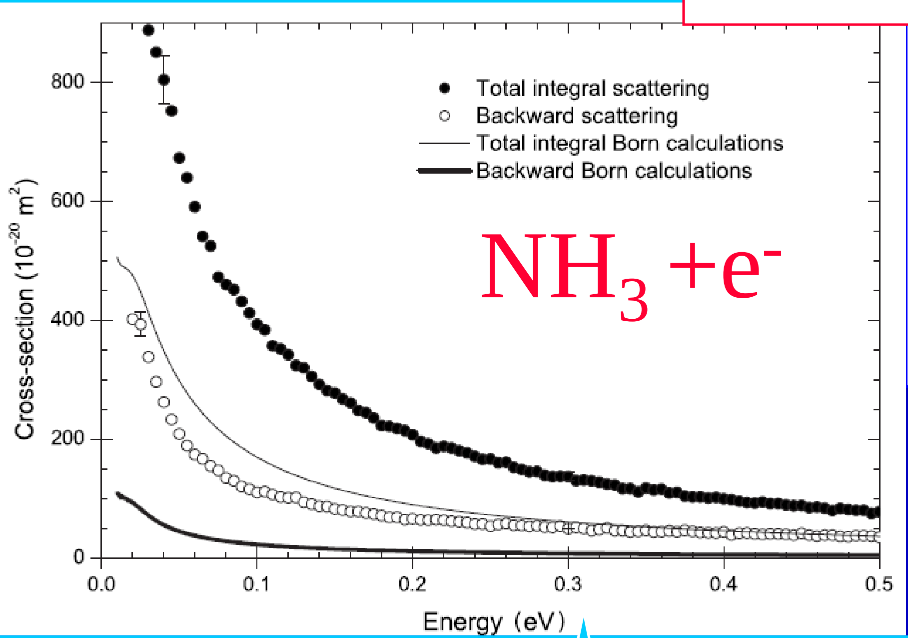

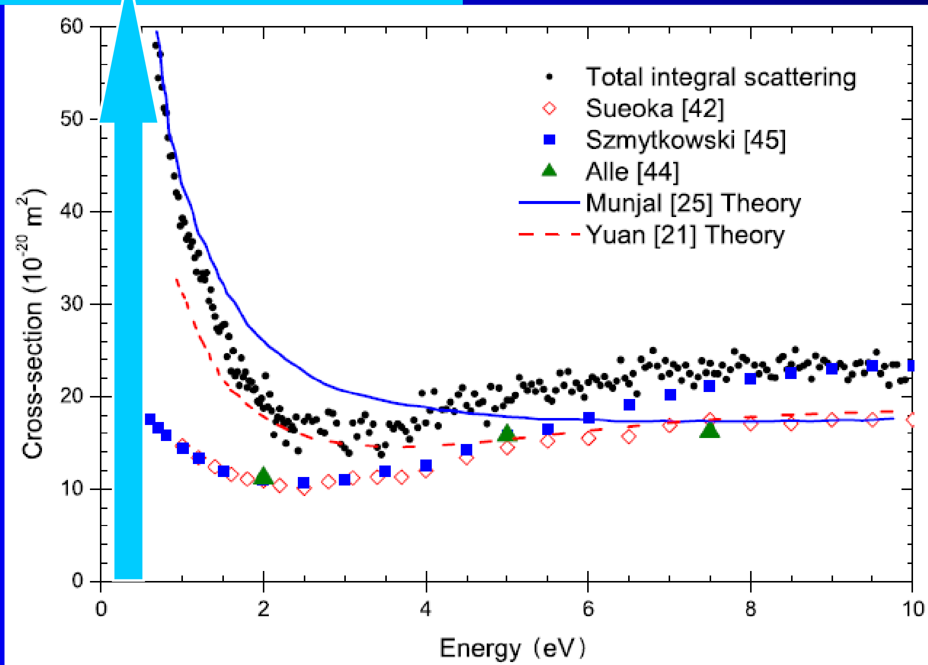

$NH_3 + e^-$

FIG. 1. (Color online) NH_3: the variation of the sum of the integral elastic and inelastic cross sections, $\sigma_{T,I}$, between 0.675 and 10 eV. Also shown are experimental data from Sueoka *et al.* [42], Szmytkowski *et al.* [45], and Alle *et al.* [44] and theoretical values from Munjal *et al.* [25] and Yuan *et al.* [21].

Molecules cross section for interaction with electrons

2008

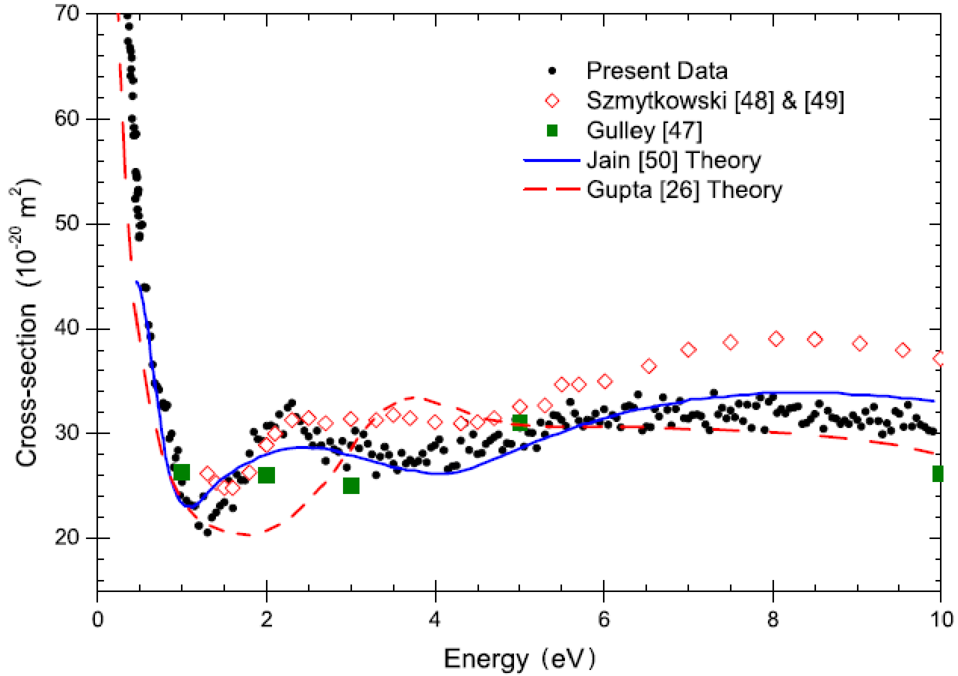

$H_2S + e^-$

FIG. 3. (Color online) H_2S: the variation of the sum of the integral elastic and inelastic cross sections, $\sigma_{T,I}$, between 380 meV and 10 eV. Also shown are experimental data in Szmytowski *et al.* [48,49] and Gulley *et al.* [47] and theoretical values from Jain *et al.* [50] and Gupta *et al.* [26].

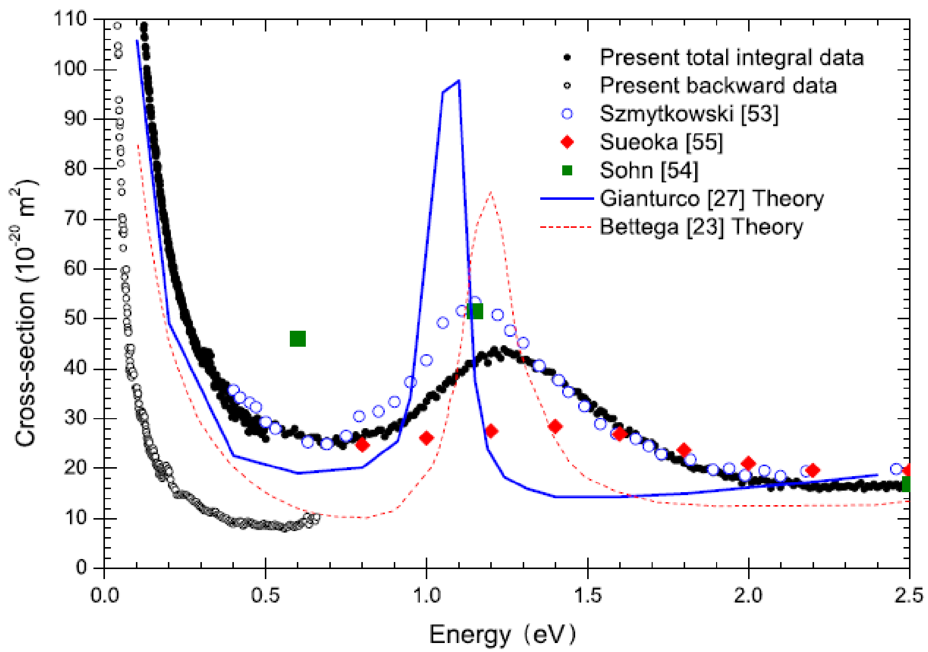

$OCS + e^-$

FIG. 5. (Color online) OCS: the variation of the sum of the integral elastic and inelastic cross sections, $\sigma_{T,I}$, between 120 meV and 2.5 eV, and the elastic and inelastic backward scattering cross section into the backward 2π sr, between 39 and 650 meV. Also shown are experimental values from Szymtkowski *et al.* [53], Sueoka *et al.* [55], and Sohn *et al.* [54] and theoretical values of integral cross sections from Gianturco *et al.* [27] and Bettega *et al.* [23].

Molecules

2006

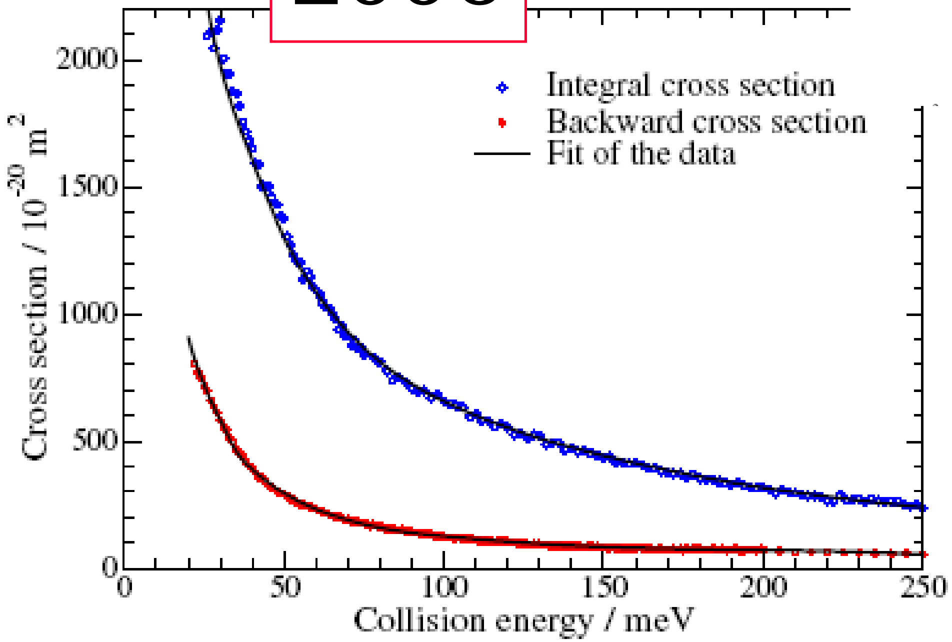

PRL **97,** 123202 (2006) PHYSICAL REVIEW LETTERS week ending 22 SEPTEMBER 2006

Rotational Excitation of H_2O by Cold Electrons

R. Čurík,[1] J. P. Ziesel,[2] N. C. Jones,[3] T. A. Field,[4] and D. Field[3,*]

[1]*J. Heyrovský Institute of Physical Chemistry, Dolejškova 3, 18223 Prague 8, Czech Republic*

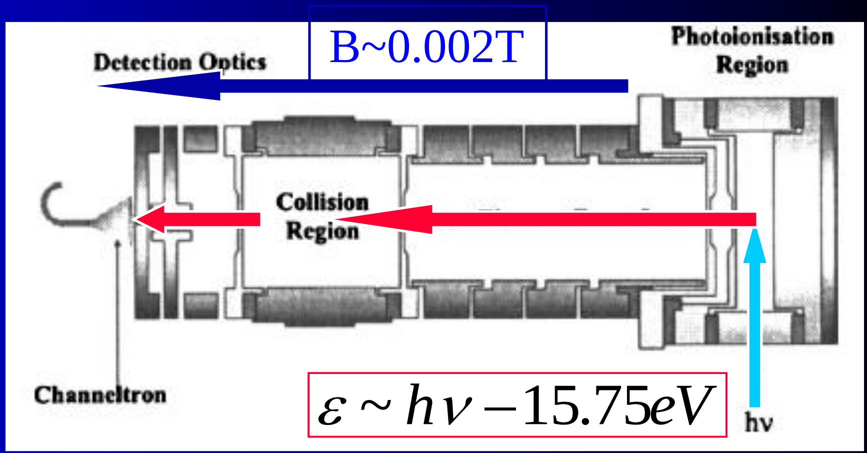

Experimental data are presented for the scattering of electrons by H_2O between 17 and 250 meV impact energy. These results are used in conjunction with a generally applicable method, based on a quantum defect theory approach to electron-polar molecule collisions, to derive the first set of data for state-to-state rotationally inelastic scattering cross sections based on experimental values.

B=2x10^{-3}T

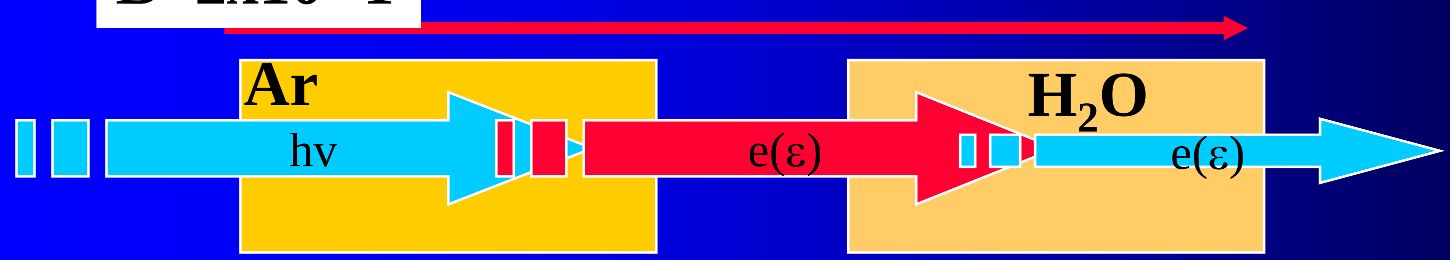

Ar +hν➔Ar$^+$+e(ε)

$$\varepsilon \sim h\nu - 15.75eV$$

H_2O (j_0) + e(ε_1)➔ H_2O($j>j_0$) + e(ε_2)

Molecules

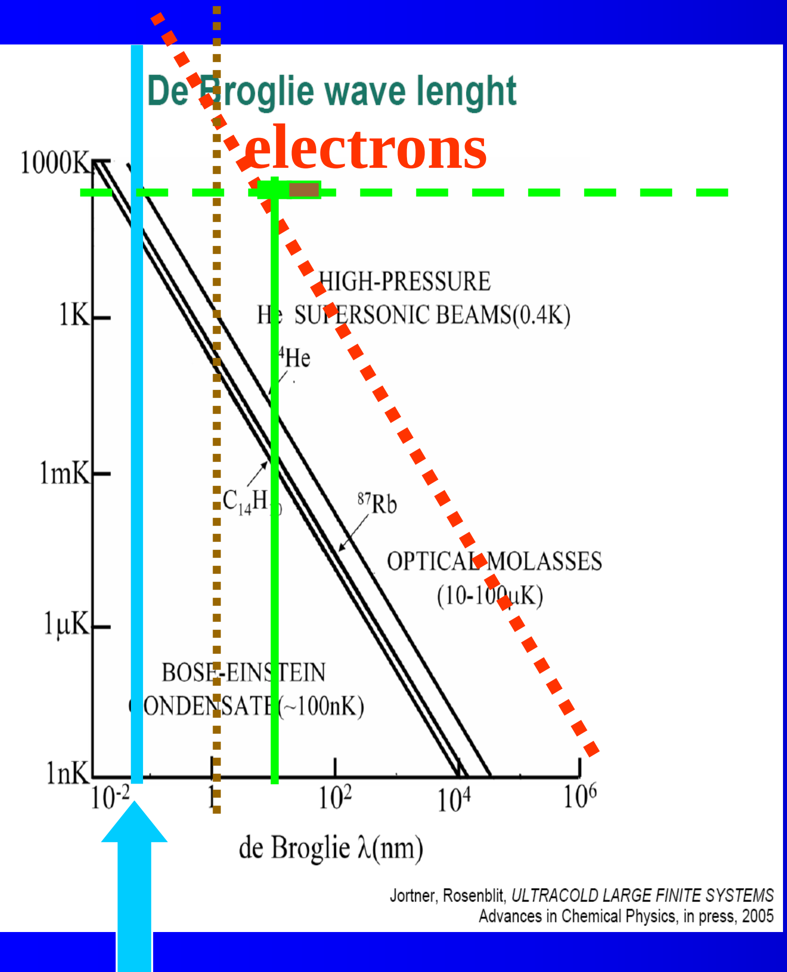

Jortner, Rosenblit, *ULTRACOLD LARGE FINITE SYSTEMS*
Advances in Chemical Physics, in press, 2005

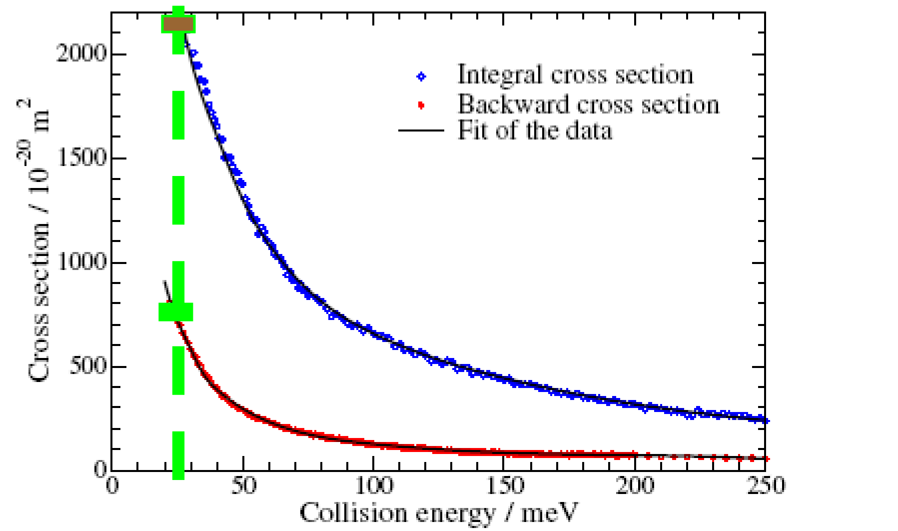

FIG. 1 (color online). Integral (upper set) and backward cross sections (lower set) for scattering of electrons by H_2O as a function of electron impact energy. Values are ±5%. The solid lines are fits to theory (see text).

$$\lambda = \frac{h}{p} = \frac{h}{mv}\sqrt{1 - \frac{v^2}{c^2}}$$

$$\sigma \sim \pi\lambda^2 \sim 1/\varepsilon$$

Molecules -rotational excitation

2006

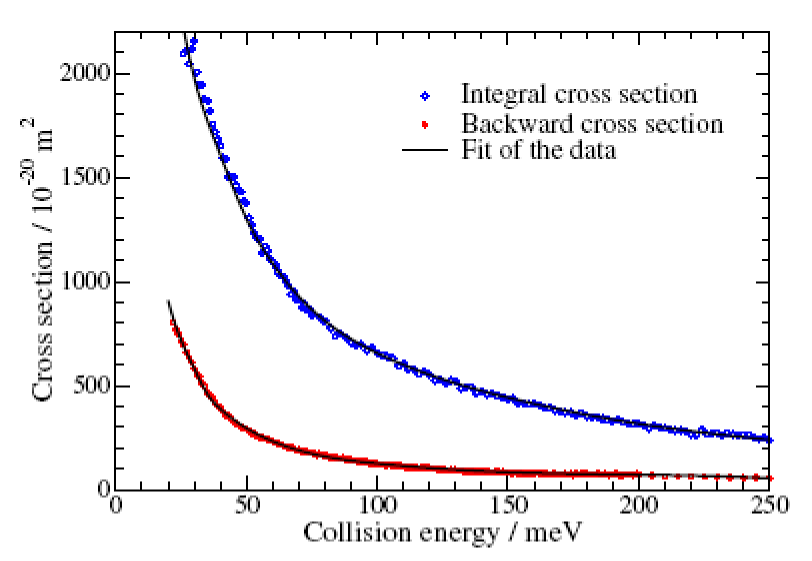

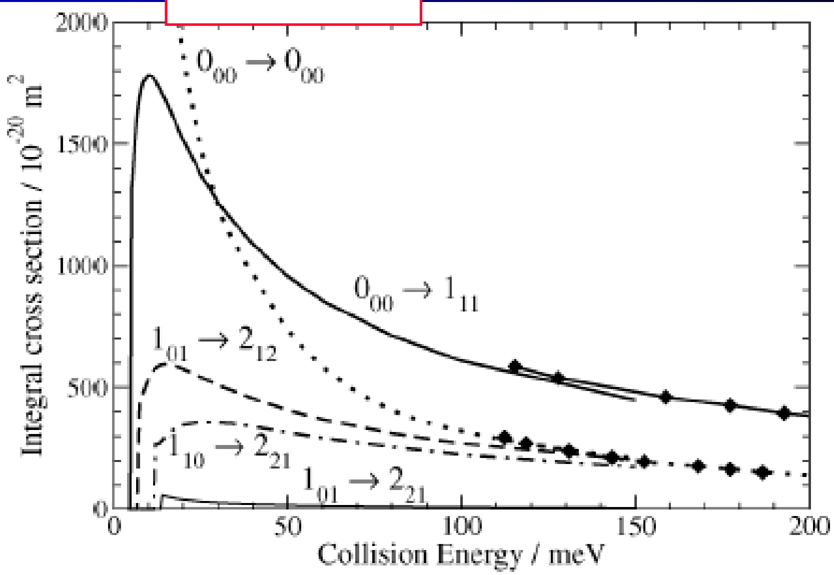

FIG. 3. Selected state-to-state integral cross sections for rotational excitation of the H_2O molecule determined from experimental data. Full curves represent results for para-H_2O and dashed for ortho-H_2O. The dotted curve represents elastic scattering for para-H_2O in its lowest rotational state. Curves with diamonds show the results of *R*-matrix calculations in Ref. [12].

$$H_2O\ (j_0) + e(\varepsilon_1) \rightarrow H_2O(j>j_0) + e(\varepsilon_2)$$

Koniec rosprávky